Chromosomal Evolution of Malaria Vectors

Ashley N. Peery

Dissertation submitted to the faculty of the Virginia Polytechnic Institute and State University in partial fulfillment of the requirements for the degree of

Doctor of Philosophy
In
Entomology

Igor V. Sharakhov, Chair
Zachary N. Adelman
Dana M. Hawley
Maria V. Sharakhovar
Zhijian Tu

April 29th 2016

Blacksburg, VA

Keywords: chromosomal evolution, vector-borne disease, malaria, mosquitoes

Chromosomal Evolution of Malaria Vectors

Ashley N. Peery

ABSTRACT

Abstract (academic):

International malaria control initiatives such as the Roll Back Malaria Initiative (RBM) and the Medicines for Malaria Venture (MMV) mobilize resources and spur research aimed at vector control as well as the treatment and eventual eradication of the disease. These efforts have managed to reduce incidence of malaria by an estimated 37% worldwide since 2000. However, despite the promising success of control efforts such as these, the World Health Organization reports a staggering 438,000 deaths from malaria in 2015. The continuing high death toll of malaria as well as emerging insecticide and antimalarial drug resistance suggests that while encouraging, success in reducing malaria incidence may be tenuous. Current vector control strategies are often complicated by ecological and behavioral heterogeneity of vector mosquito populations. As an additional obstruction, mosquito genomes are highly plastic as evidenced by the wealth or chromosomal inversions that have occurred in this genus. Chromosomal inversions have been correlated with differences in adaptation to aridity, insecticide resistance, and differences in resting behavior. However, a good understanding of the molecular mechanisms for inversion generation is still lacking. One possible contributor to inversion formation in *Anopheles* mosquitoes includes repetitive DNA such as transposable elements (TEs), tandem repeats (TRs) and inverted repeats (IRs). This dissertation provides physical maps for two important malaria vectors, *An. stephensi* and *An. albimanus* (Ch.2 and Ch. 3) and then applies those maps to the identification of inversion breakpoints in malaria mosquitoes. Repeat content of each chromosomal arm and the molecular characterization of lineage specific breakpoints is also investigated (Ch. 2 and Ch.4). Our study reveals differences in patterns of chromosomal evolution of *Anopheles* mosquitoes vs. *Drosophila*. First, mosquito chromosomes tend to shuffle as intact elements via whole arm translocations and do not under fissions or fusions as seen in fruitflies. Second, the mosquito sex chromosome is changing at a much higher rate relative to the autosomes in malaria mosquitoes than in fruit flies. Third, our molecular characterization of inversion breakpoints indicates that TEs and TRs may participate in inversion genesis in an arm specific manner.

Chromosomal Evolution of Malaria Vectors

Ashley N. Peery

General Audience Abstract:

Malaria is a complex and devastating disease vectored by the bite of a female *Anopheles* mosquito. This disease claimed an estimated 438,000 lives in 2015. The mobilization of funding and resources as part of global malaria eradication initiatives have reduced the global incidence of malaria by 37% in the last 15 years. Deaths from malaria are also 60% lower vs. the year 2000. These promising gains are threatened by the ability of *Anopheles* mosquitoes to adapt in the face of malaria control efforts. *Anopheles* mosquito chromosomes are known to be highly plastic, as evidenced by numerous chromosomal inversions. Recent years have seen increases in insecticide resistance, and behavioral change in mosquito populations that allow them to avoid insecticides and remain prolific vectors of disease. This ability of mosquito vectors to adapt threatens to unravel recent progress towards a malaria free world. The project presented in this dissertation explore mechanisms of chromosomal evolution, specifically the potential role of repetitive DNA in the generation of chromosomal inversions. The exploration of chromosomal inversions was facilitated by the creation of physical maps for *Anopheles* species. Prominent malaria vectors *An. stephensi* and*An. albimanus* were physically mapped in Chapter 2 and Chapter 3 respectively. In chapter 1 and chapter 3 physical maps are utilized for the identification of chromosomal inversion breakpoints using 2 species (Ch. 2) and many species (Ch. 4). Repeat content was quantified along each chromosomal arm (Ch 2,4) and in inversion breakpoint regions (Ch 3). This dissertation presents physical maps for two important malaria species that have been applied to the study of chromosomal evolution and will also serve as community tools for further study of malaria mosquitoes. Our work on chromosomal evolution has revealed the *Anopheles* chromosomes tend to undergo translocations as intact elements and do not under fissions and fusions as seen in fruitflies. We also find that the malaria mosquito sex chromosome changes much more rapidly relative to the autosomes than in fruitflies. Additionally, repetitive DNA including transposable elements (TEs) and tandem repeats (TRs) may be encouraging chromosomal inversions but with differing roles on different chromosomal arms.

Dedication

This dissertation is dedicated to the crazy man who decided to continue dating me, (and later marry me!) even after I warned him that I would break up with him if our relationship got in the way of my PhD. I can't imagine my life without you.

Acknowledgements

To Dr. Igor Sharakhov: Thanks for taking a chance on the enthusiastic young kid you met in 2009. You were patient enough to accept the blunders of my untrained hands and you have shaped me into the scientist that I am today.

To Dr. Maria Sharakhova: You are a master of cytogenetics and I appreciate you sharing those skills with me. Learning from you over the years has opened my eyes to the beautiful and fascinating detail of mosquito chromosomes.

To Dr. Z. Adelman, Dr. D. Hawley, and Dr. Z. Tu: Thanks so much for broadening my perspectives as I pursued my research.

To Captain Phillip J.P. George, PhD: Under your mentorship I learned scientific technique, self sufficiency, and a greater than average appreciation of NIN and Muse. Thanks for your advice on professional and personal matters over the last 7 years. I wish you happiness in your future because I have no doubt that you will be successful.

To Dr. Atashi Sharma: You are the best PhD buddy a girl could ask for and I'm so glad we became friends even if you beat me in the race to a PhD. I owe my love of chickpea curry and my chai snobbery to you. Start looking out for you! You deserve nothing less than unadulterated happiness.

To Fan Yang, MSLFS: Fan, I have enjoyed learning and working alongside you over the years. Thanks for your friendship and support.

To Dr. Maryam Kamali, Dr. Nick Kinney, and Jiyoung Lee, MS: Being in the lab for 40+ hours a week sharing the same resources means that your lab mates can feel more like your housemates. You guys are among the best housemates!

Maryam, your gentle, motherly kindness was very comforting to me in difficult periods of my work.

Nick, the quality of your cynical humor is matched only by your wit and analytical prowess. I will surely miss working with you in my next job. Thanks so much for all your help with coding.

Jiyoung, your dedication is inspiring. I admire your single-minded pursuit of your goals and your passionate defense of your opinions. Thanks for commiserating, snacking and celebrating with me as the occasion required. ***Digital HUGS***

To Sidney, Olivia, Carolyn, and Emily: Friends are the family you get to choose. Thanks for being mine and supporting me through all this. May we have parties sillier

than the lumberjack party and more beautiful than the winter wonderland in our futures.

To Alice and Steve: You two have provided me with numerous meals, jokes and afternoons unwinding with the flowers. Thanks for sharing your cathedral and being part of my life.

To my Family: It has been loooooong journey to this PhD. I couldn't have done this without you. You are always there when I need you.

Attributions

This dissertation is the result of many collaborations:

Ch2:
Conceived and designed experiments: ZT and IVS; Data generation, analysis and presentation: XJ, AP, AS, ABH, MK, MVS, AK, BW, CO, DL, KE, KM, JMCT, JMCR, MAR, MRR, MU, NP, PA, PG, RK, RS, RMW, SL, SM, VLMD, YQ, ZT; Writing of the manuscript: XJ, ABH, AAJ, AP, AS, JMCR, KDV, KM, KP, MK, MAR, MMR, SL, IVS, and ZT; Provided resources and tools and critical reviewed manuscript: XC, YS

Ch 3:
GA made cytogenetic map
GA measured proportions of each chromosome
ANP and MS made figure for ovarian nurse cell
ANP and GA performed FISH experiments
ANP and GA identified missassembly via physical mapping
ANP compared physical map to previous genetic map
MVS, IVS conceived experiments
MVS, ANP, GA, and IVS wrote the manuscript

Ch 4:
GA and AN physically mapped *An. atroparvus*
GA and ANP physically mapped *An. albimanus*
XJ identified 1:1 orthologs, syntenic blocks /chromosomal breakpoints
XJ quantified rates of rearrangement in 5 *Anopheles* species
XJ scaffolded the genomes of *An. stephensi, An. dirus,* and *An. minimus*
ANP tested scaffolding predictions in *An. stephensi*
ANP quantified TEs, IRs and TRs in breakpoint regions and 100 KB windows of *An. gambiae, An. stephensi, An.dirus* and *An. minimus* (breaks and WG)
ANP performed statistical tests
JL ran repeat masker and provided ANP with output
NAK wrote a perl script to filter output of IRs and TRs and identify overlapping repeats
ZT provided *An. stephensi* repeat library
IVS conceived experiments
ANP, XJ and IVS wrote manuscript

TABLE OF CONTENTS

CHAPTER 1. LITERATURE REVIEW

CHAPTER 2. GENOME ANALYSIS OF A MAJOR URBAN MALARIA VECTOR MOSQUITO, *ANOPHELES STEPHENSI*

LIST OF FIGURES

Chapter 2

Chapter 3

Chapter 4

LIST OF TABLES

Chapter 2

Chapter 3

Chapter 4

Chapter 1: Literature Review

1.1 The Burden of Malaria

Malaria, a complex and devastating disease is vectored exclusively by *Anopheles* mosquitoes. Although much of the burden of malaria occurs in sub-Saharan Africa, other portions of the globe including India, Asia, Central and South America, and the Middle East are also at risk [1-3]. Although only about 10% of *Anopheles* mosquitoes contribute to malaria transmission, these insects have proven very efficient agents of human disease and put more than 3.2 billion people at risk for malaria [4]. International malaria control initiatives such as the Roll Back Malaria Initiative (RBM) and the Medicines for Malaria Venture (MMV) mobilize resources and spur research aimed at vector control as well as the treatment and eventual eradication of the disease. These efforts have managed to reduce incidence of malaria by an estimated 37% worldwide since 2000 [4]. However, despite the promising success of control efforts such as these, the World Health Organization reports a staggering 438,000 deaths from malaria in 2015[4]. The continuing high death toll of malaria as well as emerging insecticide and antimalarial drug resistance suggests that while encouraging, success in reducing malaria incidence may be tenuous.

A major component of current malaria reduction efforts relies on source reduction, or control of the mosquitoes that vector malaria to humans. Traditional strategies for vector control include habitat reduction, and vector population suppression. Removal of mosquito habitats can be very effective in locations where adequate infrastructure exists for sufficient removal of mosquito breeding sites. This technique successfully eradicated malaria from the United States in the 1950s; however, as the vast majority of malaria transmission occurs in developing countries this strategy is not feasible for global malaria eradication. For this reason, population reduction tactics reliant upon the use of insecticides are most often employed at the forefront of malaria control. Current applications of insecticides most often make use of pyrethroid treated bed nets or the spraying of homes with long lasting residual pesticides. Continued use of treated bed nets and indoor residual spraying (IRS) have encouraged the selection of insecticide resistance. Modes of insecticide resistance include increased detoxification capacity and decreased sensitivity within mosquitoes. Mechanisms for the gain of these traits include gene overexpression and amplification of P450s and esterases and gene mutations that alter the target site of the insecticide. Resistance to insecticides has spread rapidly since its emergence in 1950 and resistance is now widespread in populations of An. *gambiae* and *An. funestus* [5-8].

Vector control of *Anopheles,* is additionally complicated by morphologically indistinguishable members of species complexes with intricate differences in ecology and behavior. The vast diversity of malaria vectors confounds vector control measures because they target only some of the species responsible for continuing transmission. As an additional obstruction, mosquito genomes are highly plastic, as evident by the wealth of chromosomal inversions and whole arm translocations that have taken place in the evolution of this genus [9]**.** This propensity for genome rearrangement could confound ongoing vector control efforts by allowing mosquitoes to adapt to the pressures imposed by humans as we seek to eradicate them.

The ability of mosquitoes to adapt to and overcome current control measures highlights the need to establish a better understanding of how traits impacting the spread of malaria evolve. Traits that allow adaptation of mosquitoes to new habitats including those that bring them closer to human dwellings, as well as those that facilitate new behaviors including human blood choice or indoor resting could have a large impact on the vectorial capacity of mosquitoes. Knowledge of what genetic mechanisms influence these traits as well as the genetic determinants of susceptibility to malaria parasites and insecticide resistance are of profound interest to the future of malaria control.

In the genomics era, genetic modification offers novel approaches for vector control through population suppression, lifespan shortening and population replacement[10, 11]. A more complete understanding of the genomic composition and organization of vector species' genomes can identify new gene targets for genetic modification as well as elucidate how epidemiologically important traits have evolved over time. Population suppression via genetic means strives toward the same goal as traditional insecticide based methods however, the agent responsible for death of the insect is a heritable transgene or homing endonuclease that is spread by mating of genetically modified individuals with wild type members of the population. In its earliest form, genetic population suppression was accomplished by Sterile Insect Technique (SIT)[12, 13]. In the past, male insects were made sterile by irradiation which randomly induces mutations throughout their genomes. Irradiated males are then released to mate with wild females. Females who mate with sterile males produce no viable eggs and so population size is reduced in the next generation. The history of

SIT insect control begins with the control of the agricultural pest, the new world screw worm, *Cochliomyia hominivorax.* By continued release of irradiated, sterile-male flies this obligate endoparasite was eradicated from the southern United States and Mexico. Maintenance of this program, however, requires continual release of sterile insects at the periphery of the eradication zone- an undertaking that consumes considerable money and resources[14]. Lower mating competitiveness of irradiated sterile males also poses an additional complication to this approach. Recent advances in genome editing and adaptation of these techniques to mosquito systems offers numerous approaches for the genetic control of mosquitoes[15-18]. By employing Zinc Finger nucleases (ZFNs), TALENs, and CRISPRs, researchers can now precisely edit genomes and engineer transgenes with the goal of gender specific elimination of mosquitoes at particular life stages. These methods allow scientists to affect population suppression via Release of Insects carrying a Dominant Lethal (RIDL).

The precision with which researchers are now able to manipulate genomes provides them with many options in terms of *how* they might choose to exploit SIT and RIDL methods for the control of mosquito populations. For example, lethal transgenes could target males, females, or both sexes[19]. Lethal transgenes targeting both sexes could crash a population faster than methods targeting only females and they would be self-limiting-especially if the transgene-carrying insects died before they reached reproductive age. Female killing has intuitive advantages because the disease causing culprits are removed from the population, but male carriers continue dissemination of the transgene in the population. Agent based modelling of 4 transgene RIDL scenarios suggests that a transgene lethal in the late larval stages of both sexes provides the most efficient strategy for population suppression. This scenario models best ostensibly because transgenes lethal in late stages of larval development can exploit density dependent larval mortality. Modeling favors bisex lethal transgenes over female killing because males, which can propagate the transgene in the population can also harbor the wild type alleles. A greater number of transgenic insects must be released to overcome the reservoir or wild type alleles[20].

Another approach to vector control currently being tested makes use of host manipulation resulting from infection with *Wolbachia*, a large and pervasive genus of bacteria that naturally infects as many as 60% of all arthropod species. Infection with *Wolbachia* results in very interesting manipulation of the hosts. In species naturally infected with *Wolbachia,* various outcomes including skewing of sex ratios, male killing, increased fecundity, lifespan shortening and refractoriness to parasites have been reported[21-25]. Release of *Wolbachia*-infected insects made refractory to disease pathogens or with shortened lifespans that prevent pathogen transmission could provide a means of replacing vector populations with insects that pose no threat of spreading human disease. Population suppression is also possible by exploiting *Wolbachia's* natural means of self-propagation [10]. The bacteria is maternally inherited and copulations between infected males with uninfected females results in cytoplasmic incompatibility with no viable offspring. Similarly, infected females inseminated by a male infected with a different strain of *Wolbachia* also fail to produce live offspring. Cytoplasmic incompatibility provides an avenue for the reduction of vector species populations and because methods that exploit *Wolbachia* require no direct modification of a vectors' genome, this method is sometimes viewed as a less invasive alternative to RIDL methods that make use of genetically modified insects. *Wolbachia* is known to naturally infect disease vector species including *Aedes albopictus*, the primary vector of chikungunya, and *Culex pipiens*, a vector of West Nile virus. A strain of the bacteria originating in *Drosophila*, wMelpop has also been introduced to *Aedes aegypti,* and 2 natural populations stably inheriting the bacteria now exist in Australia[26, 27]. Efforts to infect A*nopheles stephensi,* successfully incorporated an *Ae. albopictus Wolbachia*, wAlbB into a lab colony[28]. Although *Wolbachia* could offer a very promising and novel method for control of vector borne disease, the inevitable evolution of *Wolbachia* raises concerns of unintended consequences resulting from this method's use. A 2015 study by Martinez and colleagues correlated strong antiviral effects with reductions in other life history traits including fecundity and lifespan[24]. The potential for natural selection to select against antiviral activity in favor of reducing the negative impacts of infection on lifespan and fecundity equates to a potential for loss of efficacy of vector borne disease programs based on the bacteria[24].

Among the most amazing and potentially useful manipulations imposed by *Wolbachia* on its hosts is the protection from pathogen infection the bacteria can provide. In different hosts infection with *Wolbachia* has been shown to inhibit dengue virus, chikungunya, filarial worms, yellow fever virus, West Nile virus and *Plasmodium falciparum* [29]. In other scenarios however, *Wolbachia* infection can increase susceptibility of the insect to pathogen infection. *Wolbachia* infection in *Culex* *tarsalis* increases susceptibility of the mosquito to West Nile virus [30]. Although *Plasmodium falciparum* was inhibited in wAlbB infected *An. stephensi*, susceptibility to murine malaria, *P. berghei,* was increased in *An. gambiae* infected with wAlbB[31]. This result piques the possibility that human malaria parasites more closely related to *P. berghei* such as *P. ovale, P. knowleski, P. malariae* and *P. vivax* might also flourish in mosquitoes infected with wAlbB[31]. The effects of *Wolbachia* infection on these other human malaria parasites has not yet been tested, but in locations where more than one human malaria parasites coexist, malaria control efforts utilizing *Wolbachia* could inadvertently amplify one strain of malaria while limiting another. How *Wolbachia* manipulates its insect hosts remains unclear but studies associating gene expression and epigenetic changes with *Wolbachia* infection could perhaps shed some light on the interaction of the bacteria within its hosts. The availability and assembly of insect genomes will facilitate further exploration of this topic and other emerging technologies for mosquito control.

1.2 Genome mapping

The low cost of genome sequencing and concerted sequencing efforts such as the 12 Drosophila Genomes and the 16 Anopheles Genomes Projects have produced a surfeit of genome data that provides an essential platform from which comparative genomics studies become possible [9, 32]. However, draft genome assemblies are often published in databases as a collection of sequences that have been assembled to the contig or supercontig level. At this level of assembly how supercontigs fit together into chromosomes is unknown and inferences about genome landscape, population genetics, and chromosomal evolution are limited.

The assembly of sequence supercontigs into chromosomes can be achieved by considering the linkage of genetic markers (known as genetic or linkage mapping) through inheritance, or by physically mapping sequence information to chromosomal locations through the use of fluorescently labeled probes[33]. In species where a reliable source of distinct chromosomes is not available, genetic linkage mapping is used and this technique employs recombination rates to assign genetic markers to linkage groups. Linkage groups often correspond 1:1 with chromosomes and so can be analyzed in the same way as chromosomes. Historically, researchers were limited to tracking the inheritance of gene variants with measurable differences in phenotype however, this greatly limited the number of markers that were available for study. Later developments in the techniques of molecular genetics expanded the list of markers to include other markers including variable number tandem repeats (VNTRs), restriction fragment length polymorphisms (RFLPs) and single nucleotide polymorphisms (SNPs) which all have heritable polymorphisms[34, 35].

Despite the lack of easily distinguishable chromosomes, genetic linkage studies have been utilized to explore chromosomal evolution in the gene order of Lepidoptera, revealing synteny between *Haliconius melpomene* and *Bombyx mori* as well as evidence for chromosomal fusions during the evolution of this species[36]. Genetic mapping based on RFLP and microsatellite polymorphism in mosquitoes of the *Culex pipiens* complex was able to assemble 10.4% of the genome into the three linkage groups[37]. Despite the low genomic coverage of this map, the genetic markers developed in this study will be useful for population comparisons with other *Culex* species. Even greater advances were possible in *A. aegypti* where genetic mapping assigned 58% of the genome to chromosomes and corrected misassembly within the genome[38].

One advantage of genetic mapping is the ability to associate genomic loci with phenotypic variation. In *Anopheles arabiensis,* for example, quantitative trait loci (QTLs) were identified to help explain the mechanisms of resistance to pyrethroid insecticides in regions of Africa[39]. Genetic mapping has also identified genomic regions in *Aedes aegypti* that influence the interaction between host and pathogen genotype and explain variation in vectorial capacity[40].

In species that possess easily obtainable sources of visually distinct chromosomes, physically mapping genomic supercontigs to chromosomes is a good method for assembling a genome to the chromosomal level. High quality polytene chromosomes such as are produced by numerous rounds of endoreplication in the salivary glands and ovaries of Diptera including *Drosophila* and *Anopheles* render physical mapping convenient in these species. The genome sequence of *Drosophila melanogaster* was published in 2000. Later efforts in the *Drosophila* community produced 11 additional genome sequences for *Drosophila* species. Physical mapping of supercontigs to chromosomes isolated from salivary glands of these 12 species provided the basis for a large scale comparison of orthologous gene positions. Examination of gene order in these 12 species revealed that gene membership is largely conserved between homologous arms within *Drosophila* despite numerous chromosomal fusions and fissions that have taken place during the evolution of *Drosophila* [41, 42]. The identification of fixed inversion breakpoints, and estimates for rates of chromosomal evolution also became possible within this comparative genomics context.

In the major African malaria vector *An. gambiae,* nearly 2000 bacterial artificial chromosome BAC clones were physically mapped to chromosomes in the initial publication of the genome [43]. It is now known that the *An. gambiae* Pink Eye STandard (PEST) strain mosquitos that the genome sequence is based on were hybrids of two incipient species*: An. coluzzi* and *An. gambiae*. This mixed genetic background resulted in a mosaic genome of inflated size due to the presence of multiple haplotype supercontigs. Pericentromeric regions were poorly assembled in the initial publication, but later efforts aimed at improving the assembly placed an additional 5.34 MB to regions near the centromeres and also filled gaps between supercontigs. This work also removed supercontigs suspected of originating from bacterial contamination and identified sequences belonging to alternative haplotypes and the ever elusive mosquito Y chromosome [44].

The efforts of the *An. gambiae* genome project yielded a high quality genome assembly and a valuable platform for comparative genomics. Interspecies cross hybridization studies have established arm homology between *An. gambiae* and many *Anopheles* species [45-49]. Finer scale cross hybridization studies examining gene shuffling and chromosomal inversions demonstrated that different chromosomal arms exhibit varying tolerance to gene disruption, and that chromosomal inversions tend to capture similar sets of genes in species facing similar environmental pressure [49, 50]. The recent publication of 16 additional *Anopheles* genomes and the subsequent generation of low coverage physical maps for 5 species spanning 100 million years of evolutionary history allowed study of chromosomal evolution on a scale not previously obtainable in mosquitoes. This study revealed higher rates of evolution on the sex chromosomes relative to the autosomes and confirmed that like *Drosophila,* gene membership is largely conserved on homologous chromosomal arms. Unlike *Drosophila* however, chromosomal arms in *Anopheles* shuffle via whole arm translocation but do not exhibit fissions and fusions *[9]*.

Physical mapping in disease vectors belonging to *Aedes* and *Culex* is complicated by poor sequence assembly quality and a lack of high quality polytene chromosomes. However, recent developments easing the procurement and recognition of mitotic chromosomes is overcoming these obstacles [51, 52]. By employment of a two-step mapping approach, where a landmark probe is used to aid in the identification of mitotic chromosomes, localization of 45% of the *Aedes aegypti* genome and 13% of the *Culex quinquefasciatus* genome to chromosomes became possible. These advances improved not only the genome assemblies but also updated the nomenclature and integrated the physical and genetic maps for these vector species. Clustering of the QTLs in the genome of *A. aegypti* suggests that traits related to vectorial capacity and vector competence might be controlled by fewer genomic loci than previously expected [51]. Chromosome based examination of genomic features including transposable elements (TEs), satellites and genes also resulted from the physical mapping of *A. aegypti* and will eventually become possible in *C. quinquefasciatus* as the chromosomal assembly improves [52].

In insects such as mosquitoes, where selective breeding is easy and fast generation times are common- genetic mapping is possible as long as sufficient polymorphic markers exist within the population. The feasibility is limited, however, if few polymorphic markers have been identified or if the population is genetically very homogeneous. In *An. albimanus* for example, 50 microsatellite markers were sufficient to create a well-supported linkage map for chromosome 2, but very few markers segregated on chromosome 3 or the sex chromosome [53]. In *A. aegypti*, low rates of recombination across all chromosomes prevented the assignment of order and orientation to genetic markers that occupied the same mitotic band[38]. The resolution of genetic maps is further limited in areas of lower recombination. Centromeric regions have been shown to display recombination suppression spanning 20% of the chromosome in *D. melanogaster*, 40% in *An. gambiae* and 47% in *A. aegypti [38]*. Physical maps offer improved resolution compared to genetic maps but without the guidance of a genome sequence, markers can redundantly cover the same chromosomal regions and fail to provide homogenous coverage along the chromosome. The availability of genome sequences however enables the researcher to select probes with prior knowledge of which supercontigs they belong to and prevent uneven coverage.

The integration of physical and genetic maps provides an opportunity to associate chromosomal loci with phenotypic traits while also allowing the precise ordering and orientation of supercontigs along the chromosome. The improved resolution of an integrated map or iMap, will ease studies aimed at exploring how the genome landscape varies along chromosomes. Additionally, the publication of genome sequences for more species will facilitate efficient physical mapping and in turn, syntenic relationships and evolution of mosquito species can be explored in greater breadth.

1.3 Molecular characterization of insect genomes and genome landscape

Somewhat paradoxically, only a small proportion of mosquito species bear the blame for the global malaria crisis. As demonstrated by the *Anopheles gambiae* complex, vectorial capacity can vary considerably even in related species coexisting in the same locality[54]. This variation begs the question of what processes are shaping some mosquitoes into prolific disease spreaders while others are of no consequence to human health? Cytology and comparisons of gene order in several *Anopheles* species has revealed that chromosomal inversions and whole arm translocations have shuffled mosquito genomes over hundreds of millions of years, distinguishing species and providing variation within species[55].

Before genome sequencing, mosquito chromosomal inversions were detected by studying banding patterns of polytene chromosomes. Using this technique, pioneer, Mario Coluzzi was able to differentiate morphologically indistinguishable species within the *Anopheles* gambiae complex based on fixed chromosomal inversions (COLUZZI 1966). Additional study by Coluzzi and others detected extensive polymorphic inversions in interbreeding populations of the same species with alternative inversion arrangements conferring different behaviors and ecology[56-58]. Further study has catalogued numerous polymorphic inversions associated with adaptation to drier climates, changes in resting behavior and resistance to insecticides[59]. Interestingly, it has been noted that inversions occur with different frequency on different chromosomal arms [60, 61]. For example, chromosome 2R hosts a disproportionate amount of polymorphic inversions relative to all other chromosomal arms. Alternatively, the sex chromosome appears entirely devoid of polymorphic inversions but has accumulated far more fixed inversions than the autosomes[9, 60, 61]. These data suggest that different parts of the genome are more tolerant of rearrangement than others and contribute differently to the evolution and adaptation of species.

Several explanations have been proposed to explain chromosomal arm specific differences in rates evolution. The observation of breakpoint reuse in mammals and insects supplanted hypothesis of random inversions and encouraged hypothesis of some non-random “fragile regions” within the genome that are more susceptible to breakage[62-65]. A definitive reason for fragility of particular regions is still up for debate. Other ideas suggest that chromosomal breakage is limited by how tolerant a particular group of genes is to disruption. These two ideas were tested in *Drosophila* and the authors found that both mechanisms have likely been at work in this lineage[66]. Later work, however, engineered a chromosomal inversion in a very well conserved syntenic region that was thought to be preserved by “functional contraints”. They were unable to determine any reduction in fitness to the organism[67].

The development of molecular cloning, DNA sequencing, and algorithms for the detection of repeats has provided a means of exploring the content of specific inversion breakpoint regions of both fixed and polymorphic inversions. A study of the fixed $2R^{+o}$ inversion in the *An. gambiae* complex uncovered degraded remains of transposable elements (TEs)[68]. Polymorphic inversion 2Rj was flanked by two segmental duplications (SDs) [69]. Other studies in mosquito, fruitfly, yeast and human have uncovered various repeats including TEs, SDs, inverted repeats (IRs) and tandem repeats (TRs) in the vicinity of chromosomal inversions[70-76]. The proximity of these repeats to breakpoints hints at a possible role played by repeats in the formation of chromosomal inversions. Despite some evidence for the occurrence of repetitive elements in inversion breakpoints of Diptera, other studies have also failed to detect repeats in inversion breakpoints[77, 78]. One particularly large study undertaken by Ranz and colleagues found that more than half of the 29 breakpoints they considered lacked repetitive elements. In fact, they only found repeats in 2/29 breaks [79]. This evidence, and lack thereof, highlights the ongoing debate about the molecular context of inversion genesis in Diptera.

The inclination for mosquito genomes to change imparts tremendous adaptive potential and spells disastrous consequences for humankind as we seek to eradicate mosquito-borne disease. Unraveling the role of repeats in inversion genesis will assist humans in disarming our winged foe. At present we are facing a dearth of clear evidence elucidating the causative mechanisms for chromosomal inversion in Diptera; however the availability of many new genome sequences and assembled genomes provides exciting opportunities for testing of these hypotheses in *Anopheles.*

Chapter 2: Genome analysis of a major urban malaria vector mosquito, *Anopheles stephensi*

Xiaofang Jiang[1,2]*, Ashley Peery[3]*, A. Brantley Hall[1,2], Atashi Sharma[3], Xiao-Guang Chen[4], Aleksey Komissarov[5], Michelle M. Riehle[6], Yogesh Shouche[7], Maria V. Sharakhova[3], Dan Lawson[8], Robert M. Waterhouse[9,10,11,12], Nazzy Pakpour[13], Peter Arensburger[14], Victoria L. M. Davidson[15], Karin Eiglmeier[16], Scott Emrich[17], Phillip George[3], Ryan Kennedy[18], Chioma Oringanje[19], Yumin Qi[2], Robert Settlage[20], Marta Tojo[21], Jose M. C. Tubio[22], Maria Unger[23], Bo Wang[13], Kenneth D. Vernick[16], Jose M. C. Ribeiro[25], Anthony A. James[24], Kristin Michel[15], Michael A. Riehle[19], Shirley Luckhart[13], Igor V. Sharakhov[1,3§], Zhijian Tu[1,2§]

[1]Program of Genetics, Bioinformatics, and Computational Biology, Virginia Tech, Blacksburg, VA, USA
[2]Department of Biochemistry, Virginia Tech, Blacksburg, VA, USA
[3]Department of Entomology, Virginia Tech, Blacksburg, VA, USA
[4]Department of Pathogen Biology, Southern Medical University, Guangzhou, Guangdong, China
[5]Theodosius Dobzhansky Center for Genome Bioinformatics, St. Petersburg State University, and Institute of Cytology Russian Academy of Sciences, St. Petersburg, Russia
[6]Department of Microbiology, University of Minnesota, Minneapolis, MN, USA
[7]National Center for Cell Science, Pune University Campus, Ganeshkhind, Pune, India
[8]European Molecular Biology Laboratory, European Bioinformatics Institute, Wellcome Trust Genome Campus, Hinxton, Cambridge CB10 1SD, United Kingdom
[9]Department of Genetic Medicine and Development, University of Geneva Medical School, rue Michel-Servet 1, 1211 Geneva, Switzerland
[10]Swiss Institute of Bioinformatics, rue Michel-Servet 1, 1211 Geneva, Switzerland
[11]Computer Science and Artificial Intelligence Laboratory, Massachusetts Institute of Technology, 32 Vassar Street, Cambridge, MA, USA
[12]The Broad Institute of MIT and Harvard, 7 Cambridge Center, Cambridge, MA, USA
[13]Department of Medical Microbiology and Immunology, University of California, Davis, CA, USA
[14]Biological Sciences Department, California State Polytechnic University Pomona, CA, USA
[15]Division of Biology, Kansas State University, Manhattan, KS, USA
[16]Department of Parasitology and Mycology, Unit of Insect Vector Genetics and Genomics, Institut Pasteur, Paris, France and CNRS Unit of Hosts, Vectors and Pathogens (URA3012), Paris, France.
[17]Department of Computer Science and Engineering, University of Notre Dame, Notre Dame, IN, USA
[18]Department of Bioengineering and Therapeutic Sciences, University of California, San Francisco, California, USA
[19]Department of Entomology, University of Arizona, Tucson, AZ, USA
[20]Virginia Bioinformatics Institute, Virginia Tech, Blacksburg, VA, USA

[21]Department of Physiology, School of medicine – CIMUS, Instituto de Investigaciones Sanitarias, University of Santiago de Compostela, Spain
[22]Wellcome Trust Sanger Institute, Hinxton, Cambridgeshire, UK.
[23]Department of Biological Sciences, University of Notre Dame, Notre Dame, IN, USA
[24]Departments of Microbiology & Molecular Genetics and Molecular Biology & Biochemistry , University of California, Irvine CA, USA
[25]Section of Vector Biology, Laboratory of Malaria and Vector Research, National Institute of Allergy and Infectious Diseases, Rockville, MD, USA

* Equal contribution, listed by alphabetical order
§ Corresponding authors

Email addresses:
ZT: jaketu@vt.edu
IVS: igor@vt.edu

Email addresses of other authors are provided during online submission.

2.1 Abstract

Background

Anopheles stephensi is the key vector of malaria throughout the Indian subcontinent and Middle East and an emerging model for molecular and genetic studies of mosquito-parasite interactions. The “type” form of the species is responsible for the majority of urban malaria transmission across its range.

Results

Here we report the genome sequence and annotation of the Indian strain of the “type” form of *An. stephensi*. The 221 Mb genome assembly represents >92% of the entire genome and was produced using a combination of 454, Illumina, and PacBio sequencing. Physical mapping assigned 62% of the genome onto chromosomes, enabling chromosome-based analysis. Comparisons between *An. stephensi* and *An. gambiae* revealed a high rate of gene order reshuffling on the X chromosome, exceeding not only the rate on the autosomes but also the rate on the *Drosophila* X chromosome. *Anopheles stephensi* has more heterochromatin in pericentric regions but less repetitive DNA in chromosome arms than *An. gambiae*. We also identified a number of Y-chromosome contigs and BACs. Interspersed repeats constitute 7.1% of the assembled genome while LTR retrotransposons alone comprise >49% of the Y contigs. RNA-seq analyses provide new insights into mosquito innate immunity, development, and sexual dimorphism.

Conclusions

The genome analysis described in this manuscript provides a resource and platform for fundamental and translational research into a major urban malaria vector. Chromosome-bases investigations provide unique perspectives on *Anopheles* chromosome evolution. RNA-seq analysis and studies of immunity genes offer new insights into mosquito biology and mosquito-parasite interactions.

2.2 Background

Mosquitoes in the genus *Anopheles* are the primary vectors of human malaria parasites and the resulting disease is one of the most deadly and costly in history[80, 81]. Publication and availability of genome sequences accelerates research that not only enhances our basic understanding of vector biology and vector-parasite interactions, but also contributes to new strategies for combating malaria[43]. Recent application of next-generation sequencing technologies to mosquito genomics offers exciting opportunities to expand our understanding of mosquito biology in many important vector species and harness the power of comparative genomics. Such information will further facilitate the development of new strategies to combat malaria and other mosquito-borne diseases. *Anopheles stephensi* is among the ~60 species considered important in malaria transmission and is the key vector of urban malaria on the Indian subcontinent and the Middle East[82, 83]. Of the three forms: type, mysorensis, and intermediate, the former is responsible for the majority, if not all, of urban malaria transmission across its range and accounts for approximately 12% of all transmission in India[84]. Thus efforts to control it can be expected to contribute significantly to the malaria eradication agenda[85, 86]. *Anopheles stephensi* is amenable to genetic manipulations such as transposon-based germline transformation[87], genome-wide mutagenesis[88], site-specific integration[89], genome-editing[90] and RNAi-based functional genomics analysis[91]. Our understanding of the interactions between *An. stephensi* and the malaria parasites is rapidly improving[28, 92-96]. Thus *An. stephensi* is emerging as a model species for genetic and molecular studies. We report here the genome sequence of the Indian strain of the “type” form of *An. stephensi* as a resource and platform for fundamental and translational research. We also provide unique perspectives on *Anopheles* chromosome evolution and offer new insights into mosquito biology and mosquito-parasite interactions.

2.3 Results and discussion

2.3.1 Draft genome sequence of An. stephensi: Assembly and verification

The *An. stephensi* genome was sequenced using 454 GS FLX, Illumina HiSeq, and PacBio RS technologies (Additional file 1: Table S1). The 454 reads comprised 19.4x coverage: 12.2x from single-end reads, 2.2x from 3 kilobase (kb) paired-end reads, 3.4x from 8 kb paired-end reads, and 1.7x from 20 kb paired-end reads. The majority of 454 reads ranged from 194 to 395 base-pairs (bp) in length. A single lane of Illumina sequencing of male genomic DNA resulted in 86.4x coverage of 101 bp paired-end reads with an average insert size of ~200 bp. Ten cells of PacBio RS sequencing of male genomic DNA produced 5.2x coverage with a median length of 1,295 bp. A hybrid assembly combining 454 and Illumina data produced a better overall result than using 454 data alone (Materials and methods). The resulting assembly was further improved by filling gaps with error-corrected PacBio reads and scaffolding with BAC-ends. The current assembly, verified using various methods as described in Materials and methods, contains 23,371 scaffolds spanning 221 Mb that includes 11.8 Mb of gaps (Table 2.12.2.12.1). The N50 scaffold size is 1.59 Mb and the longest scaffold is 5.9 Mb. The number of scaffolds is inflated because we choose to set the minimum scaffold length to 500 bp to include repeat-rich short scaffolds. The assembled size of 221 Mb is consistent with the previous estimate of the *An. stephensi* genome size of ~235 Mb[97].

2.3.2 Physical mapping

Mapping of 227 probes was sufficient to position 86 scaffolds on the *An. stephensi* polytene chromosomes (Figure 2.11.1; Table 2.12.2; Additional file 2). These 86 scaffolds comprise 137.14 Mb or 62% of the assembled genome. Our physical map includes 28 of the 30 largest scaffolds and we were able to assign orientation to 32 of the 86 scaffolds. We expect that relatively little of the heterochromatin was captured in our chromosomal assembly based on the morphology of the chromosomes in regions to which the scaffolds mapped. For this reason, subsequent comparisons with *An. gambiae* on molecular features of the genome landscape exclude regions of known heterochromatin from the *An. gambiae* dataset. *Anopheles stephensi* and *An. gambiae* have different chromosome arm associations with 2L of *An. gambiae* homologous to 3L of *An. stephensi[49]*. Therefore, all ensuing discussion of synteny between the two species refers to *An. stephensi* chromosome arms listed in homologous order to those of *An. gambiae*: X, 2R, 3L, 3R, and 2L. While draft genomes also are available for *An. darlingi* and *An. sinensis*[98, 99], we focused our comparative analysis on *An. stephensi* and *An. gambiae*, the only two species that have chromosome-based assembly.

2.3.3 Gene annotation

A total of 11,789 protein-encoding genes were annotated in the *An. stephensi* genome using a combination of homology and *de novo* prediction. These gene models have been submitted to NCBI (GCA_000300775.2) and are hosted at VectorBase (https://www.vectorbase.org/Anopheles_stephensiI/Info/Index). The average transcript length was 3,666 bp and the average number of exons per transcript was 4.18. A total 10,492 (89.0%) of the 11,789 predicted *An. stephensi* protein-encoding genes had orthologs in *An. gambiae*, *Aedes aegypti* and *Drosophila melanogaster* (Figure 2).

2.3.4 Global Transcriptome Analysis

Eleven RNA-seq samples were prepared from 0-1, 2-4, 4-8, and 8-12 hour post-egg deposition embryos, larvae, pupae, adult males, adult females, non-blood-fed ovaries, blood-fed ovaries, and 24 hours post-blood-fed female carcass without ovaries[100]. The corresponding genes were clustered into 20 distinct groups ranging in size from 8 to 2,106 genes per group on the basis of similar expression patterns (Figure 2.11.3). Many of the clusters correspond to either a specific developmental stage or sex (Additional files 3 and 4). A search for over-represented gene ontology (GO) terms in the 20 clusters found that many of the co-regulated genes have similar inferred functions or roles. Adult females require a protein-rich blood-meal for oogenesis and thus are the most interesting sex from a health perspective. Genes in clusters 1, 10, and 17 are induced after blood-feeding in the female soma. These clusters are enriched for genes encoding proteins with proteolytic activity, including serine peptidases, involved in blood-meal digestion. Mosquitoes have undergone lineage-specific amplification of serine peptidases when compared to *Drosophila*, many of which are found in the three clusters described above. Cluster 9 contains 258 genes that showed peak expression in the pupa and it is enriched for genes whose products are involved in exoskeleton development. GO analyses of other clusters are described in the supplementary text.

We also identified 241 and 313 genes with female- or male-biased expression, respectively (Additional file 5). The male-biased genes were enriched for those whose products are involved in spermatogenesis and the detection of sound. Male mosquitoes detect potential mates using their Johnston's organ, which has twice the number of sensory neurons as that of the females [101, 102]. The female-biased genes were enriched for those whose products are involved in proteolysis and other metabolic processes likely relevant to blood digestion.

2.3.5 Immunity genes

Manual annotation was performed on genes involved in innate immunity including those that encode the LRR immune (LRIM) and the *Anopheles Plasmodium*-responsive leucine-rich repeat 1 (APL1) proteins, and the genes of the Toll, immune deficiency (IMD), insulin/insulin-like growth factor signaling (IIS), mitogen-activated protein kinase (MAPK) and TGF-β signaling pathways. A number of studies have demonstrated the importance of these genes or pathways in mosquito defense against parasites or viruses[92-96, 103-105]. Manual analysis showed overall agreement with the automated annotation and improved the gene models in some cases (Additional files 6 and 7). A high level of orthology is generally observed between *An. stephensi* and *An. gambiae* and we highlight here a few potentially interesting exceptions. *Anopheles stephensi* may have only one APL1 gene (ASTEI002571) instead of the three APL1 gene cluster found in *An. gambiae* (Additional file 1: Figure S1). We also observed the apparent lack of TOLL1B and 5B sequences in *An. stephensi*, which in *An. gambiae* are recent duplications of TOLL1A, 5A, respectively. Whether these differences between the two species are true or simply artifacts resulting from mis-assembly requires further experimental validation[106].

Expression profiles of all immunity genes were analyzed using the 11 RNA-seq samples to provide insights into their biological functions (Additional file 8). For example, FKBP12, a protein known to regulate both transforming growth factor

(TGF)-β and target of rapamycin (TOR) signaling, showed abundant transcript levels across immature stages and adult tissues (Additional file 1: Figure S2). The high expression levels of AsteFKBP12 in all examined stages and tissues were remarkable and unexpected. Examination of existing publicly-available microarray data confirmed these expression levels and patterns[107]. FKBP12 in mammals forms a complex with rapamycin and FKBP-rapamycin-associated protein (FRAP) to inhibit TOR[108]. Given that TOR signaling is fundamental to many biological functions in mammals[109] and cumulative data support the same for *D. melanogaster*[110], a high level of FBKP12 expression may be critical for tight regulation of TOR activity in *An. stephensi* and perhaps *An. gambiae*[111]. Expression patterns of the *An. gambiae* FKBP12 ortholog (AGAP012184) from microarray datasets (http://funcgen.vectorbase.org/expression-browser/gene/AGAP012184) support the hypothesis that this protein is involved in a broad array of anopheline physiologies, including development, bloodfeeding, molecular form-specific insecticide resistance, circadian rhythm, desiccation resistance, mating status, and possibly also broad regulation of infection based on studies with murine (*Plasmodium berghei*) and human (*Plasmodium falciparum*) malaria parasites. Whether these same physiologies and others are regulated by FKBP12 in *An. stephensi* will require experimental confirmation. Given that signaling pathways regulating embryonic pattern formation in *Drosophila* (e.g., the Toll pathway[112]) have been co-opted in the adult fly for regulation of various physiologies including metabolism and immune defense, the data presented here support the hypothesis that pathways integral to adult biology in adult anophelines also have been similarly co-opted from important developmental roles.

2.3.6 Salivary genes

Saliva of blood feeding arthropods contains a cocktail of pharmacologically active components that disarm their host's blood clotting and platelet aggregation, induce vasodilation and affect inflammation and immunity. These salivary proteins are under accelerated evolution most likely due to their host's immune pressure. A previous salivary gland transcriptome study identified 37 salivary proteins in *An. stephensi*, most of which are shared with *An. gambiae*, including mosquito and *Anopheles*-specific protein families[113]. The current assembly of the *An. stephensi* genome allowed for insights into the genomic organization of salivary gland genes, many of which occur as tandem repeated gene families that arose by gene duplication events. Tandem repeated gene families often are poorly annotated by automated approaches, therefore, manual annotation was necessary to improve the salivary gland gene models (Additional files 9 and 10). In particular, *An. gambiae* has 8 genes of the D7 family, which has modified odorant binding domains (OBD) that strongly bind agonists of platelet aggregation and vasoconstriction (histamine, serotonin, epinephrine and norepinephrine)[114].Three of these genes have two OBD’s while the remaining five only have one domain each. As in *An. gambiae*, the short forms are oriented in tandem and in the opposite orientation of the long form genes. However, *An. stephensi* has apparently collapsed the second long form to create a sixth short form.

2.3.7 Repeat content

Transposable elements (TEs) and other unclassified interspersed repeats constitute 7.1% of the assembled *An. stephensi* genome (Table 2.12.3; Additional file 11). TE occupancy of the euchromatic genome in *D. melanogaster* and *An. gambiae* is 2% and 16%, respectively[43]. Thus variations in the size of the genomes correlate with different amounts of repetitive DNA in these three species. More than 200 TEs have been annotated. DNA transposons and miniature inverted-repeat TEs (MITEs) comprise 0.44% of the genome. Non-LTR retrotransposons (or LINEs) comprise 2.36% of the genome. Short intersperse nuclear elements (SINEs), although less than 300 bp in length, are highly repetitive and comprise 1.7% of the genome. There is considerable diversity among the LTR-retrotransposons although they occupy only 0.7% of the genome. Approximately 2% of the genome consists of interspersed repeats that remain to be classified.

2.3.8 Genome landscape: a chromosomal arm perspective

The density of genes, TEs, and short tandem repeats (STRs) for each chromosome were determined based on the physical map (Figure 2.11.4). The average numbers of genes for each chromosome arm are consistent with those in *An. gambiae*. The X had the lowest number of genes per 100 kb, and the highest densities of genes per 100 kb were seen on 2R and 3L (Figure 2.11.5; Additional file 1: Tables S2 and S3). Chromosomes 2R and 3L also contain the greatest numbers of polymorphic inversions[115]. Genes functioning as drivers of adaptation could be expected to occur in greater densities on chromosome arms with higher numbers of polymorphic inversions[116].

Anopheles stephensi has a lower density of transposable elements across all chromosome arms than *An. gambiae* (Figure 2.11.5; Additional file 1: Tables S2 and S3; Additional file 12). The density of transposable elements on the *An. stephensi* X is more than twice that of the autosomes. A comparison of the *An. stephensi* simple repeat densities with those in *An. gambiae* euchromatin showed that densities in the latter were ~2-2.5x higher (Figure 2.11.5; Additional file 1: Tables S2 and S3). The greatest densities of simple repeats were found on the X chromosome and this is consistent with a previous study in *An. gambiae*[50]. Although *An. stephensi* shows lower densities of simple repeats across all arms compared to *An. gambiae*, its X appears to harbor an overrepresentation of simple repeats compared to its autosomes. Scaffold/Matrix-associated regions (S/MARs) can potentially affect chromosome mobility in the cell nucleus and rearrangements during evolution[117, 118] and these were found to be enriched in the 2L and 3R arms (Figure 2.11.5; Additional file 1: Tables S2 and S3).

2.3.9 Molecular organization of pericentric heterochromatin

We observed clear differences in heterochromatin staining patterns when comparing mitotic chromosome squashes prepared from imaginal discs of *An. gambiae* and *An. stephensi*. *An. stephensi* appears to have more pericentric heterochromatin than *An. gambiae* (Additional file 1: Figure S3). This is particularly evident in sex chromosomes. Mitotic X chromosomes in *An. stephensi* possess much more pericentric heterochromatin compared with X chromosomes from several different strains of *An. gambiae*. Finally, the Y chromosome in *An. stephensi* has a large block of heterochromatin. We further investigated whether particular tandem repeats are concentrated in heterochromatin. Aste72A and Aste190A, the two repeats with highest coverage in raw genomic data reads, were selected as probes for FISH analysis (Additional file 13). Aste72A, which comprises approximately 1% of the raw genomic reads, was mapped to the pericentric heterochromatin of X and Y chromosomes (Figure 2.11.6). Aste190A, which comprises approximately 2% of the raw genomic reads, was mapped to centromere of both autosomes (Additional file 1: Figure S4). The Aste72A tandem repeat has a 26.7% mean GC-content and contributes significantly to the AT-rich peak in the plot of GC distribution of raw genomic reads (Additional file 1: Figure S5).

2.3.10 Y chromosome

Anopheles mosquitoes have heteromorphic sex-chromosomes where males are heterogametic sex (XY) and females homogametic (XX)[119]. The high repetitive DNA content of Y chromosomes makes them difficult to assemble and they often are ignored in genome projects. An approach called the chromosome quotient[120] was used to identify 57 putative Y sequences spanning 50,375 bp (Additional files 14 and 15). All of these sequences are less than 4,000 bp in length and appear to be highly repetitive. Five BACs that appeared to be Y-linked based on the CQs of their end sequences were analyzed by sequencing and their raw PacBio reads were assembled with the HGAP assembler[121]. Eleven contigs spanning 196,498 bp of predicted Y-linked sequences were obtained (Additional files 16 and 17). The 57 Y-linked sequences and 11 contigs from the Y-linked BACs represent currently the most abundant set of Y sequences in any *Anopheles* species. RepeatMasker analysis using the annotated *An. stephensi* interspersed repeats showed that the *An. stephensi* Y sequences comprise ~65% interspersed repeats. LTR retrotansposons alone occupy ~49% of the annotated Y (Additional files 18 and 19).

2.3.11 Synteny and gene order evolution

We used the chromosomal location and orientation of 6,448 1:1 orthologs from *An. gambiae* and *An. stephensi* to examine synteny and estimate the number of chromosomal inversions between these two species (Figure 2.11.7; Additional file 20). Syntenic blocks were defined as those in which all genes within the block had the same order and orientation with respect to one another in both genomes. The X chromosome has markedly more inversions than the autosomes. The number of chromosomal inversions that might have happened since *An. stephensi* and *An.*

gambiae last shared a common ancestor were determined with GRIMM[122] and SPRING[123]. We calculated the density of inversions per chromosome arm ignoring breakpoint reuse and assuming two breakpoints per inversion (Additional file 1: Tables S4 and S5). The length of *An. gambiae* euchromatin was used as a proxy for the size of the *An. stephensi* chromosomes[124]. The density of inversions per megabase on the X chromosome supports the conclusion that it is much more prone to rearrangement than the autosomes. Another way of analyzing chromosome evolution is to consider how likely genes are to be rearranged into a different order on any given chromosome. We calculated the density of breaks per 100 genes for each chromosomal arm. The results are consistent with the density of breaks per megabase. Genes on the X are greater than four times more likely to change order than those on the autosomes.

2.3.12 Rates of chromosome evolution in *Drosophila* and *Anopheles*

Recent studies have established that both *Anopheles* and *Drosophila* species have high rates of chromosomal evolution as compared with mammalian species[42, 50, 125-131]. We compared the number of breaks per gene and breaks per megabase for each chromosome to understand the differences in the rates of chromosome evolution between *Drosophila* and *Anopheles* (Additional file 1: Tables S6 and S7). These results reveal a high rate of gene order reshuffling in the mosquito X chromosome as compared with autosomes, and even with the *Drosophila* X chromosome, which was thought to have a high rate of rearrangements (Figure 2.11.8). We correlated densities of different molecular features including simple repeats, TEs, genes, and S/MARs with the rates of rearrangement calculated for each arm (Additional file 1: Tables S8-S13). The strongest correlations were found among the rates of evolution across all chromosome arms and the densities of microsatellites, minisatellites and satellites in both *An. gambiae* and *An. stephensi*. The highly-positive correlations between rates of inversion across all chromosome arms and satellites of different sizes are due most likely to the co-occurring abundance of satellites and inversions on the X chromosome. Rates of inversions and satellite densities are much lower on the autosomes. From the autosomal perspective, S/MARs were moderately correlated negatively with fixed inversions and polymorphic inversions.

2.4 Conclusions

The genome assembly of the type-form of the Indian strain of *An. stephensi* was produced using a combination of 454, Illumina, and PacBio sequencing and verified by analysis of BAC clones and ESTs. Physical mapping was in complete agreement with the genome assembly and resulted in a chromosome-based assembly that includes 62% of the genome. Such an assembly enabled analysis of chromosome arm-specific differences that are seldom feasible in next-gen genome projects.

Comparative analyses between *An. stephensi* and *An. gambiae* showed that the *Anopheles* X has a high rate of chromosomal rearrangement as compared with autosomes, despite the lack of polymorphic inversions in the X chromosomes in both species. Additionally, the difference between the rates of X chromosome and autosome evolution is much more striking in *Anopheles* than in *Drosophila*. The high rate of evolution in X correlates well with the density of simple repeats. Our data indicate that overall high rates of chromosomal evolution are not restricted to *Drosophila* but may be a feature common to Diptera.

The genome landscape of *An. stephensi* is characterized by relatively low repeat content compared to *An. gambiae*. *Anopheles stephensi* appears to have larger amount of repeat-rich heterochromatin in pericentric regions but far less repetitive sequences in chromosomal arms as compared with *An. gambiae*. Using a newly developed chromosome quotient method, we identified a number of Y-chromosome contigs and BACs, which together represent currently the most abundant set of Y sequences in any *Anopheles* species.

The current assembly contains 11,789 predicted protein coding genes, 127 miRNA genes, 434 tRNA genes, and 53 fragments of rRNA genes. *Anopheles stephensi* appears to have fewer gene duplications than *An. gambiae* according to orthology analysis, which may explain the slightly lower number of gene models.

This genome project is accompanied by the first comprehensive RNAseq-based transcriptomic analysis of an *Anopheles* mosquito. Twenty gene clusters were identified according to gene expression profiles, many of which are stage or sex-specific. GO term analysis of these gene clusters provided biological insights and leads for important research. For example, male-biased genes were enriched for genes involved in spermatogenesis and the detection of sound.

Close attention was paid to genes involved innate immunity including LRIMS, APL1, and proteins in the Toll, IMD, insulin, and TGF-β signaling pathways. High level of orthology is generally observed between *An. stephensi* and *An. gambiae.* RNAseq analysis, which was corroborated by other expression analysis methods, provided novel insights. For example, a protein known to interact with both TOR and TGF-β signaling pathways showed intriguingly abundant mRNA expression in a wide range of tissues, providing new leads for insights into both TOR and TGF-β signaling in mosquitoes.

2.5 Methods

2.5.1 Strain selection

We chose to sequence the Indian strain of *An. stephensi*, a representative of the type form. The lab colony from which we selected mosquitoes for sequencing was originally established from wild mosquitoes collected in India. The lab colony has been maintained continuously for many generations so we did not attempt to inbreed it.

2.5.2 Sample collection

DNA was isolated from more than 50 adult male and female *An. stephensi* using the Qiagen (Hilden, Germany) DNeasy Blood and tissue kit following the suggested protocol. The integrity of the DNA was verified by running an aliquot on a 1% agarose gel to visualize any degradation. Total RNA was isolated using the standard protocol of the mirVana RNA isolation kit (Life Technologies, Carlsbad, CA).

2.5.3 Sequencing

The *An. stephensi* genome was sequenced to 19.4x coverage using 454 FLX Titanium sequencing performed by the Virginia Bioinformatics Institute (VBI) core laboratory. Sequencing was performed on four different libraries: a single-end shotgun library, and 3 kb, 8 kb and 20 kb mate-pair libraries. A 200bp insert size library produced from male *An. stephensi* genomic DNA was prepared and subjected to a single lane of Illumina HiSeq. Genomic DNA from male *An.* sequence was subjected to 10 SMRT cells of Pacific Biosciences (PacBio) v1 sequencing. Sanger sequencing performed by Amplicon Express was used to sequence 7,263 BAC-ends.

2.5.4 Genome assembly

We used several approaches to combine the Illumina and 454 data to generate a better assembly. Newbler can take raw Illumina data as input, so we tried a Newbler assembly with the 454 and Illumina data. However, this resulted in a worse assembly than 454 alone. We had much more success with the strategy used to assemble the *Solenopsis invicta* genome[132]. First we assembled the Illumina data then cut the assembly into pseudo-454 reads, and then used these reads along with the real 454 data as input to Newbler[133].

2.5.5 *De novo* Illumina assembly with Celera

We assembled the paired-end Illumina reads using the Celera assembler[134] with the parameters: ”overlapper = ovl; unitigger = bogart; utgBubblePopping = 1; kickOutNonOvlContigs = 1; cgwDemoteRBP = 0; cgwMergeMissingThreshold = 0.5; merSize = 14”. The Celera assembler output comprise 41,213 contigs spanning 212.8 Mb. The N50 contig size of this assembly was 16.8 kb.

2.5.6 *De novo* 454 and Illumina pseudo-454 reads assembly with Newbler 2.8

The contigs of the aforementioned Illumina assembly were shredded informatically into 400 bp pieces with overlapping 200 bp to approximate 454 reads. To artificially simulate coverage depth, we started the shredding at offsets of: 0, 10, and 20. Shredding the Illumina assembly resulted in 2,452,038 pseudo-454 reads simulating 4.17x coverage.

We generated an assembly of the 454 and pseudo-454 reads with Newbler 2.8 using the ”-het -scaffold -large -s 500” parameters. The resulting assembly contained 23,595 scaffolds spanned 221 Mb. The scaffold N50 size was 1.34 Mb. Mitochondrial DNA (1 scaffold), and other contamination (87 scaffolds) were identified by blastn and removed from the assembly.

2.5.7 Gap-filling with PacBio Reads

PacBio data was used to fill gaps in the scaffolds to further improve the genome assembly. We error-corrected raw PacBio reads using the 454 sequencing data with the Celera pacBioToCa pipeline. pacBiotoCa produced 0.88 Gb of error-corrected PacBio reads. Using the error-corrected PacBio data as input, Pbjelly[135] was used to fill gaps with parameters: ”-minMatch 30 -minPctIdentity 98 -bestn 10 -n Candidates 5 -maxScore -500 -nproc 36-noSplitSubreads”. Pbjelly filled 1,310 gaps spanning 5.4 Mb.

2.5.8 Further Scaffolding with BAC-ends

The scaffolds of the assembly were improved subsequently through the integration of 3,527 BAC-end pairs (120 kb ± 70 kb) using the Bambus scaffolder[136] (Additional file 21). The BAC-end sequences were mapped to the scaffolds using Nucmer[137]. The output files were used to generate the ”.contig” format files required for Bambus. In total, 275 links between scaffolds were detected. Of these, 169 were retained as potential valid links, which are links connected by uniquely mapped BAC-ends. Links confirmed by less than two BAC-ends were rejected. A total of 46 links were retained that together connected 22 scaffolds, increasing the N50 scaffold size from 1,378 kb to 1,572 kb.

2.5.9 Assembly Validation

CEGMA (Core Eukaryotic Genes): We used CEGMA[138] to search for the number of core eukaryotic genes to test the completeness and correctness of the genome assembly. CEGMA provides additional information as to whether the entire core eukaryotic genes are present (>70%) or only partially present (>20% and <70%). In total, CEGMA found 96.37% of the 248 core eukaryotic genes to be present, and 97.89% of the core eukaryotic genes to be partially present.

BAC-ends: We checked whether BAC-ends align concordantly to the genome to study the structural correctness of the *de novo* assembly. BAC-ends were aligned to the scaffolds using NUCMER. In order to ensure unambiguous mapping, only sequences that aligned to a unique location with >95% coverage and 99% identity were used. In total, 21.6% of the BAC-end sequence pairs could be aligned to a unique position in the *An. stephensi* genome with these stringent criteria. Pairs of BAC-end sequence that aligned discordantly to a single scaffold were considered indicative of potential mis-assembly. Only 4 of 717 aligned BAC-end pairs aligned discordantly with the assembly confirming overall structural correctness.

ESTs*: An. stephensi* EST sequences were downloaded from both the NCBI and VectorBase. We screened the EST sequences to remove any residual vector sequence. The screened ESTs were aligned to the assembly with GMAP[139]. In total, 35,367 out of 36,064 ESTs aligned to the assembly. Of these, 26,638 aligned over at least 95% of their length with an identity >98%. The high percentage of aligned ESTs demonstrates the near-completeness of the *An. stephensi* genome assembly.

Fluorescent in situ hybridization (FISH) - Slides were prepared from ovaries of lab reared, half-gravid females of the *An. stephensi* Indian wild-type strain. Slide preparation and hybridization experiments followed the techniques described in Sharakhova et al[124]. Fluorescent microscope images were converted to black and white and inverted in adobe photoshop. FISH signals were mapped to specific bands or interbands on the physical map for *An. stephensi* presented by Sharakhova et al[140].

2.5.10 Constructing the Physical Map

For the chromosomal based genome assembly, all probes mapped by in situ hybridization by Sharakhova[140] and this study were aligned to the final version of the *An. stephensi* genome using NCBI blast+ blastn. Different blastn parameters were used for probes from different sources to determine if the probe was kept in the final assembly. An e-value of 1e-40 and an identity of >95% was required for probes from *An. stephensi*. An e-value of 1e-5 was required for probes from species other than *An. stephensi*. Probes that mapped to more than one location in the genome were discarded. The work by Sharakhova *et al*[140] hybridized 345 probes however, only ~200 probes from that study were maintained in the final chromosomal assembly. An additional 27 PCR products and BAC clones were hybridized to increase the coverage of our chromosomal assembly.

2.5.11 Annotation

The genome assembly was annotated initially using the MAKER pipeline[141]. This software synthesizes the results from *ab initio* gene prediction with experimental gene evidence to produce final annotations. Within the MAKER framework, RepeatMasker[142] was used to mask low-complexity genomic sequence based on the repeat library from previous prediction. First, ESTs and proteins were aligned to the genome by MAKER using BLASTn and BLASTx, respectively. MAKER uses the program Exonerate to polish BLAST hits. Next, within the MAKER framework, SNAP[143] and AUGUSTUS[144] were run to produce *ab initio* gene predictions based on the initial training data. SNAP and AUGUSTUS were run once again inside of MAKER using the initial training obtained from the ESTs and protein alignments to produce the final annotations.

2.5.12 Orthology

Orthologs of predicted *An. stephensi* genes were assigned by OrthoDB[145]. Information about orthologous genes for *An. gambiae*, *Ae. aegypti*, and *D. melanogaster* also were downloaded from OrthoDB. Enrichment analysis was performed for categories of orthologs using the methods provided in the ontology section.

2.5.13 Transcriptomics

RNA-seq from 11 samples including: 0-1, 2-4, 4-8, and 8-12 hour embryos, larva, pupa, adult males, adult females, non-blood-fed ovaries, blood-fed ovaries, and female carcass without ovaries as described[100] were used for transcriptome analysis. These RNA-seq samples are available from the NCBI SRA (SRP013839). Tophat[146] was used to align these RNA-seq reads to the *An. stephensi* genome and HTSeq-count [147] was used to generate an occurrence table for each gene in each sample. The numbers of alignments to each gene in each sample then were clustered using MBCluster.Seq[148], an R package designed to cluster genes by expression profile based on Poisson or Negative-Binomial models. MBCluster.Seq generated 20 clusters. To visualize these results we performed regularized log transformation to the original occurrence tables for all 20 clusters using DESeq2[149]. The results were plotted using ggplot2[150].

2.5.14 Ontology

Gene ontology (GO) terms were assigned for the 20 clusters of predicted *An. stephensi* genes. GO terms were assigned using Blast2Go[151]. The predicted proteins is blasted against the NCBI non-redundant protein database and scanned with InterProScan[152] against InterPro's signatures. We also identified enzymatic functions according to the KEGG map module within Blast2GO. After GO terms were assigned, GO-slim results were generated for the available annotation based on the Generic GO slim mapping. The GO terms assigned by Blast2GO were subject to GO term enrichment. Overrepresented GO terms were identified using a hypergeometric test using the GOstats package in R[153].

2.5.15 noncoding RNA

We used tRNAScan-SE[154] with the default eukaryotic mode to predict 434 tRNAs in the *An. stephensi* genome (Additional file 1: Table S14; Additional file 22). Other noncoding RNAs were predicted with INFERNAL[155] by searching against Rfam database version 11.0[156]. A total of 53 fragmental ribosomal RNA, 34 snRNA, 7 snoRNA, 127 miRNA, and 148 sequences with homology to the *An. gambiae* self-cleaving riboswitch were predicted at an e-value cutoff of 1e-5.

2.5.16 Transposable elements and other interspersed repeats

Transposable element discovery and classification were performed on the *An. stephensi* scaffold sequences using previously-described pipelines for LTR-retrotransposons, non-LTR-retrotransposons, SINEs, DNA-transposons, and MITEs, followed by manual inspection[157]. The manually-annotated TE libraries then were compared with the RepeatModeler output to remove redundancy and to correct mis-classification by RepeatModler. A repeat library was produced that contains all manually-annotated TEs and non-redundant sequences from RepeatModeler. The repeat library was used to run RepeatMasker at default settings on the *An. stephensi* assembly to calculate TE copy number and genome occupancy.

2.5.17 Simple repeats

To quantify the number of microsatellites, minisatellites, and satellites present in the mapped scaffolds for each chromosome, these scaffolds were divided into strings of 100,000 bp and then concatenated into a multi-FASTA file representing an *An.*

stephensi pseudo chromosome. Scaffolds were oriented when possible, and all unoriented scaffolds were given the default positive orientation for that chromosome. The multiFASTA file for each pseudo-chromosome was analyzed using a local copy of TandemRepeatsFinder v 4.07b[158]. Parameters for the analysis followed those used by Xia et al, 2010: microsatellites were those of period size 2-6 with copy number of 8+. Minisatellites had period size 7-99 while repeats were considered satellites if they had a period size of 100+. Both satellites and minisatellites were considered only if they had a copy number of 2+. Simple repeats were recorded only if they had at least 80% identity.

2.5.18 Identification of S/MARs

Scaffold/matrix associated regions were identified using the SMARTest bioinformatic tool provided by Genomatix[159]. Densities of genes and TEs per 100 kb window were calculated using Bedtools coverage based on the genome annotation and TE annotation respectively.

2.5.19 Synteny, gene order evolution, and inversions

One-to-one orthologs from *An. gambiae* and *An. stephensi* were identified using OrthoDB and their locations on the *An. gambiae* and *An. stephensi* scaffolds determined. Comparative positions of the genes on the scaffolds based on ontology relationships were plotted using genoPlotR. Scaffolds that mapped using two or more probes were oriented properly, but those anchored by only one probe were used in their default orientation. The number of synteny blocks for each pair of homologous chromosome arms between *An. stephensi* and *An. gambiae* was determined from the images output from genoPlotR. Two criteria were imposed to determine the number of synteny blocks: the orientation of orthologous genes, and whether genes remained in the same order on the chromosome of *An. stephensi* as in *An. gambiae*. Thus, a group of genes is assigned to the same synteny block if it has the same orientation and order in both species. Synteny blocks were numbered 1,2,3,4 ...etc. along the chromosome by assigning *An. gambiae* as the default gene order. *Anopheles stephensi* was considered rearranged compared to *An. gambiae* when the numbering of synteny blocks was the same in both species but the order was rearranged in *An. stephensi*. After quantifying the number of synteny blocks and the amount of gene rearrangement between the two species, we estimated the number of chromosomal inversions between them using the programs Genome Rearrangements in Mouse and Man (GRIMM[122]) and Sorting Permutation by Reversals and block-INterchanGes (SPRING [123]).

2.6 Data access

The *An. stephensi* genome assembly has been deposited in GenBank under the accession number ALPR00000000 and is available at www.VectorBase.org. The raw sequence data used for genome assembly is available in the NCBI SRA: 454 - SRP037783, Illumina - SRP037783 and PacBio - SRP037783. The BAC-ends used for scaffolding are available from the NCBI dbGSS accession numbers: KG772729 - KG777469. RNA-Seq data can be accessed at the NCBI SRA with ID SRP013839.

2.7 Additional files

Additional file 1: this file includes supplemental text, supplemental figures, and supplemental Tables.

Additional files 2-22 are provided as Additional_Files2-22.tar.gz. We also provide a link for all additional files in case the reviewers find it useful (http://tu08.fralin.vt.edu/share/Additional%20Files/)

Additional file 2: Physical Map Data.xlsx
Additional file 3: Lists of genes in clusters.xlsx
Additional file 4: Cluster ontology.txt
Additional file 5: Sex-biased genes list and GO terms.xlsx
Additional file 6: Revised annotation for immunity-related genes.gff3
Additional file 7: Sequences of immunity-related genes.fasta
Additional file 8: RNA-seq expression profile of immunity-related genes.xlsx
Additional file 9: Revised annotation for salivary genes
Additional file 10: Sequences of salivary genes
Additional file 11: Repeat sequences
Additional file 12: Genome Landscape.xlsx
Additional file 13: Tandem repeat sequences.fa
Additional file 14: Chromosome quotients of putative Y-linked scaffolds
Additional file 15: Sequences of putative Y-linked scaffolds
Additional file 16: Chromosome quotients of Y-linked BACs
Additional file 17: Sequences of Y-linked BACs
Additional file 18: Repeat masker output of Y-linked BACs and Y-linked scaffolds
Additional file 19: Repeat masker output of Y-linked BACs
Additional file 20: Synteny Blocks.docx
Additional file 21: BAC-ends dbGSS accession numbers.txt
Additional file 22: Non-coding RNA annotation.txt

2.8 Author contributions

Conceived and designed experiments: ZT and IVS; Data generation, analysis and presentation: XJ, AP, AS, ABH, MK, MVS, AK, BW, CO, DL, KE, KM, JMCT, JMCR, MAR, MRR, MU, NP, PA, PG, RK, RS, RMW, SL, SM, VLMD, YQ, ZT; Writing of the manuscript: XJ, ABH, AAJ, AP, AS, JMCR, KDV, KM, KP, MK, MAR, MMR, SL, IVS, and ZT; Provided resources and tools and critical reviewed manuscript: XC, YS

2.9 Acknowledgements

This work is supported by the Fralin Life Science Institute and the Virginia Experimental Station, and by NIH grants AI77680 and AI105575 to ZT, AI094289 and AI099528 to IVS, AI29746 to AAJ, AI095842 to KM, AI073745 to MAR, AI080799 and AI078183 to SL, AI042361 and AI073685 to KDV. RMW is supported by Marie Curie International Outgoing Fellowship PIOF-GA-2011-303312. XC is supported by GDUPS (2009). YS thanks the Department of Biotechnology, Government of India for the financial support.

Figures

Figure 2.10.1: Physical Map

A physical map of the *An. stephensi* genome was created from FISH on polytene chromosomes comprising 227 probes and 86 scaffolds. These 86 scaffolds comprise 137.14 Mb or 62% of the *An. stephensi* genome. Orientation was assigned to 32 of the 86 scaffolds. The physical map includes 28 of the 30 largest scaffolds.

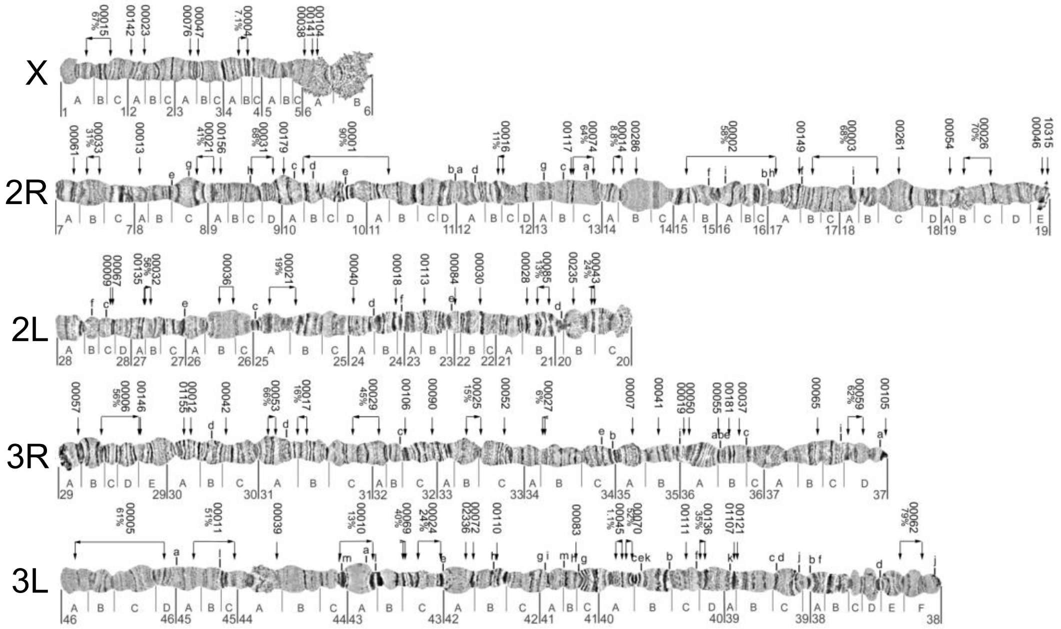

Figure 2.10.2 Orthology

Comparative analysis of orthologs from *An. stephensi*, *An. gambiae*, *Ae. aegypti*, and *D. melanogaster*. Orthologous genes were retrieved from OrthoDB. 7,305 genes were shared among all four species, 1,297 genes were specific to *An. stephensi*, 653 genes were *Anopheles* -specific, and 1,863 genes were mosquito-specific.

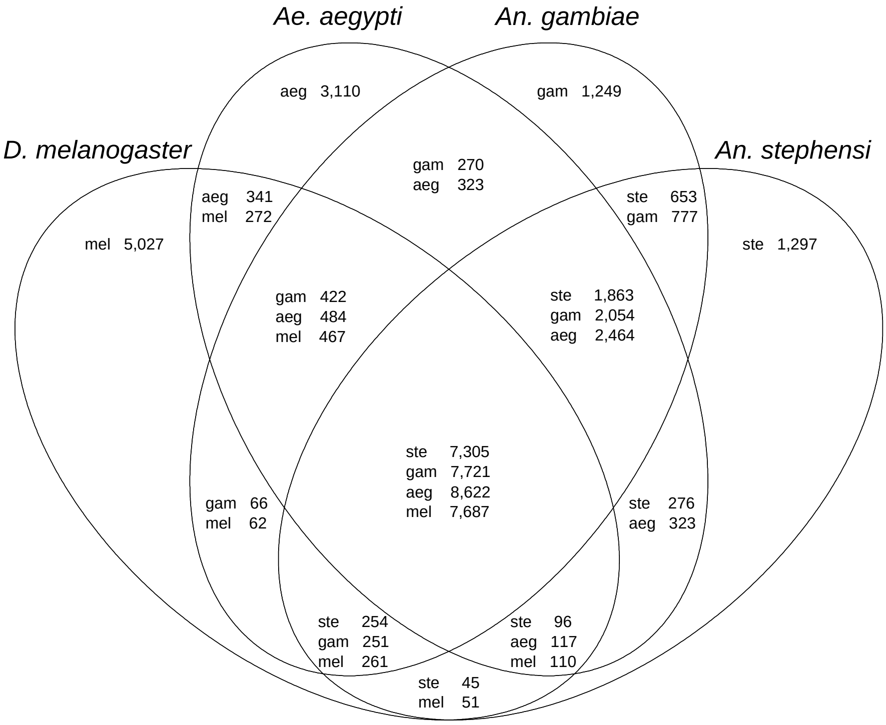

Figure 2.10.3 Gene clustering according to expression profile.

Twenty groups of genes were clustered by expression profile. The expression profiles used for grouping were generated using 11 RNA-seq samples spanning developmental time points including: 0-1, 2-4, 4-8, and 8-12 hour embryos, larva, pupa, adult males, adult females, non-blood-fed ovaries, blood-fed ovaries, and 24 hours post-blood-fed female carcass without ovaries. Male stage are colored blue, female stages are colored green, ovary samples are colored yellow, embryo samples are colored red, larva samples are colored pink, and pupa samples are colored purple. Many of these clusters correspond to either a specific developmental stage or specific sex.

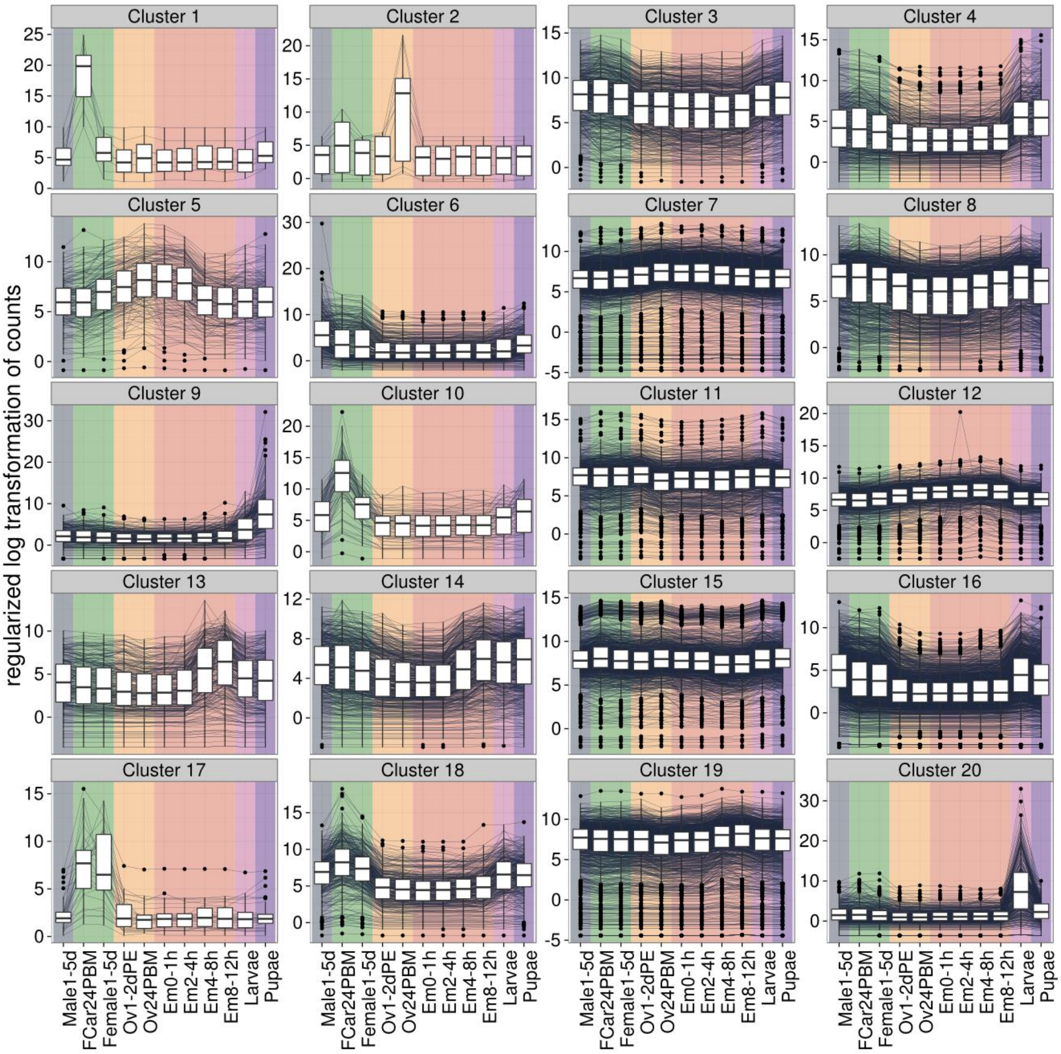

Figure 2.10.4 Genome Landscape

Density of genes (black vertical lines), transposable elements (TEs; green vertical lines), and short tandem repeats (STRs, red vertical lines) in 100 kb windows of mapped scaffolds. Based on the physical map, scaffolds were ordered and oriented respective to their position in the chromosomes and then 100 kb non-overlapping windows were generated for each scaffold (X-axis). The density of genes and TEs (Y-axis) was determined using coverageBed. Satellite sequences were identified using TandemRepeatFinder. The short tandem repeats track is a combination of the number of microsatellites, minisatellites and satellites per 100 kb window.

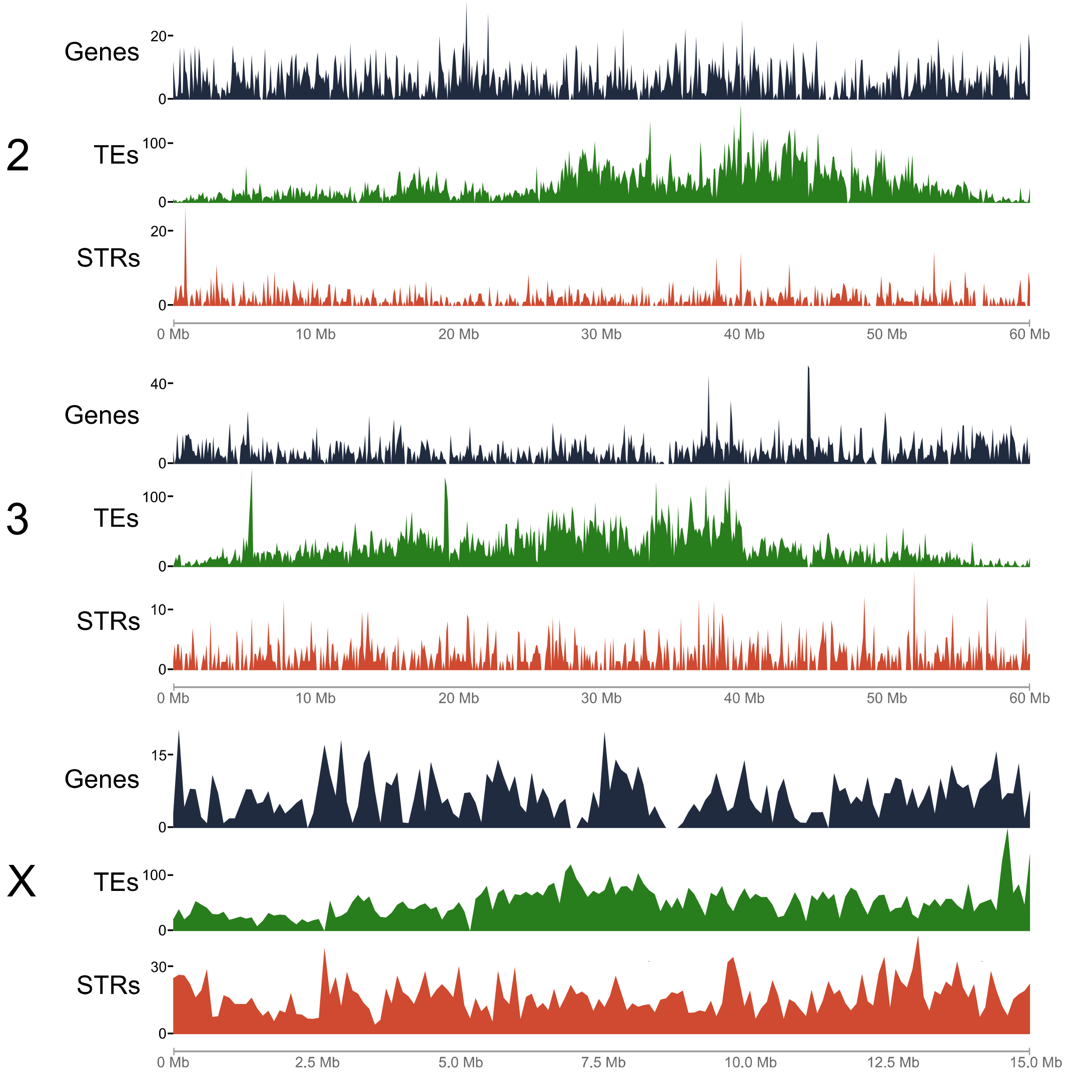

Figure 2.10.5 Average Density / 100kb / ARM

A comparison of the average density per 100 kb of genes, TEs, S/MARS, microsatellites, minisatellites, and satellites between chromosome arms.

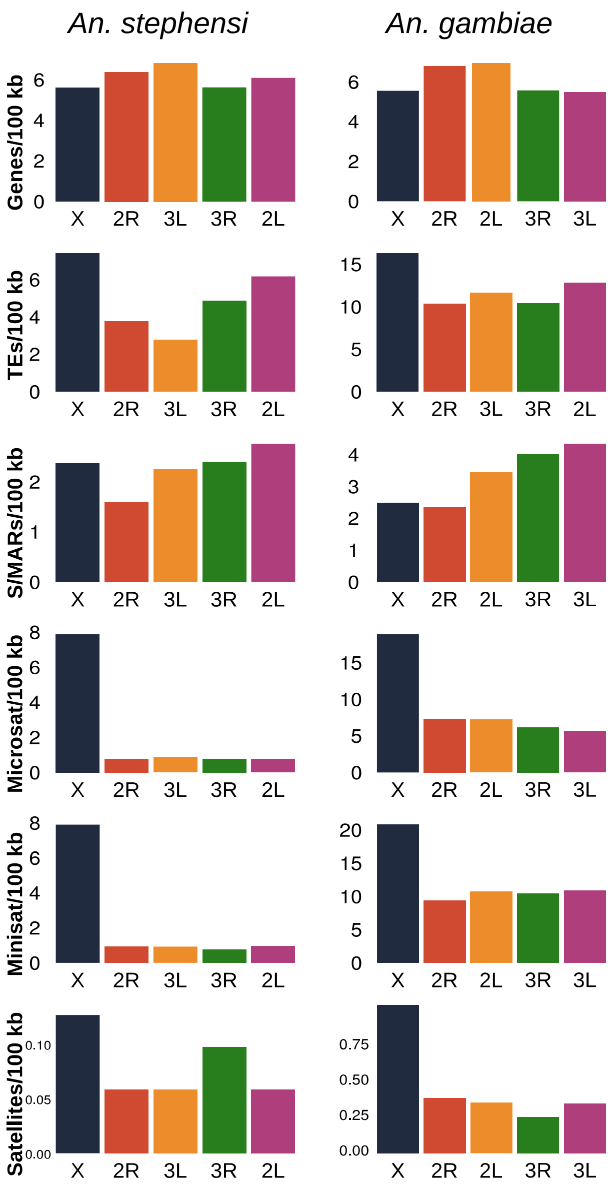

Figure 2.10.6 FISH with Aste72A, rDNA and DAPI on mitotic chromosomes

The pattern of hybridization for satellite DNA Aste72A on mitotic sex chromosomes of *An. stephensi.* Aste72A hybridizes to pericentric heterochromatin in both X and Y chromosomes while ribosomal DNA locus maps next to the heterochromatin band in sex chromosomes.

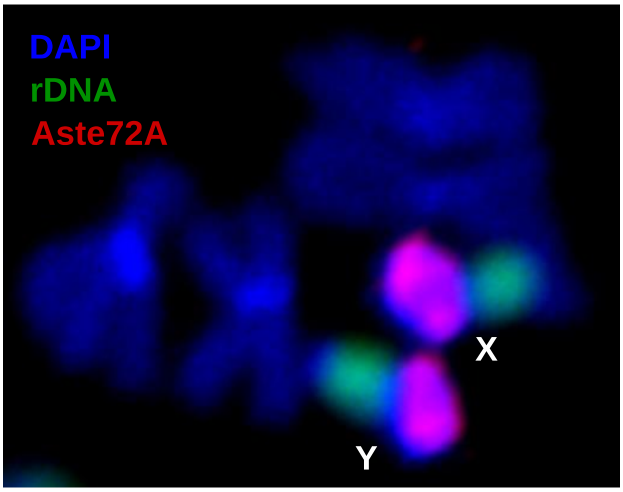

Figure 2.10.7 Synteny

Synteny between *An. stephensi* and *An. gambiae* based on 6,448 single-copy orthologs. Orthologs with the same orientation in *An. stephensi* and *An. gambiae* are connected with red lines and orthologs with the opposite orientation are connected with blue lines. Orthologous genes from *An. stephensi* and *An. gambiae* were retrieved from OrthoDB. The physical map was used to identify the relative locations of genes on the *An. stephensi* chromosomes. The relationship of the position between the *An. stephensi* and *An. gambiae* orthologs were plotted with GenoPlotR. 75 syntenic blocks were identified on the X chromosome. 69 and 54 syntenic blocks were identified on 2R and 2L (3L in *An. stephensi*). 48 and 28 syntenic blocks were identified on 2R and 3L (2L in *An. stephensi*). Therefore, the X chromosome has undergone the most rearrangements per megabase.

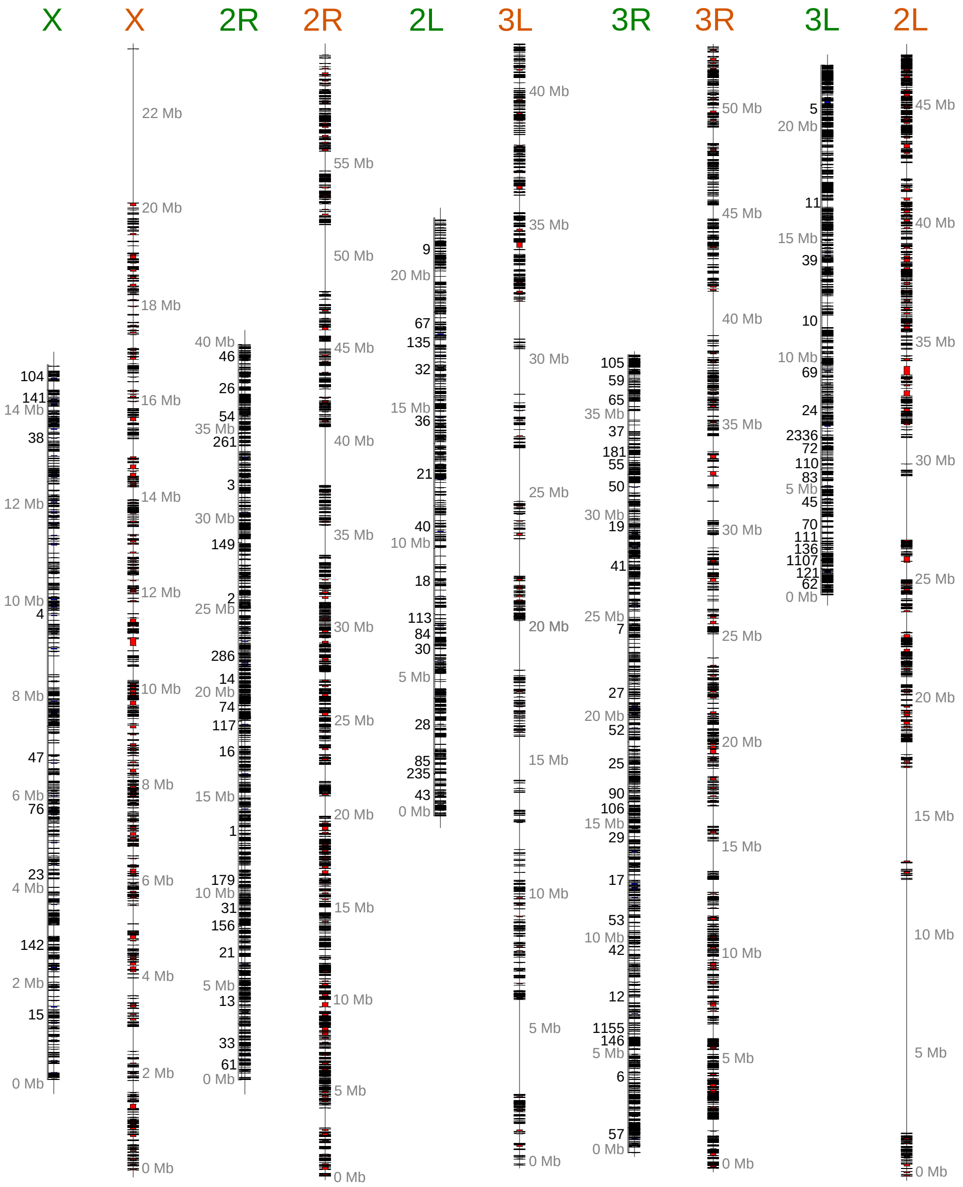

Figure 2.10.8 Breaks per 100 Genes per million years in *Anopheles* and *Drosophila*.

These results reveal a high rate of gene order reshuffling in the X chromosome as compared with autosomes, and even with the *Drosophila* X chromosome.

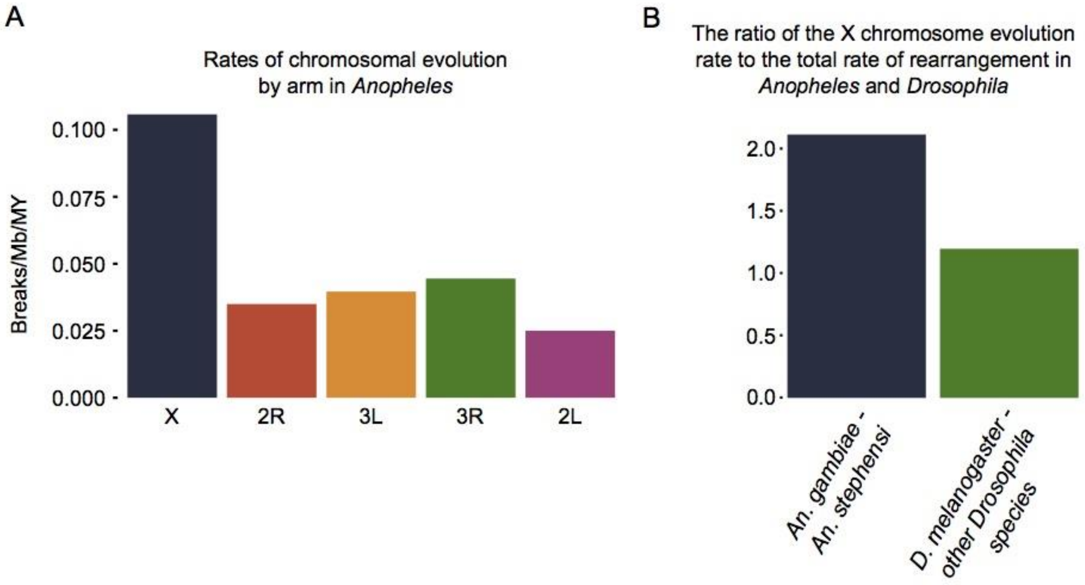

Tables

Table 2.11.1: Assembly Statistics

Statistic	Value
Scaffolds (n)	23,371
Scaffold N50 size	1,591,355
Maximum Scaffold Length	5,975,090
Minimum Scaffold Length	486
Total Length of Scaffolds	221,309,404
Percent Ns	5.35 %
Contigs (n)	31,761
Contig N50 size	36,511
Maximum Contig Length	475,937
Minimum Contig Length	347
Total Length of Contigs	209,483,518
GC Percent	44.80 %

Table 2.11.2: Physical Map Information

Arm	Scaffolds per Arm (n)	Length (Mb)	% Mapped Genome	% of Total Genome
X	9	14.95	10.90	6.77
2R	21	39.50	28.80	17.87
2L	15	22.40	16.33	10.14
3R	24	37.83	27.59	17.12
3L	17	22.45	16.37	10.16
Total	86	137.14	100	62.05

Scaffolds mapped to each chromosome, total bp to each chromosome, percent of the predicted genome covered.

Table 2.11.3: Transposable elements and other interspersed repeats

Type	Elements (n)	Length Occupied (bp)	Percent of Genome
SINEs	30,514	3,739,253	1.69
LINEs	22,022	5,231,240	2.36
LTR elements	4,359	1,499,282	0.68
DNA elements	4,611	966,667	0.44
Unclassified	30,611	4,322,468	1.95
Total	92,117	15,758,910	7.12

Chapter 3: A physical genome map of Neotropical malaria vector *Anopheles albimanus*

3.1 Abstract

The genome assembly of the Neotropical malaria vector *Anopheles albimanus* is the smallest among 16 malaria mosquito genomes. Preliminary physical mapping placed ~75% of the genome to the drawn cytogenetic map. However, a detailed physical genome map was still lacking. In this study we develop a high resolution photomap with completely straightened polytene chromosomes from the salivary glands of the mosquito. Based on this map we construct a physical genome map utilizing fluorescent *in situ* hybridization of PCR amplified DNA probes to the chromosomes. This physical map orders and orients 32 genomic supercontigs comprising 96% of the genome and currently represents the most compete physical genome map among *Anopheles*. The study reveals that several of the largest genomic supercontigs are misassembled. Based on additional sequence analysis these supercontigs are now divided into 2-4 smaller supercontigs. Thus, our study demonstrates that physical mapping is a powerful tool for improving the quality of draft genome assemblies for mosquitoes.

3.2 Introduction

Anopheles albimanus is one of the dominant malaria vectors in the Americas [160]. This species is widely distributed in the Neotropical region stretching from the southern United States to northern Peru and the Caribbean Islands. It is the major contributor to malaria transmission in the coastal areas of this region. Like other species from this Neotropical region, *An. albimanus* is a member of subgenus Nyssorhynchus. Unlike other species from genus *Anopheles* that usually belong to species complexes, no evidence for cryptic species of this vector has been described [161, 162]. The availability of morphological mutants and biochemical markers allowed development of a genetic linkage map for *An. albimanus* [163]. This map was later integrated with microsatellite markers [53].

Like other mosquitoes from the genus *Anopheles*, *An. albimanus* has high quality polytene chromosomes in salivary glands, [164] and this species is well studied cytogenetically. The first drawn map and detailed description of chromosomal banding patterns for *An. albimanus* was developed by W. Keppler in 1973 [165]. This paper also determined that chromosomes of *An. albimanus* are remarkably uniform, with no rearrangements between strains. This lack of chromosomal polymorphism is unusual for *Anopheles* [60, 61]. A comprehensive cytogenetic study conducted later, on samples from 11 distant localities in Columbia, found only one small inversion on chromosome X. This inversion was present in low frequency and only in certain populations [162]. Comparisons of the chromosomal banding patterns also revealed no similarities between *An. albimanus* chromosomes and other *Anopheles* from subgenus *Cellia* and *Anopheles* [165]. Recognizable banding patterns that can be used for arm homology reconstruction were only found within the species from subgenus *Nyssorhynchus*, which includes *An. albimanus*. The first successful *in situ* hybridization on chromosomes of *An. albimanus* was performed using histone genes from *Drosophila melanogaster* [166].

The first cytogenetic photomap for the salivary gland polytene chromosomes of *An. albimanus* delineated further banding details relative to previously published drawn maps, and represented a vast improvement in photomapping in this species [47]. After molecular cytogenetic techniques were developed for the African malaria vector, *An. gambiae* [167, 168], *An. albimanus* was the first mosquito investigated for interspecies chromosome comparison by cross *in situ* hybridization [47]. Direct mapping of 17 DNA probes from *An. gambiae* onto chromosomes of *An. albimanus* allowed reconstruction of arm homology between the species from two different subgenera- *Cellia* and *Nyssorhynchus*. It was demonstrated that autosomes of these mosquitoes are rearranged in a whole-arm translocation manner. The study also found numerous paracentric inversions within chromosomal arms but no pericentric inversions or partial arm translocations. . Interspecies *in situ* hybridization was later applied to explore chromosomal rearrangements in other *Anopheles* species [50, 125, 169]. These studies revealed that the whole-arm translocations and paracentric inversions within chromosomal arms are common rearrangements in genus *Anopheles*.

The genomics era has offered new opportunities to study chromosomal evolution in mosquitoes. The *An. albinamus* genome was sequenced within the 16 *Anopheles* genome project which has allowed validation of chromosomal evolution hypothesis on a previously unattainable scale. [9]. The genome assembly generated by Illumina sequencing for *An. albinamus* was relatively small compared to other species of *Anopheles*. At 170 Mb, the genome consists of 204 scaffolds with N50=18 Mb. This study utilized previously mapped markers [47].to develop a physical map covering 75% of the *An. albinamus* genome. An interspecies chromosome comparison was then conducted on 5 mosquito species which also possessed chromosomal genome assemblies. In addition to *An. albimanus,* the study included three species from subgenus *Cellia*: *An. gambiae, An. stephensi*, and *An. funestus*; and one species from subgenus *Anopheles*: *An. atroparvus*. The study supports the hypothesis that chromosomal arms in *Anopheles* reshuffle between chromosomes via whole-arm translocations, but unlike *Drosophila*, do not undergo fissions or fusions. This work also revealed that the sex chromosome, X, exhibits the highest rate of the chromosomal rearrangements among chromosomal arms, and displays the highest rate of gene movement to other chromosomes. Although it was not included in publication of 16 Anopheles genome cluster [9], the physical map used for that study raised the question of possible misassembly within the *An. albimanus* genome. During the alignment of the previously mapped markers [47] to the genome assembly one large scaffold, KB672397, contained probes which were physically mapped to different chromosomal arms. Further investigation by identifying the chromosomal positions of orthoglous genes in *An. gambiae* revealed likely misassembly within 6 *An. albimanus* supercontigs. The suspected misassemblies broke scaffolds sized 1.8 MB-24 MB into 2-4 pieces of variable sizes.

Here we report a chromosomal genome assembly of the *An. albimanus* reflecting 96% genome assignment to chromosomes. To facilitate physical mapping we developed a detailed cytogenetic photomap for polytene chromosomes from salivary glands of *An. albimanus*. Chromosomes on this map were completely straightened that make them convenient for physical mapping of the genomic supercontigs. To further assist in physical mapping we also provide detailed description of major cytogenetic landmarks for all chromosomal arms. Our physical mapping corrects misassembly within the genome and tests scaffold gluing predictions resulting in the most complete chromosomal assembly for any mosquito to date. Our study identifies 15 misassemblies in 6 supercontigs within the current genome assembly of this mosquito. Based on these data and additional sequence alignments the *An. albimanus* genome to the reference genome of *An. gambiae* these misassemblies are corrected in the reference *An. albimanus* genome hosted by Vectorbase. The availability of genome assemblies for multiple *Anopheles* species also allowed the development of a computational technique called “scaffold gluing” wherein syntenic gene order from many related species can be used to predict the merging or "gluing" of scaffolds in other species. Our study demonstrated that this technique is useful for filling gaps in chromosomal assemblies and improving genome assembly quality. With these findings our work demonstrates that physical mapping can be effectively used for improvement of mosquito genome assemblies. The physical map developed in this study for Neotropical malaria vector *An. albimanus* can be further utilized for exploration of chromosomal evolution in mosquitoes.

3.3 Material and methods

3.3.1 Mosquito strain and larvae preservations

We utilized *An. albimanus,* STECLA strain mosquitoes from a laboratory colony hosted in the Fralin Life Science Institute, Virginia Tech, USA. The strain was originally colonized from an El Salvador population and the Virginia Tech colony was obtained courtesy the Malaria Research and Reference Reagent Resource (MR4) (MRA-126, MR4, ATCC Manassas Virginia). Larvae were grown in a growth chamber at 27ºC, with 12 hours of light and darkness per day. Fourth instar specimens were fixed in cold Carnoy`s solution (3 ethanol : 1 glacial acetic acid by volume) for no less than two weeks at -20 ºC.

3.3.2 Chromosome preparation and map development

For one chromosome preparation, salivary glands were dissected from one or two larvae. Salivary glands were bathed in a drop of 50% propionic acid for 5 minutes, and squashed as previously described [124]. The quality of the preparation was assessed on an Olympus CX41 (Olympus America Inc., Melville, NY) phase contrast microscope. High quality preparations were then flash frozen in liquid nitrogen and immediately placed in cold 50% ethanol. After a minimum of two hours, preparations were dehydrated in an ethanol series (70%, 90%, and 100%) and air dried. Chromosome images were observed using Olympus BX41 microscope (Olympus America Inc., Melville, NY) with attached CCD camera Qcolor5 (Olympus America Inc., Melville, NY). Images were combined, straightened, shaped, and cropped in AdobePhotoshop CS2 (George et al., 2010). The chromosome nomenclature was adopted from previously published chromosome maps for salivary glands of *An. albimanus* [47, 165] .

3.3.3 Fluorescent *in situ* hybridization

For probe preparation gene-specific primers were designed to amplify unique exon sequences from the beginning and end of each of the scaffold using the Primer-blast software (Ye et al., 2012) developed at NCBI (http://www.ncbi.nlm.nih.gov/tools/primer-blast/). Primer design was based on gene annotations from the *An. albimanus* Vectorbase genome assembly AalbS1 (www.vectorbase.org/organisms/anopheles-albimanus/stecla/aalbs1). PCR was performed using 2X Immomix DNA polymerase (Bioline USA Inc, MA, USA) and standard Immomix amplification protocol. Amplified fragments were labeled by random primers with Cy3 and Cy5 fluorescent dyes (GE Health Care, UK Ltd, Buckinghamshire, UK and Enzo Biochem, Enzo Life Sciences Inc., Farmingdale, NY) or TAMRA-5-dUTP (Biosan, Novosibirsk, Russia), using Random Primers DNA Labeling System (Invitrogen, Carlsbad, CA, USA). Fluorescent *in situ* hybridization (FISH) was performed using previously described standard protocol (Sharakhova et al. 2006). DNA probes were hybridized to the chromosomes at 39°C overnight in hybridization solution (50% Formamide; 10% Sodium Dextransulfate, 0.1% Tween 20 in 2XSSC, ph 7.4). Then the chromosomes were washed in 0.2XSSC (Saline-Sodium Citrate: 0.03M Sodium Chloride, 0.003M Sodium Citrate) and counterstained with DAPI in ProLong Gold Antifade Mountant (Thermo Fisher Scientific Inc., USA).

3.4 Results

3.4.1 A cytogenetic photomap of *An. albimanus*

An. albimanus exhibits a chromosomal complement typical for *Anopheles* where 2n=6. The chromosomes are represented by two pairs of metacentric autosomes and one pair of subtelocentric sex chromosomes [164]. Because of homologous pairing, the chromosomal complement in salivary glands of *An. albimanus* is represented by 5 chromosomal arms: the smallest arm is the X-chromosome, the longest the 2R arm, and almost equal in length the 2L, 3R and 3L arms (**Table 3.7.1**). A typical chromosomal spread is shown in **Figure 3.8.1**. The autosomal centromeres are visibly bound together in a chromocenter and the short X chromosome has dissociated from the autosomes but remains nearby. In this study, we constructed a photomap for the polytene chromosomes from salivary glands of *An. albimanus* (**Figure 3.8.2**) using phase contrast images of unstained chromosomes. This approach allowed us to obtain clear banding pattern of the chromosomes. Chromosomes were straightened using AdobePhotoshop and divided into 45 numbered divisions and 110 lettered subdivisions. The division borders and nomenclature were adopted from a drawn map [165] and a photomap [47] that were previously developed for polytene chromosomes from the salivary glands of *An. albimanus.*

Chromosomal arms of *An. albimanus* have regions with reproducible, distinct morphology, or landmarks, that can be used for arm recognition. The lengths of the X chromosome and 2R arm make them easily identifiable as shortest and longest arms among the rest of the chromosomal complement. Additional landmarks for X-chromosome are a bell-shaped telomere end with a pair of dark bands in the middle of region 1a and a light puffy area in the second part of region 3A. All autosomal telomeres of *An. albimanus* have flared ends with only slight differences in morphology thus using them as landmarks for arm identification is difficult. Centromeres are usually significantly underpolytenized and often are not properly spread due to the formation of a chromocenter. For these reasons we rely on internal chromosomal regions for arm identification of *An. albimanus.* Three very thin bands in region 7A, and a dark thick band surrounded by two thin bands close to the centromere in region 15B can be used as robust landmarks for arm 2R. Despite their nearly equal length, 2L, 3R, and 3L arms can be easily distinguished by distinct landmarks in the middle of the arms. A pair of dark bands in 17A-B and a wide dark band in the middle of the arm in region 20A can be recognized as landmarks for arm 2L. The major landmark for arm 3R is a wide granulated band surrounded by two dark bands in region 34B. A series of three dark bands surrounded by light areas in region 30A and a wide thick band in region 28B can be used as additional landmarks for this arm. In some specimens we observed a big puff in region 31A-31B that looks like a Balbiani ring. If present, this puff can be also utilized as a strong landmark for 3R. Arm 3L can be recognized by a pair of bands in region 37B that are located near the chromocenter and usually surrounded by unstructured chromatin. Additional landmarks for this arm are a light puffy area in region 39B-38A surrounded by two bands (region 39A, 38B).

3.4.2 A physical map for the *An. albimanus* genome

A physical mapping via FISH placed 24 of the 204 supercontigs included in the *An. albimanus* assembly hosted by Vectorbase. Due to a large N50 value for the *An. albimanus* assembly these 24 supercontigs were sufficient to assign ~98% of the genome to chromosomal locations. The largest supercontig, KB672286 (30.8 MB) covers nearly all of chromosomal arm 3L, from region 38C to 45A. Our Genome analysis and physical mapping identified and corrected a total of 13 misassemblies within 6 scaffolds. We propose that misassembled scaffolds be renamed using letters to denote different fragments originating from misassembly within a supercontig. For example, supercontig KB672435 (15.38 MB) was found to be composed of 3 misassembled fragments that localized to 2 places on 2R and one location on 2L. We have named these pieces KB672435**A** (3.38MB), KB672435**B** (7.09 MB), and KB672435**C** (3.72 MB). Our study found that all 13 physically mapped cases of misassembly are associated with physical gaps between genomic contigs that were erroneously bridged by a longer read. A summary of all identified and mapped misassembled supercontigs is provided in **Table 3.7.2.**

Using our proposed nomenclature where each misassembled fragment of a supercontig is counted as its own supercontig we have placed a total of 32 supercontigs **(Table 3.7.3)**. Euchromatic regions of chromosomal arms are well covered on our map with the exception of one gap on 3R in region 33A. Gaps also remain in the heterochromatic centromeres of arms X, 2R, 3R, and 3L. The sizes and numbers of supercontigs necessary to cover each arm varied considerably, even among arms of similar size. Arm 2L, for example, is nearly completely covered by 3 large scaffolds. In contrast, supercontigs comprising sequences of 3R are contained in 8 scaffolds (**Table 3.7.2, Figure 3.8.1**).

Six of the mapped scaffolds were predicted to be merged into larger scaffolds based on synteny data published in the supplemental materials of Neafsey *et al.,* 2015. We confirmed merging predictions on X, 2R and 3R (**Table 3.7.2, in red text**).

3.5 Discussion

This study developed a physical map for the genome of the dominant malaria vector in Central America, *An. albimanus.* To proceed with physical mapping we constructed a new cytogenetic map for the salivary gland polytene chromosomes of this mosquito. Although the original publication of the drawn chromosome map described banding patterns of *An. albimanus* chromosomes, in general this map was too simple to be used for physical mapping (Keppler et al., 1973). The photomap developed later for *An. albimanus* significantly improved the overall clarity of the chromosomes' structure [47] and allowed positioning of 17 DNA probes that were hybridized to the chromosomes using *in situ* hybridization. After the genome of *An. albimanus* was released, availability of this physical map allowed placement of 75%

of the genome to chromosomes [9]. However, the first cytogenetic photomap developed for *An. albimanus* chromosomes was not designed for large-scale physical genome mapping and this map hindered efforts for a more complete chromosomal assembly in this species. The cytogenetic photomap constructed in this study has two advantages that make it convenient for physical mapping applications. First, chromosomes are completely straightened and flattened, so that relative position of bands along the arm are not obscured. Second, major landmarks for arm recognition are described in detail, rendering identification of chromosomal arms much easier. This improved map allowed placement of 98% of the *An. albimanus* genome to the chromosomes resulting in the most complete physical genome map developed for any mosquito.

Our study supplements a classical molecular biology technique with computational approaches of the genomics era. The results demonstrate how bioinformatic approaches can work synergistically with physical mapping to efficiently map the largest supercontigs, systematically identify and correct misassembly, and fill gaps within genomes for higher quality assemblies. Misassemblies identified computationally certainly could have been identified using FISH alone but the process of identifying boundaries of the misassembly within supercontigs would have been much more time consuming. As chromosomal assemblies are developed for many more *Anopheles* species the predictive power of orthologous positions within related species will become an immensely powerful tool for the identification of genome misassembly.

The identification of misassembly within multiple supercontigs in the genome of *An. ablimanus* highlights the need for physical mapping to validate the accuracy of genome assemblies. All cases of misassembly were accompanied by physical gaps between contigs that were incorrectly bridged. The generation of the *An. albimanus* genome assembly made use of large insert mate pairs with inserts ranging from 38-40kb that assisted in assembly across repetitive regions within mosquito genomes[170]. Although large inserts were necessary to traverse repetitive regions these large inserts can introduce error into genome assemblies by the creation of chimeric mate pairs that unite random segments of sequence within the assembly[171-173]. Physical mapping will provide an essential quality control in the assembly of these genomes to the chromosomal level.

The availability of a genetic map for chromosome 2 allowed us to compare the order of scaffolds on physical map to the order of genetic markers published earlier (Penilla *et al.,* 2009). The analysis revealed a strong correspondence between the order of scaffolds on physical map and the microsatellites on the genetic map. The correspondence in position in centi-Morgans (cM) on the genetic map with the order of scaffolds on physical map has a strong linear relationship with R^2=0.8705. The correlation between position on the two maps is strong and positive with R=0.933 (**Figure 3.8.3, Table 3.7.4**). The position of 2 microsatellites, 0008, and 0125 reside in contradictory locations between our physical map and the cM distance indicated in the previous study (Penilla *et al.,* 2009). This disparity is most likely due to a lack of resolution near the telomere of 2R on the genetic map.

3.6 Conclusions

The genome map developed in this study for Neotropical malaria vector *An. albimanus* demonstrates the power of integrating cytogentic and physical mapping with sequence and synteny information from related species. Using this approach we were able to generate a high coverage physical map for *An. albimanus* that surpasses that of even the best studied malaria mosquito, *An. gambiae.* Additionally, our physical mapping efforts placed 13 fragments within 6 misassembled supercontigs highlighting the importance of physical mapping for accurate genome assembly. By drawing upon syntenic relationships in related species we were able to confirm that 6 supercontigs could be merged into larger supercontigs as predicted earlier (Neafsey *et al*, 2015). The ability to fill gaps in genome assemblies promises to assist in improving the accuracy of fixed inversion breakpoint identification in studies of chromosomal evolution and also facilitate the reconstruction of more accurate genome landscapes.

3.7 Tables

Table 3.7.1: Measurements and proportion of *An. albimanus* polytene chromosomes

Chromosome	X	2	3
Average length (µm)	58.6	412.2	322
Relative length (%)	7.4	52	40.6
Centromere position (%)	Not applicable	40.6	50

Table 3.7.2: Misassemblies within the *An. albimanus* genome- Six supercontigs were revealed as misassembled as a result of bioinformatic analysis and physical mapping. Bioinformatic comparison of orthologous position predicted 13 supercontig fragments and physical mapping identified two more for a total of 15 supercontig fragments. Physical mapping has confirmed the location of 13/15 fragments.

Supercontig	**Size MB**	**Boundary coordinates within original supercontig**	**Chromosomal location**
KB672397A	11,932,447	KB672397:1-11932447	2L: 23A-25A
KB672397B	5,005,411	KB672397:11932448-16937859	2R: 10C-11B
KB672397C	6,156,850	KB672397:16937860-23094710	2R: 9B-10B
KB672397D	922,501	KB673397:23094711-24017212	2R: 14C
KB672287A	2,751,045	KB672287: 2660-2755249	3R: 26A-26B
KB672287B	208,834	KB672287: 2890973-3099807	3R: 34A
KB672298A	426,296	KB672298: 1-426296	2R: 12A
KB672298B	2,440,770	KB672298: 455149-2895919	3R: 32A-32C
KB672435A	3,388,532	KB672435: 1- 3388532	2L: 16C-17A

KB672435B	7,093,667	KB672435: 3656459 - 10750126	2R: 12A-13A
KB672435C	3,720,697	KB672435:11658498 - 15379195	2R: 14C-15A
KB672468A	5,883,756	KB672468: 1-5883756	2R: 13C-14B
KB672468B	285,889	KB672468:5883757-6169646	NOT MAPPED
KB672353A	1,741,901	KB672353:1-1741901	2R: 15A-15B
KB672353B	103,535	KB672353:1741902-1845436	NOT MAPPED

Table 3.7.3: Sizes and chromosomal positions of *An. albimanus* supercontigs-The order and location of 32 physically mapped *An. albimanus* supercontigs. Positive orientation on X, 2R, and 3R is towards the centromere. Positive orientation on 2L and 3L is towards the telomere.

ARM	**LOCATION**	**Scaffold**	**Size**
X	1A-3A	KB672457	8,610,254
X	3A-3C	KB672404	1,315,522
X	3C-4A	KB672407	636,932
X	4A-4C	KB672406	778,592
2R	6A-9A	KB672446	9,735,467
2R	9B-10B	KB672397C	6,156,850
2R	10B-10C	KB672331	2,547,207
2R	10C-11B	KB672397B	5,005,411
2R	11C-12A	KB672320	2,643,688
2R	12A	KB672298A	426,296
2R	12A-13A	KB672435B	7,093,667

2R	13A-13C	KB672479	4,205,160
2R	13C-14B	KB672468A	5,883,756
2R	14C	KB672397D	922,501
2R	14C-15A	KB672435C	3,720,697
2R	15A	KB672409	300,361
2R	15A-15B	KB672353	1,845,436
2L	16C-17A	KB672435A	3,388,532
2L	17A-23A	KB672413	22,635,183
2L	23A-25A	KB672397A	11,932,447
3R	26A-26B	KB672287A	2,751,045
3R	26B-32A	KB672424	18,068,499
3R	32A-32C	KB672298B	2,440,770
3R	33A-33B	KB672309	2,815,218
3R	33C	KB672386	1,286,344
3R	34A	KB672287B	208,834
3R	34A-34B	KB672364	1,390,780
3R	34B	KB672405	851,493
3R	35A-35B	KB672375	1,459,936
3L	36A-37B	KB672398	1,248,850
3L	37B-38C	KB672342	1,994,720
3L	38C-45A	KB672286	30,179,321

Table 3.7.4: Correspondence of *An. albimanus* physical map with previously published genetic map-Microsatellite sequences were aligned to the *An. albimanus* genome hosted on Vectorbase.org.

Chromosome (Genetic Map)	**Microsatellite**	**Position (cM)**	**Scaffold**	**Chromosome (Physical Map)**	**Order Agree?**
2	0025	0	KB672**397A**	2L	Yes
2	0125	10	KB672**397A**	2L	No
2	0128	13	KB672**413**	2L	Yes
2	0108	25	KB672**413**	2L	Yes
2	*Ebony*	28	KB672**413**	2L	Yes
2	0114	38	KB672**413**	2L	Yes
2	0034	46	KB672**413**	2L	Yes
2	0038	56	KB672**468**	2R	Yes
2	0113	73	KB672**435B**	2R	Yes
2	0032	86	KB672**298A**	2R	Yes
2	0100	92	KB672**320**	2R	Yes
2	0117	106	KB672**397B**	2R	Yes
2	0008	111	KB672**446**	2R	No
2	0135	116	KB672**397B**	2R	Yes
2	0109	124	KB672**397B**	2R	Yes

3.8 Figures

Figure 3.8.1: A typical salivary gland nucleus from *An. albimanus*- Chromosome arm names are indicated at each telomere. The chromocenter is labeled *CC*.

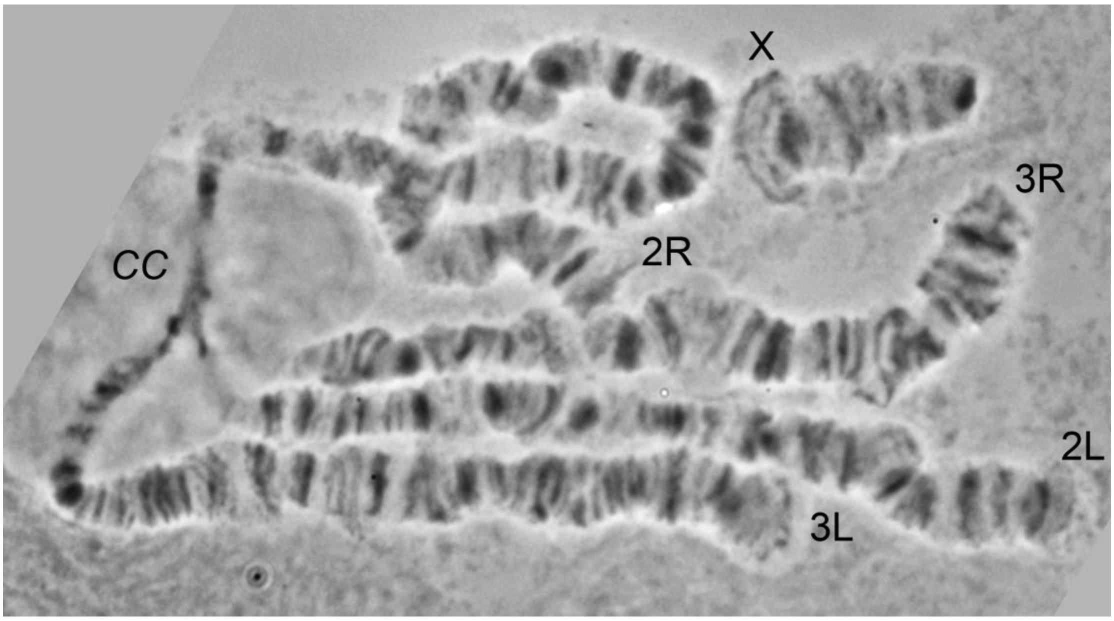

Figure 3.8.2: A physical map for *An. albimanus*- Scaffold names are indicated above each chromosome. Orientation of scaffolds is shown by arrows. Misassembled scaffolds originating for single scaffolds in the assembly are indicated by a scaffold name followed by a capital letter.

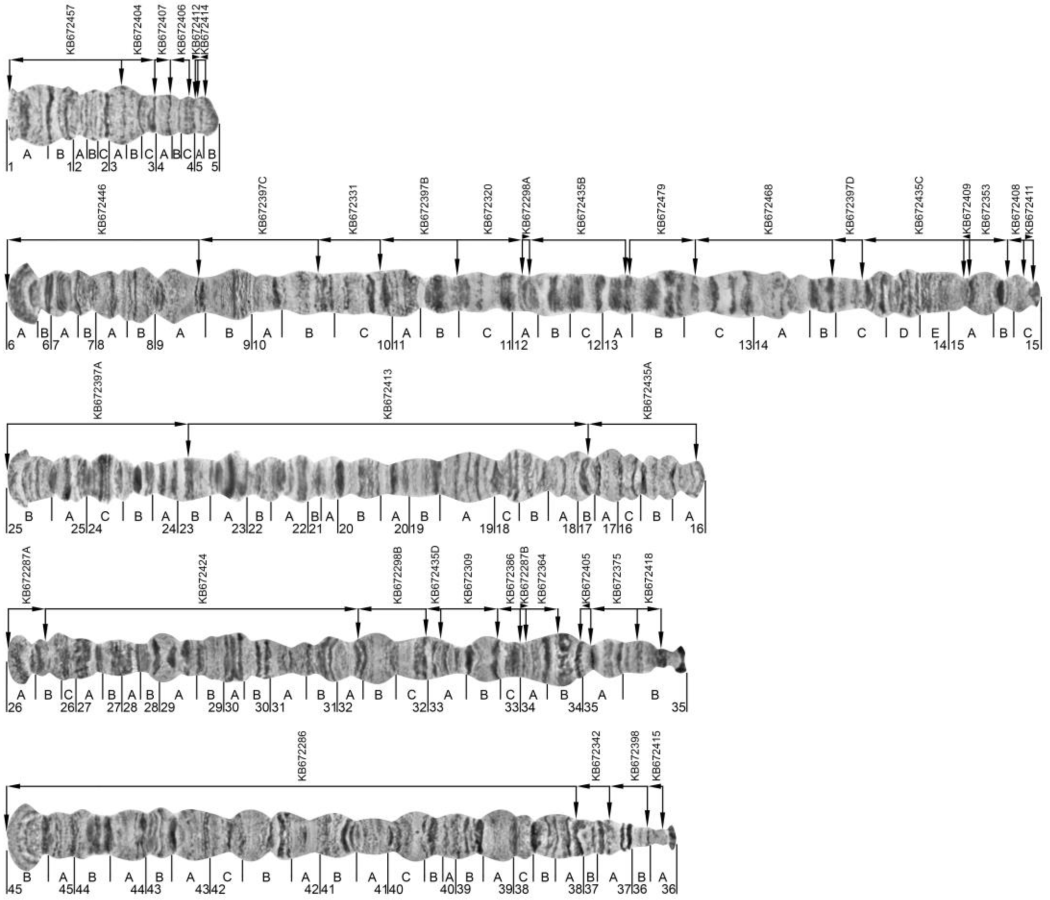

Figure 3.8.3: A comparison of genetic and physical maps for chromosome 2- The genetic map adapted from Penilla et. al, 2009 is compared to our physical map for chromosome 2. The maps correspond nearly completely with the exception of microsatellite marker 0008 and 0125.

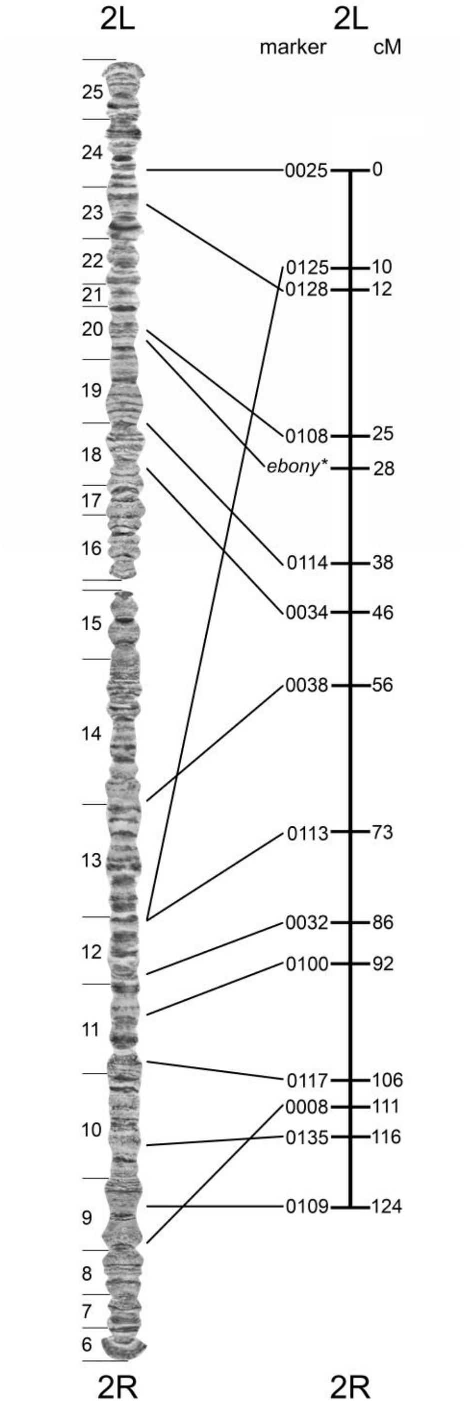

Chapter 4: Insights into rates and mechanisms of chromosomal evolution in *Anopheles* from multi-species genomic analysis.

4.1 Abstract

Until recently, a lack of well assembled genomes hindered genome evolution studies in *Anopheles* species; however recent sequencing efforts and the combined power of computational and physical mapping approaches have yielded several assemblies which are suitable for whole genome comparison. In this work, we present an improved chromosomal assembly for *An. stephensi,* identified species specific fixed chromosomal inversion breakpoints, and explored the repeat content of inversion breakpoint regions. We found that the sex chromosome is evolving the fastest in all species and it also contains significantly more transposable elements (TEs) tandem repeats (TRs) and inverted repeats (IRs) in all species. Our results indicate unique distributions of TEs, and TRs in the genomes of *An. dirus, An. gambiae, An. minimus* and *An. stephensi.* The densities of repeats vary by chromosomal arm, however TEs were consistently overrepresented in the breakpoint regions of all species. Correlations between repeat coverage and the rate of chromosomal breakage indicates that repeats may be contributing differently to evolution on different chromosomal arms. These findings demonstrate high rates of chromosomal evolution in mosquitoes and provide the ground work for further investigation into mechanisms and biological significance of genome rearrangements. Additionally, genome assembly improvements and the identification of evolutionarily conserved blocks will aide in the search for novel candidates for genetic control strategies of disease vectors.

4.2 Introduction

Insect adaptation for blood-feeding on humans is a relatively rare occurrence, but this behavior imparts resounding consequences for the human race. Although only about 100 of the ~10,000 described species who blood feed do so preferentially on humans, the recent upsurge in mosquito borne diseases such as Zika and chikungunya showcase the social and economic effects of vector borne disease[174, 175]. In better studied mosquito borne diseases such as malaria and dengue, mosquito vectors are rapidly evolving metabolic and behavioral mechanisms for counteracting chemical means of mosquito control[176-178]. The rapid evolution and capacity of disease vectors to adapt leaves governments and public health agencies in great need of new tools and a better understanding of how mosquitoes are adapting to overcome existing control strategies.

Previous work has demonstrated a rapid rate of chromosomal evolution in Dipteran genomes as evidenced by the extensive reshuffling of genes that takes place even between very closely related species[42, 179]. It is also clear that rates of evolution are not uniform throughout the genome[9, 50, 62, 66]. The molecular basis of non-uniform rates of evolution as of yet remains poorly understood, but the investigation of specific inversion breakpoints in *Drosophila* and *Anopheles* have found inverted repeats (IRs), tandem repeats (TRs), segmental duplications (SDs), and the vestiges of transposable elements (TEs)[69, 125, 180, 181]. The presence of these repeat sequences in inversion breakpoints potentially aids in ectopic recombination or double stranded break (DSB) formation, and suggests a possible role for these repeats in the genesis of chromosomal inversions.

In *Drosophila*, analysis of 29 interspecific chromosomal breakpoints revealed that inverted duplications of genes rather than repetitive sequences were more common in breakpoint regions suggesting that staggered breaks were the most common mechanism for inversion genesis[79]. A subsequent study investigating two models for genome evolution, “fragile regions” and “functional constraints” concluded that some combination of the two forces was at work in shaping genome evolution of *Drosophila* species with fragile regions being more common especially on the sex chromosome[66]. Other work in *D. mojavensis* supports multiple mechanisms of breakpoint genesis including ectopic recombination between inverted stretches of non-repetitive DNA, and possible fragile regions[181].

In mosquito species, Xia et al. explored whether arm specific differences in inversion frequency are correlated with differences in the genomic landscape of each chromosomal arm. They explored this hypothesis using comparative mapping of *An. gambiae* and *An. stephensi,* and applied Bayesian statistical models to analyze the genomic landscape of individual *An. gambiae* chromosomal arms. Their results indicated that differences in chromosomal arm content with respect to repeats, genes, and scaffold/matrix associated regions (S/MARs) likely contribute to the differences in inversion fixation rate and rates of evolution observed between different arms[50]. Later work by Sharakhova et al., compared gene order in *An. gambiae, An. stephensi* and *An. funestus* and demonstrated that different chromosomal arms exhibit varying tolerance to gene disruption, and that chromosomal inversions tend to capture similar sets of genes in species facing similar environmental pressure[49]. This study demonstrated that the fastest evolving 2R autosomal arm was enriched with gene blocks conserved between only a pair of species. In contrast, all identified syntenic blocks were preserved on the slowly evolving 3R arm of *An. gambiae* and on the homologous arms of *An. funestus* and *An. stephensi*. These works represent the first investigation into the molecular context for chromosomal evolution in *Anopheles.* With genomic data now available for many more species, analysis of *Anopheles* patterns of evolution is now possible on a much greater scale.

Because syntenic relationships between species can be leveraged to detect misassembly and further assemble related genomes, the availability of many mosquito genomes empowers the vector biology community in ways that were not previously possible[182]. More complete genome assemblies can be utilized to investigate evolutionary processes or for fine scale interrogation of the genetic factors controlling epidemiologically important traits. Additionally, well assembled genomes ease the development of genetic tools for mosquito control and vector borne disease prevention.

Recent, concerted efforts to sequence and assemble the genomes of many medically and agriculturally important arthropods have provided a wealth of genome data that can be used in comparative genomics studies and allow patterns of evolution to be discerned. Efforts by individual researchers and collaborative efforts such as the *Anopheles* 16 Genomes consortium (AGC) have produced the genomes of more than 20 vector and non-vector *Anopheles* species. Comparative genomic studies of these genomes have already begun to bear fruit and shed light on patterns of genome evolution in *Anopheles*. By utilizing gene order information from 6 physically mapped *Anopheles* species the AGC has confirmed and established several principles of chromosomal evolution of malaria mosquitoes:

A) Genes shuffle extensively within chromosomal arms and arm association changes occur as the result of whole arm translocations rather than the fission or fusion of arms as seen in *Drosophila* (see figure from supplementary material of *Neafsey* et al. below:)

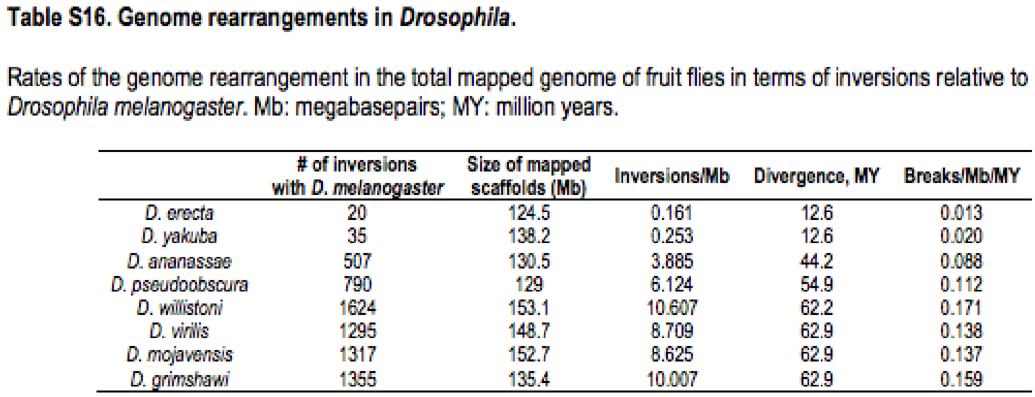

Table S16. Genome rearrangements in *Drosophila*.

Rates of the genome rearrangement in the total mapped genome of fruit flies in terms of inversions relative to *Drosophila melanogaster*. Mb: megabasepairs; MY: million years.

	# of inversions with *D. melanogaster*	Size of mapped scaffolds (Mb)	Inversions/Mb	Divergence, MY	Breaks/Mb/MY
D. erecta	20	124.5	0.161	12.6	0.013
D. yakuba	35	138.2	0.253	12.6	0.020
D. ananassae	507	130.5	3.885	44.2	0.088
D. pseudoobscura	790	129	6.124	54.9	0.112
D. willistoni	1624	153.1	10.607	62.2	0.171
D. virilis	1295	148.7	8.709	62.9	0.138
D. mojavensis	1317	152.7	8.625	62.9	0.137
D. grimshawi	1355	135.4	10.007	62.9	0.159

Table S16 from supplementary material of From Neafsey, D.E., et al., *Mosquito genomics. Highly evolvable malaria vectors: the genomes of 16 Anopheles mosquitoes.* Science, 2015. **347**(6217): p. 1258522. Reprinted with permission from AAAS.

B) Conserved gene order deteriorates very rapidly within chromosomal arms

C) Rates of evolution vary by chromosomal arm with the sex chromosome (e1) evolving the fastest and e4 exhibiting the slowest rate of change across 4 species

D) *Anopheles* sex chromosomes exhibits a greater propensity for gene loss than the autosomes

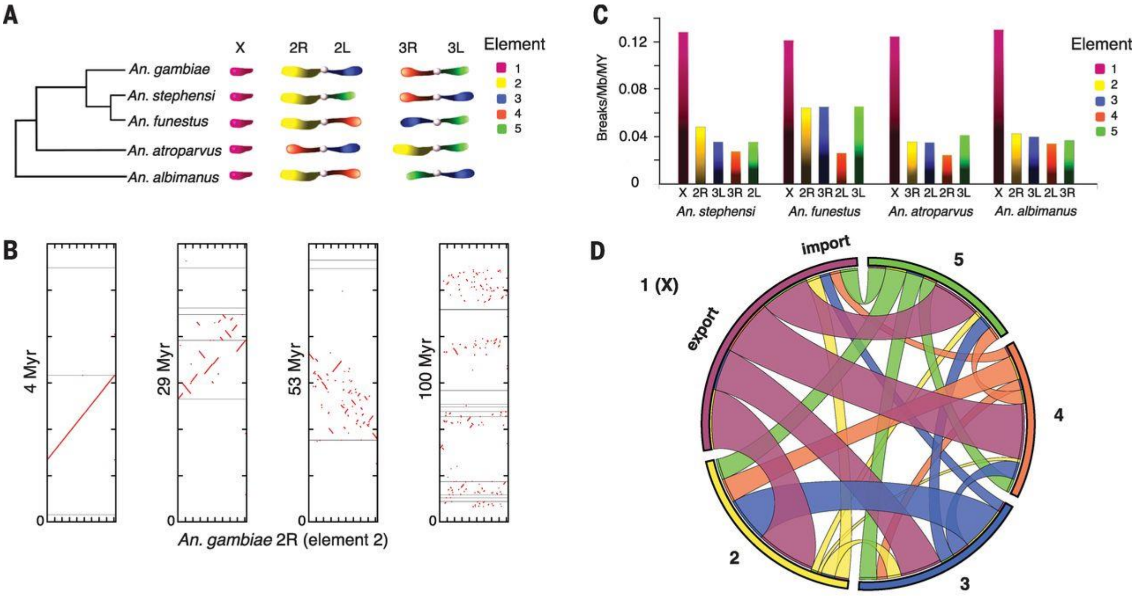

From Neafsey, D.E., et al., *Mosquito genomics. Highly evolvable malaria vectors: the genomes of 16 Anopheles mosquitoes.* Science, 2015. **347**(6217): p. 1258522. Reprinted with permission from AAAS.

Despite being based on fragmented chromosomal assemblies (~40% *An. stephensi, An. atroparvus; ~35% An. funestus*) the findings and multi-discipline approach of this study have provided a strong foundation for both the current work and future exploration of mosquito genomics.

Since the completion of the *Anopheles* 16 genomes project the combined approaches of bioinformatics and physical mapping have continued to improve the chromosomal assemblies of *Anopheles* species. Currently, *Anopheles gambiae, An. stephensi, An. atroparvus,* and *An. albimanus* possess relatively complete assemblies (~80% or greater) with both physical mapping and bioinformatic support[44, 183](Artemov et al, in preparation, Artemov and Peery et al, in preparation). Computational approaches have constructed high coverage predicted genomes for two more species, *An. dirus* and *An. minimus.* Collectively these six species represent malaria vectors from 4 continents and more than 100 million years of evolution.

In the current work we combine this profusion of physical mapping information with new algorithms which permit the identification of synteny/loss of synteny based on multiple species alignments rather than simple pairwise comparisons to *An. gambiae* which were employed in the 2015 publication. These new resources allow for greater confidence in our study of rearrangement rates in *Anopheles.* Additionally, this study leverages syntenic relationships to identify misassembly for the improvement of genome assemblies in multiple malaria mosquitoes. Finally, we further expand upon the foundation of the *Anopheles 16 Genomes* project to dissect the repeat content of species specific fixed chromosomal inversion breakpoints and investigate arm specific dynamics of genome evolution.

4.3 Results

4.3.1 Identification of genome misassemblies

As shown in **Table 4.6.1**, 16 misassemblies were detected (eight in *An. albimanus*, one in each *An. atroparvus*, *An. epiroticus*, *An. farauti* and five in the *An. stephensi* SDA strain). For *An. albimanus*, we compared the predicted misassemblies with the verified misassemblies identified from physical mapping (**Table 4.6.2** and Supplementary Information: **Albimanus_physical_map.pptx**). All misassemblies that fused regions on different chromosomal elements into one scaffold were included by the HMM prediction. However, this method cannot identify misassemblies that merged regions on the same chromosomal element, such as KB672287A and KB672287B. For *An. stephensi* SDA strain, the five misassemblies were verified by comparing with the gene order in the *An. stephensi* Indian strain. The other misassemblies need to be verified by additional physical mapping. In fact our physical mapping determined that scaffolds KB672353 and KB672375 are broken by real pericentric inversions, not by misassembly (Supplementary Information: **Supplementary figure 1**). The accuracy of the physical mapping was confirmed by the comparison of the order of markers on chromosome 2 between genetic and physical maps of *An. albimanus* (Supplementary Information: **Genetic_map-vs-Physical_map-Albimanus.jpg**).

4.3.2 Scaffolding genomes based on conserved syntenic segments and genome rearrangement

By studying the gene orders of one-to-one orthologs between each pair of genomes, the evidence showing how scaffolds are linked (Supplementary Information: **Linkage Inference.xlsx**) was obtained. **4.6.1** shows the scaffold linkage information of the *An. stephensi* Indian strain inferred from the *An. stephensi* SDA strain. In total, 125 linkages were identified. Combined with additional 66 linkages inferred from other species, five large chains of scaffolds were built, which represented the five chromosomal arms. The inference of linkages from other species is under the assumption that the synteny is conserved at the linkage site. However, if chromosomal rearrangement occurs at the linkage site, the inference will be invalid. Therefore, additional physical mapping is necessary to check the linkages.

4.3.3 Genome rearrangement analysis

Table 4.5.1 shows the number of one-to-one orthologs identified for each chromosomal element. 1721 synteny blocks composed of 6166 single-copy orthologs were identified. The detailed information about orthologs and synteny blocks is presented in Supplementary Information: **Synteny Block Analysis.xlsx**. Genome rearrangements were evaluated both at the whole genome scale and at the individual chromosomal level. Rearrangement rates were calculated as the number of rearrangements per thousand genes per million years (**Figure 4.6.2**). We used the number of genes instead of Mb in the rearrangement analysis because the same number of orthologs was identified in all species. However, the sizes of the fasta files that represent the arm lengths in each species vary. Therefore, if we want to calculate rate per Mb, we should use only one species such as *An. gambiae* as reference or the average of all species. Two different divergence times estimated from previous publications were used for the calculation:

(1) from Table S13 of Neafsey et al 2015 Science:

An. albimanus diverged from *An. gambiae, An. atroparvus, and An. stephensi* - 100 MYA

An. atroparvus diverged from *An. gambiae* and *An. stephensi* - 58 MYA
An. gambiae diverged from *An. stephensi* - 30.4 MYA

(2) from Figure S10A of Neafsey et al 2015 Science:
An. albimanus diverged from *An. gambiae, An. atroparvus,* and *An. stephensi* - 100 MYA
An. atroparvus diverged from *An. gambiae* and *An. stephensi* - 80.3 MYA
An. gambiae diverged from *An. stephensi* - 41.5 MYA.

The Fontaine et al 2015 paper reports much smaller divergence times for *An. epiroticus* and *An. christyi* than those proposed in Figure S10A of Neafsey et al 2015 Science. The X chromosome showed significantly higher evolution rate over time compared with the autosomes.

4.3.4 Physical mapping and confirmation of gluing predictions in *An. stephensi* Indian strain

Physical mapping allowed us to place probes from 36 supercontigs which were not previously mapped for a total of 124 (122 on map) supercontigs mapped in this species. The newly mapped probes added 39.78 MB to the mapped genome of *An. stephensi* and bring the total mapped genome for this species to 176.375 MB or ~79.6%. (**Figure 4.6.4**). This level of coverage, while still less than *An. gambiae* and *An. albimanus,* was considered sufficient for whole genome comparisons.

Physical mapping demonstrated large scale agreement between our mapped order of supercontigs and the order predicted by gluing. Glued and mapped positions of supercontigs agree in 108/115 supercontigs that were common to both procedures. The 7 conflicts between the two procedures occur on X, 2R and 2L. On X, supercontigs 00142 and 00015 are in opposite order in mapped vs. predicted location. On 2R, 00077 and 00149 are in reversed order on the physical map. On 2L, two groups of supercontigs are in an inverted order on the physical map relative to gluing predictions: 00049, 00030, 00028 and 00085, and 00043, 00093, and 00066. There are 3 inconsistencies in the predicted orientation of supercontigs vs their mapped orientation. Supercontigs 00034 (2L), 00044 (2L), 00025 (3R) all have a mapped orientation opposite that predicted by gluing. **(Figure 4.6.4: Physical Map for *An. stephensi,* Table 4.5.3: Mapped supercontigs in *An. stephensi*)**

4.3.5 Transposable Elements

Transposable element coverage varied between species and between chromosomal elements within species. Of the 4 species considered, *An. gambiae* was by far the most repeat rich with an average of 9.66% TEs/100kb. The *An. stephensi* genome possessed an average of 3.46% TEs per 100kb while *An. minimus* and *An. dirus* were far more modest at an average of 2.23% and 1.53% TEs per 100kb respectively. These differences in mean %TEs were statistically significant according to a one-way ANOVA at the p< .05 level [F(3, 8074) = 826.12, p<.0001]. **(Figure: 4.6.2; Table 4.5.2)**

Based on previous data we expected to see clear differences in %TE of the sex chromosome (e1) vs. the autosomes. Our results demonstrate this trend in all species except *An. stephensi* where the e5 (M=4.503, SD=3.36) has a mean %TEs that is not statistically different from e1 (M=4.901, SD= 3.42), according to a post-hoc comparison by a Tukeys HSD test. If all autosomes are pooled however, the average % TEs in autosomes is lower than that of e1 (one-way ANOVA at p<.05 [F(1,1895)=35.50, p<.0001]).

Autosomal elements of all species clustered into 2 or 3 groups when tested for statistically significant differences in mean %TEs. In *An. gambiae,* autosomes e3, e4, and e5 all had similar means while e2 clustered alone with significantly lower %TEs (Tukeys HSD, e3(M=9.661, SD=10.82), e4(M=8.581, SD=8.35), e5(M=9.604, SD=10.07), e2(M=7.343, SD=8.68)). In *An. stephensi,* mean %TE of e2 was significantly lower than e4, but the mean of e3 did not differ from the either e2 or e4 (Tukeys HSD, e2(M=2.698, SD=2.34), e4(M=3.34, SD=3.082), e3(M=3.109, SD=2.95)). In *An. dirus,* the sex chromosome clustered alone with the highest mean %TEs (e1(M=3.184, SD=2.70)). Element 5 had significantly greater % TEs relative to the other autosomes but not as high as that seen in e1(e5(M=1.623, SD=1.70)). Element 4 clustered alone with the lowest %TEs while e2 and e3 were similar to both e4 and e5 in terms of mean %TEs (e4(M=1.266, SD=1.63), e2(M=1.339, SD=1.59), e3(M=1.336, SD=1.40)). *Anopheles minimus* autosomes clustered into 3 groups: e5 had the highest mean %TEs (e5(M=2.622, SD=2.27). Element 3 had lower % TEs than e5 and e2 but higher than e4 which had substantially lower mean %TEs relative to the other autosomes (e3(M=2.144, SD=2.16), e2(M=2.483, SD= 2.22), e4(M=.6301, SD=.560)). Mean %TEs of e2 was similar to both e5 and e3(**Figure 4.6.3; Figure 4.6.4; Table 4.5.3)**

4.3.6 Inverted repeats in 4 species

The inverted repeat content in *An. dirus, An. gambiae, An. minimus,* and *An. stephensi* was very low, at least an order of magnitude lower than the coverage of tandem repeats and 2 orders of magnitude lower than transposable elements. Even at these very low coverages the *An. gambiae* genome contains the greatest coverage of IRs (.042%) followed by *An. dirus* (.023%) while *An. minimus* (.009%) and *An. stephensi* (.006%) were similar in terms of IRs and no statistically significant differences were detected between these two species (One-way ANOVA [F(3,8074)=101.1, p<.0001], Tukeys HSD *An. gambiae* (M=.041, SD=.112), *An. dirus* (M=.023, SD=.067), *An. minimus* (M=.008, SD=.036), *An. stephensi* (M=.005, SD=.047)).

When considering possible differences between the chromosomal elements within each species our analysis revealed that the sex chromosome contains the greatest coverage of IRs in all species. A post-hoc Tukey HSD test finds significant difference in mean %IRs in *An. dirus* and *An. gambiae* e1 vs the autosomes, but no differences between e1 and the autosomes in *An. stephensi* (*An. dirus* e1(M=.0451, SD=.093, *An. gambiae* (M=.0965, SD=.186)). In *An. minimus* e5 was similar to both e1 and other autosomes (*An. minimus* e1(M=.0200, SD=.053), e5(M=.0115, SD=.039)). There were no differences between autosomes in *An. dirus, An. gambiae* and *An. stephensi* but minimus autosomes clustered into 3 overlapping groups (*An. minimus* (e2(M=.0074, SD=.035), e3(M=.0092, SD=.037), e4(M=.0027, SD=.017)). **(Figure 4.6.3; Figure 4.6.4; Table 4.5.3)**.

4.3.7 Simple tandem repeats in 4 species

Simple tandem repeats were present in the genomes of *An. dirus, An. gambiae, An. minimus* and *An. stephensi* at lower coverage than TEs; a one-way ANOVA detected significant differences between each of the four species [F(3,8074)=390.69, p>.0001]. *Anopheles gambiae* had the greatest average coverage of TRs (M=1.28%, SD= 1.73) followed by *An. dirus* (M=.713%, SD=.66), *An. stephensi* (M=.393%, SD=.28) and *An. minimus* (M=.328%, SD= .37). **(Table 4.5.2)**

A post-hoc Tukeys HSD test demonstrates that the sex chromosome harbors greater average coverage of TRs compared to the autosomes in all 4 species. Average coverage of TRs on the autosomes varied by species. *Anopheles gambiae* presented no statistically significant differences between autosomes while mean %TRs in *An. dirus, An. minimus* and *An. stephensi* autosomes clustered into 2 statistically different groups.(*An. gambiae* e1(M=2.492, SD=1.15), e2(M=1.013, SD=1.18), e3(M=1.161, SD=1.24), e4(M=1.206, SD=2.49), e5(M=1.193, SD=1.75)), (*An. dirus* e1(M=1.618, SD=1.00), e2(M=.6149, SD=.348), e3(M=.6143, SD=.471), e4(M=.5854, SD=.363), e5(M=.7302, SD=.942)), (*An. minimus* e1(M=.6072, SD=.447), e2(M=.3133, SD=.329), e3(M=.3434, SD=.428), e4(M=.2076, SD=.262), e5(M=.3059, SD=.346)), (*An. stephensi* e1(M=.6808, SD=.331), e2(M=.3553, SD=.262), e3(M=.3689, SD=.233), e4(M=.3390, SD=.213), e5(M=.4139, SD=.344)) **(Table 4.5.2; Figure 4.6.4)**

4.3.8 Comparison of breakpoints to the whole genome

Our hypothesis posits that repeats such as transposable elements, simple tandem repeats and inverted repeats increase the fragility in regions of the genome where they accumulate and thus increase the likelihood of chromosomal breakage, misrepair of double stranded breaks (DSBs) and inversion formation. With that hypothesis we expected to see greater coverage of TEs, TRs and IRs in breakpoint regions relative to the rest of the genome. Our results demonstrate this trend for TEs, but a less straight forward relationship between TRs and IR content in breakpoint regions **(Table 4.5.4)**.

We compared the average coverage of TEs, IRs, and TRs in breakpoint regions and the whole genome in 4 species. The average coverage of TEs was at least 1.9X greater in breakpoint regions relative to the rest of the genome and these differences were statistically significant in *An. dirus, An. gambiae, An. minimus* and *An. stephensi.* Significant differences in tandem repeats were also observed in all species. The average density of simple tandem repeats was 1.6x and 2.4x higher in *An. gambiae* and *An. stephensi,* respectively, but ~1.5x lower in breakpoint regions of *An. dirus* and 1.6x lower in *An. minimus.* Inverted repeats were overrepresented in the breakpoints of *An. stephensi* and underrepresented in breakpoint regions of *An. dirus* and *An. minimus. Anopheles dirus* breaks contained 4x less inverted repeats on average than the rest of the genome. Breakpoints of *An. minimus* were entirely devoid of inverted repeats. The average density of IRs in breakpoints of *An. gambiae* were not significantly different from the whole genome.

4.3.9 Rates of inversion in *Anopheles*

To assess possible differences in the rate of inversion of different chromosomal arms we pooled the rate of inversion for each chromosomal arm across *An. albimanus, An. atroparvus, An. gambiae, An. stephensi* and *An. minimus.* We then used a one-way ANOVA followed by a Tukey HSD test [F (4, 20) =8.89, p<.0003]; (e1(M=3.328, SD=1.57), e2(M=.924, SD=.428), e3(M=.836, SD=.402), e4(M=.826, SD=.55), e5(M=.792, SD.575). This test divides the mean rate of evolution for chromosomal elements into 2 groups. The sex chromosome clusters alone in one group while all autosomes are pooled in a second group. These results indicate that the sex chromosome is evolving at different rate than the autosomes. **(Table 4.5.5)**

4.3.10 Correlation of Repeats with Rate of Chromosomal Breakage

We correlated the rate of chromosomal breakage with the mean coverage of TEs, TRs and IRs for each chromosomal arm in *An. gambiae* and *An. stephensi* **(Table 4.5.6)**. In *An. gambiae*, if all chromosomal arms are considered then we observe strong positive correlations with all repeat types. To determine if any chromosomal arm was biasing our correlations we repeated the analysis removing each chromosomal arm one at a time. The strong positive correlation persists unless the sex chromosome is excluded from the analysis. These results suggest that the high coverage of repeats and fast rate of evolution on e1 account for most of the the observed positive correlation. To determine if any one autosome was responsible for the negative correlations observed we repeated the analysis excluding e1 and each of the autosomes one at a time. In the absence of e1 and e2 correlations between rate of chromosomal breakage and mean coverage of repeats becomes positive for all repeat types indicating that e2, with the highest rate of autosomal breakage and among the lowest coverage of repeats, was responsible for much of the negative correlation. Although the correlation coefficients become positive with the exclusion of e1 and e2 the correlation between rate of breakage and the different repeat types are not particularly strong suggesting that these repeats do not explain much of the variation in rate of breakage for e3, e4, or e5 in *An. gambiae.*

In *An. stephensi,* correlations between rate of breakage and coverage of repeats with all chromosomal arms reveal strong positive correlations between rate of breakage and the mean coverage TRs and IRs but only a weak positive correlation is observed for %TEs. Removal of e1 from that analysis changes the correlation values for all repeat types to negative values. As in *An. gambiae*, it appears that the high coverage and high rate of breakage on e1 accounts for most of the positive correlations between rate of chromosomal breakage and coverage of these repeat types. The weak positive correlation between %TEs and the rate of breakage (.48) for all chromosomal arms appears to result from the effects of e5. Removal of e5 changes the correlation value to a strong positive .87. This effect of e5 is most likely due to the low rate of breakage on e5 and the high coverage of TEs on this arm. In *An. stephensi*, the mean %TEs of e5 is not statistically different from e1, however, the rate of chromosomal breakage on this arm is much lower than e1. Removal of e1 and e5 from the correlation analysis produces a strong positive correlation (.74) between the rates of breakage and mean %TR in e2, e3, and e4. These results could suggest differing roles of tandem repeats on e5 relative to the other autosomes.

4.4 Discussion/Conclusions

At present, many genomes are being published as unfinished collections of supercontigs and the applications of genomes in this state are limited. Computational tools such as the syntenic scaffolding described here is an invaluable tool that promises to increase the coverage of genome assemblies and permit further study of genome evolution and chromosomal landscapes that are not otherwise possible. Although our computational approach for genome assembly to the chromosomal level requires further validation, the high level of agreement between predicted and mapped supercontig order in *An. stephensi* suggests that this method can help bring unfinished genomes to a level of completion that is more useful to the scientific community. Additionally, computational predictions of genomic misassembly can be combined with physical mapping to speed the process of chromosomal assembly and yield more accurate genome assemblies. More accurate genome assemblies in turn will assist in identification of novel gene targets and position effects of transgene insertions.

Our results reveal striking differences in the dynamics of sex chromosome vs. autosome evolution in the genus *Anopheles*. The chromosome is rearranging more than three times as quickly as the autosomes in all species and this faster rate of chromosomal rearrangement corresponds with our hypothesis of much greater densities of TEs, TRs and IRs on e1 contributing to chromosomal rearrangement. Because of the disproportionate contribution of sex chromosomes to hybrid incompatibility and speciation, extensive shuffling of genes underscores the potential capability for malaria mosquitoes to evolve and further differentiate into new species[184-186].

The vastly excessive accumulation of repeats on the sex chromosome coupled with high rate of gene loss points to a “heterochromatization” of the sex chromosome in *Anopheles[170]*. A lack of recombination between the X and the Y could explain both the accumulation of repeats and the loss of genes from e1, and indeed most evidence suggests that the X and Y do not recombine though occasional exchange of genetic material has been postulated in *An. gambiae* and few other *Anopheles* subgenera[187-190]. This pattern of occasional recombination would do very little to prevent the accumulation of repeats resulting in the high rates of rearrangements on e1.

Our arm by arm correlation analysis provides clues that different repeat types could contribute to arm specific mechanisms of breakage. Given that mosquito chromosomal arms remain intact over evolutionary time, displaying no partial arm translocations or pericentric inversions, the possibility of distinct mechanisms for breakage is not unexpected. In *An. gambiae*, we find that the negative correlation between rate of breakage on autosomes and %TEs is due to e2. Despite the fast rate of breakage this arm has a lower coverage of TEs. Its possible that other molecular features with recombinogenic power, such as segmental duplications, populate the breakpoint regions of e2. Previous work and recent studies are highlighting the recombinogenic effect of segmental duplications (SDs) in the genomes of human, primates and fruitflies [191-193]. Xia et al found that segmental duplications are present in higher proportions on the fastest evolving autosomes: 2R and 3L of *An.*

gambiae. The coverage of SDs on these arms was in even higher proportions then on the sex chromosome. Further studies should be able to delineate if SDs co-occur with higher rates of evolution on autosomes of other mosquito species.

In *An. stephensi* e5 accounts for the negative correlation between %TRs and rate of breakage in autosomes. Removal of this arm from the analysis yields a strong positive correlation (.749) for the rate of breakage in e2, e3, and e4 and the coverage of TRs. Tandem repeats are significantly higher in break points of *An. stephensi* so these elements may be playing a major role in the evolution of e2, e3, and e4 but not e5.

The negative correlation between coverage of TEs and rate of autosomal breakage is contradictory to our finding of greater coverage of TEs in breakpoints of all chromosomal arms in all species that we considered. There are several possible reasons for this apparent contradiction in our data. One possible explanation involves the important distinction that not all TEs are capable of causing DNA DSBs. A finer analysis is necessary to determine if the TEs present within the breakpoints are actually capable of generating the DNA DSBs that are necessary for the formation of chromosomal inversions. A more detailed analysis of the TEs within breakpoints may remove repeats that mislead our correlations.

Another explanation for the contradiction in our results could be that TEs do not actually relate to the induction of chromosomal breakage. A correlation does not indicate causation and the co-localization of TEs with other features that encourage breakage or misrepair could lead to spurious correlations. In yeast, strong correlations between origins of replication, tRNAs and Ty elements and LTRs and rearrangement sites have been established. These different features co-localize within the yeast genome so it is entirely possible that one or two of the features encourage genomic rearrangement and the others have accumulated in the repair process but have no role in genomic instability[194]. Although yeast and mosquitoes are very different organisms a similar confounding effect of TEs with other true causes of chromosomal fragility is possible. The erosion of TE sequences over time further complicates the untangling of TEs as a cause or effect of genomic instability. Our analysis only allows investigation of inversion breakpoints as they exist in the present. However, if further analysis of TEs in recently derived inversion breakpoints revealed young, intact TEs that are still active and capable of causing breakage then this might provide stronger implication of the role of TEs in inversion generation.

This study has considered fixed chromosomal inversions that distinguish different species. The fixation of chromosomal inversions, however, is the result of two processes: the generation of inversions through chromosomal breakage and misrepair, and the selection of those inversions that leads to their eventual fixation in different species. Chromosomal inversions change the order of genes along segments of the chromosome and this activity can lead to differential expression of genes in individuals with different chromosomal arrangements[195]. Evidence for the effect of chromosomal inversion on gene expression are documented in yeast, human, and mosquitoes, and the variation between alternative inversion karyotypes provides phenotypic deviation that natural selection can act on[196-198]. The dual processes of breakage and selection that are responsible for producing the inversions considered in this study have likely each played a role in the the rates of inversion for each chromosomal arm. With this in mind, the observed differences in rate of inversion between the chromosomal arms could result from greater propensity for breakage or greater effects of selection on some arms than others. Our study focuses only on factors related to chromosomal breakage and cannot comment on the differential effects of selection on each arm.

Although this work has focused primarily on the breaks in synteny that occur during speciation there is also quite a lot that can be learned from the conserved regions of mosquito genomes. Highly conserved blocks of genes that have remained uninterrupted over long periods of evolutionary time are thought to be preserved in a particular order to maintain essential functions within an organism's genome. These so called "ultra conserved regions" are present in very distantly related taxa such as birds, mammals, and fish and, are often related to essential functions such as development[199]. Because of their vital function, ultra conserved genes could be good targets for genetic control strategies as changes to these genes would be expected to have detrimental impact to the organism. Evolutionarily conserved blocks of genes were identified in *Drosophila* species as part of a study of genome evolution and these syntenic blocks were presumably maintained by "functional contraints" [66]. The researchers subsequently disrupted one of these ultra conserved regions by an engineered chromosomal inversion but found no detrimental effect to the organism's fitness[67]. The modified organisms did display some different responses to volatile chemicals so it is unclear if these differences could translate to a reduction in fitness outside of the lab.

Our study which has localized evolutionarily conserved blocks and sites of genomic rearrangement within the genomes of malaria mosquitoes provides the ground work for further exploration of evolutionary dynamics in *Anopheles* mosquitoes. Further study promises to elucidate the role of different classes of interspersed repeats in shaping malaria vector genomes. Upon completion of sequencing and assembly of multiple *Culex* and *Aedes* species comparisons of evolutionary dynamics within *Culicidae* will also be possible. Comparisons of genome evolution among these genera can provide insights into how evolutionary processes might differ in more repeat rich genomes.

4.5 Tables

Table 4.5.1 The number of one-to one orthologs identified for each chromosomal element

chromosomal element	# of orthologs	# of synteny blocks
e1	496	300
e2	2041	528
e3	1464	331
e4	1282	347
e5	883	215

Table 4.5.2 The number of genome rearrangements for individual chromosomal elements on different tree branches

The scheme below shows the branches

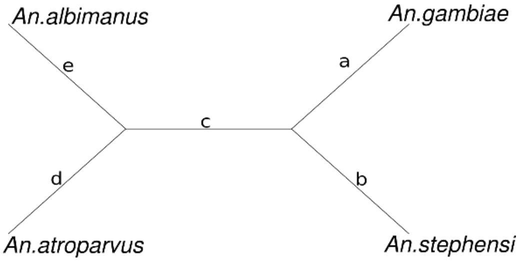

	Chromosomal elements					Time (MYA)	
Branch	e1	e2	e3	e4	e5	A	B
a	41	88	41	38	30	30.4	41.5
b	32	36	20	6	1	30.4	41.5
c	79	67	60	49	36	27.6	38.8
d	58	46	48	26	20	58	80.3
e	199	213	111	163	82	100	100

Table 4.5.3 Mapped supercontigs in *An. stephensi*

Arm	Location	Scaffold	Size (bp)	Orientation
X	1A- 1B	scaffold_00015	2717355	(-)
X	1C	scaffold_00142	244011	not oriented
X	1C-2A	scaffold_00058	1184849	(-)
X	2A-C	scaffold_00023	2215234	(-)
X	3A	scaffold_00076	861362	Not oriented
X	3B	scaffold_00047	1353894	Not oriented
X	4A- 4B	scaffold_00004	5098044	(+)
X	5A	scaffold_00038	1690795	Not oriented
X	6A	scaffold_00141	244011	Not oriented
X	6A	scaffold_00104	528361	Not oriented
2R	7A	scaffold_00061	1129359	Not oriented
2R	7B	scaffold_00033	1882624	(-)
2R	8A	scaffold_00013	2876150	Not oriented
2R	8C	scaffold_00020	2346360	(-)
2R	9A	scaffold_00156	138726	Not oriented
2R	9A	scaffold_00060	1144152	
2R	9C-9D	scaffold_00031	1955281	(+)
2R	10A	scaffold_00179	86345	Not oriented
2R	10A-11A	scaffold_00001	5975090	(-)
2R	11B	scaffold_00096	592562	
2R	11C	scaffold_00089	654626	

2R	12A	scaffold_00022	2225538	
2R	12AB	scaffold_00056	1207362	
2R	12B-12C	scaffold_00016	2461092	(-)
2R	13B	scaffold_00055	1245807	
2R	13B	scaffold_00117	401431	Not oriented
2R	13C	scaffold_00074	863053	(+)
2R	14A-14B	scaffold_00014	2766867	(-)
2R	14B	scaffold_00286	17030	Not oriented
2R	15A-17A	scaffold_00002	5961939	(+)
2R	17A	scaffold_00149	205987	Not oriented
2R	17AB	scaffold_00077	830129	Not oriented
2R	17B-18B	scaffold_00003	5630514	(-)
2R	18C	scaffold_00063	1014770	
2R	18C	scaffold_00261	22170	Not oriented
2R	18C	scaffold_00079	793214	Not oriented
2R	18D	scaffold_00048	1332325	Not oriented
2R	19A	scaffold_00054	1283538	Not oriented
2R	19B-19C	scaffold_00026	2124590	(-)
2R	19D	scaffold_00073	878309	(-)
2R	19E	scaffold_00046	1368814	Not oriented
2R	19E	scaffold_10315	853	Not oriented
2L	20C	scaffold_00066	971934	Not oriented
2L	20C	scaffold_00093	604418	Not oriented
2L	20C-20B	scaffold_00043	1551626	(+)

2L	20B	scaffold_00235	30195	Not oriented
2L	21B	scaffold_00085	736451	(+)
2L	21B	scaffold_00028	2078127	Not oriented
2L	22B	scaffold_00030	1990510	Not oriented
2L	22A	scaffold_00049	1325362	Not oriented
2L	22A	scaffold_00084	736794	Not oriented
2L	23B	scaffold_00071	895107	Not oriented
2L	23B	scaffold_00113	438679	Not oriented
2L	23A	scaffold_00091	623304	Not oriented
2L	24B	scaffold_00018	2434081	Not oriented
2L	24B	scaffold_00075	861362	Not oriented
2L	24A	scaffold_00040	1631802	Not oriented
2L	25C	scaffold_00080	788890	Not oriented
2L	25A-25B	scaffold_00021	2346360	(-)
2L	25A	scaffold_00095	594721	Not oriented
2L	26C	scaffold_00100	544206	Not oriented
2L	26B	scaffold_00036	1737740	Not oriented
2L	26A-27C	scaffold_00034	1819477	(-)
2L	27B	scaffold_00032	1942051	(-)
2L	27A	scaffold_000135	270198	Not oriented
2L	28D-27A	scaffold_00044	1453912	(-)
2L	28C	scaffold_00067	962451	Not oriented
2L	28C	scaffold_00009	3514595	Not oriented
3R	29A	scaffold_00057	1190389	Not oriented

3R	29B-29E	scaffold_00006	4219845	(+)
3R	29E	scaffold_00146	232801	Not oriented
3R	30A	scaffold_01155	3227	Not oriented
3R	30A	scaffold_00012	3035404	Not oriented
3R	30C	scaffold_00042	1579480	Not oriented
3R	31A	scaffold_00053	1295374	(+)
3R	31A	scaffold_00099	559588	Not oriented
3R	31B	scaffold_00017	2453200	(-)
3R	31B-32A	scaffold_00029	2074802	(-)
3R	32C	scaffold_00106	508607	Not oriented
3R	32C	scaffold_00097	580229	Not oriented
3R	32C	scaffold_00090	654006	Not oriented
3R	33A	scaffold_00094	597473	Not oriented
3R	33B-33C	scaffold_00025	2202290	(+)
3R	33C	scaffold_00052	1299898	Not oriented
3R	34B	scaffold_00027	2102516	(-)
3R	35A	scaffold_00007	4015228	Not oriented
3R	35B	scaffold_00041	1581406	Not oriented
3R	36A	scaffold_00050	1312856	(-)
3R	36A	scaffold_00055	1245807	
3R	36B	scaffold_00181	84367	Not oriented
3R	36B	scaffold_00037	1737740	Not oriented
3R	36C	scaffold_00019	2358289	Not oriented
3R	37B	scaffold_00065	973771	Not oriented

3R	37D	scaffold_00059	1145648	(+)
3R	37D	scaffold_00105	528361	Not oriented
3L	38F-38E	scaffold_00062	1115343	(-)
3L	38C-38D	scaffold_00035	1814618	(+)
3L	38B	scaffold_00081	776269	Not oriented
3L	38A	scaffold_00088	699487	Not oriented
3L	38A-39C	scaffold_00068	961948	(-)
3L	39C-39B	scaffold_00051	1303419	(-)
3L	39B	scaffold_00121	352369	Not oriented
3L	39A	scaffold_01107	3313	Not oriented
3L	39A	scaffold_00092	619269	Not oriented
3L	40D	scaffold_00087	722457	Not oriented
3L	40D	scaffold_00078	803307	Not oriented
3L	40D	scaffold_00136	256842	(-)
3L	40C	scaffold_00111	457603	Not oriented
3L	40B	scaffold_00086	725040	Not oriented
3L	40B	scaffold_00064	999561	Not oriented
3L	40A	scaffold_00070	937869	(-)
3L	40A	scaffold_00045	1432165	(+)
3L	41C	scaffold_00082	761370	
3L	41B	scaffold_00083	761370	Not oriented
3L	41B-42C	scaffold_00008	3725231	(+)
3L	42B	scaffold_00110	466204	Not oriented
3L	42A	scaffold_00072	895107	Not oriented

3L	42A	scaffold_02336	2126	Not oriented
3L	43C	scaffold_00024	2206587	(-)
3L	43C	scaffold_00069	948256	(-)
3L	44C	scaffold_00010	3481139	(-)
3L	44A	scaffold_00039	1662464	Not oriented
3L	45C-45A	scaffold_00011	3233111	(-)
3L	46C-46B	scaffold_00005	4240566	(+)
		Total BP	176375888	
		% Mapped	0.796912617	

Table 4.5.4: Species differences in Mean % Repeats

Species Differences	# of Windows	Mean % Inverted Repeats	Mean % Tes	Mean % TRs
An. dirus	2073	0.0232	1.5286	0.7087
An. gambiae	2307	0.0416	9.6557	1.2789
An. minimus	1801	0.0089	2.2344	0.3276
An. stephensi	1897	0.0056	3.4603	0.3934

Means that are statistically different are different colors for each column

Table 4.5.5: Differences in Repeats by Element (Mean, SD is reported)

Transposable Elements				
Elements	*An. dirus*	*An. gambiae*	*An. minimus*	*An. stephensi*
e1	A(3.184, 2.70)	A(17.917, 15.34)	A(3.8187, 3.87)	A(4.901, 3.42)
e2	BC(1.339, 1.59)	C(7.343, 8.68)	BC(2.4831, 2.22)	C(2.698, 2.34)
e3	BC(1.336, 1.40)	B(9.661, 10.82)	C(2.1441, 2.16)	BC(3.109, 2.95)
e4	C(1.266, 1.63)	BC(8.581, 8.35)	D(.6301, .560)	B(3.340, 3.082)
e5	B(1.623, 1.70)	B(9.604, 10.07)	B(2.6223, 2.27)	A(4.503, 3.36)

Inverted Repeats				
Elements	*An. dirus*	*An. gambiae*	*An. minimus*	*An. stephensi*
e1	A(.0451, .093)	A(.0965, .186)	A(.0200, .053)	A(.0141, .046)
e2	B(.0172, .065)	B(.0314, .102)	BC(.0074, .035)	A(.0038, .019)
e3	B(.0241, .064)	B(.0384, .100)	BC(.0092, .037)	A(.0031, .017)
e4	B(.0188, .055)	B(.0272, .070)	C(.0027, .017)	A(.0035, .019)
e5	B(.0270, .071)	B(.0469, .118)	AB(.0115, .039)	A(.0100, .099)

Tandem Repeats				
Elements	*An. dirus*	*An. gambiae*	*An. minimus*	*An. stephensi*
e1	A(1.618, 1.00)	A(2.492, 1.15)	A(.6072, .447)	A(.6808, .331)
e2	C(.6149, .348)	B(1.013, 1.18)	B(.3133, .329)	C(.3553, .262)
e3	C(.6143, .471)	B(1.161, 1.24)	B(.3434, .428)	BC(.3689, .233)
e4	C(.5854, .363)	B(1.206, 2.49)	C(.2076, .262)	C(.3390, .213)
e5	B(.7302, .942)	B(1.193, 1.75)	B(.3059, .346)	B(.4139, .344)

Means that are statistically different are connected by different letters.

Table 4.5.6: Breaks vs. Whole Genome

Species	# of Breaks	Mean % IRs (Breaks)	Mean % TEs (Breaks)	Mean % TRs (Breaks)
An. dirus	237	0.0058*	2.9793*	0.4591*
An. gambiae	115	0.0434	25.7298*	2.0487*
An. minimus	67	0*	3.5204*	0.1933*
An. stephensi	80	0.0312	7.5924*	0.9461*

Means with * are significantly different from the whole genome mean for that species

Table 4.5.7: Rates of Inversion by element (all species pooled)

e1	3.328	A
e2	0.924	B
e3	0.836	B
e4	0.826	B
e5	0.792	B

*Means followed by the same letter are not significantly different

Table 4.5.8: Correlation of Inversion rates with Repeat content of each chromosomal arm

An. gambiae

Element	Rate of Breakage	Mean % TR	Mean % TE	Mean % IR
e1	2.72	2.492	17.917	0.0965
e2	1.42	1.013	7.343	0.0314
e3	0.92	1.161	9.661	0.0384
e4	0.98	1.206	8.581	0.0272
e5	1.12	1.193	9.604	0.0469
CORRELATION (all elements)	*An. gambiae*	0.9297	0.8915	0.9236
without e1		-0.8647	-0.8499	-0.109
without e2		0.9963	0.9929	0.976
without e3		0.936	0.9174	0.9377
without e4		0.9368	0.8863	0.9147
without e5		0.9268	0.8916	0.9445
without e1 & e2		0.5105	0.1631	0.6222
without e1 & e3		-0.9673	-0.7962	-0.0031
without e1 & e4		-0.8386	-0.926	-0.5503
without e1 & e5		-0.9445	-0.971	-0.2508

An. stephensi

Element	Rate of Breakage	Mean % TR	Mean % TE	Mean % IR
e1	2.12	0.68	4.79	0.0141
e2	0.58	0.356	2.703	0.0038
e3	0.45	0.368	3.109	0.0031
e4	0.15	0.34	3.366	0.353
e5	0.04	0.413	4.502	0.01
CORRELATION (all elements)	*An. stephensi*	0.9249	0.4819	0.6865
Without e1		-0.4479	-0.892	-0.6842
Without e2		0.9519	0.5647	0.7126
Without e3		0.9275	0.4655	0.699
Without e4		0.9144	0.4484	0.6392
Without e5		0.9875	0.876	0.9799
without e1 & e2		-0.3768	-0.8192	-0.7429
without e1 & e3		-0.4763	-0.8869	-0.6262
without e1 & e4		-0.9995	-0.9999	-0.9476
without e1 & e5		0.7494	-0.9382	0.2152

4.6 Figures

Figure 4.6.1 Scaffold linkage in *An. stephensi* Indian strain

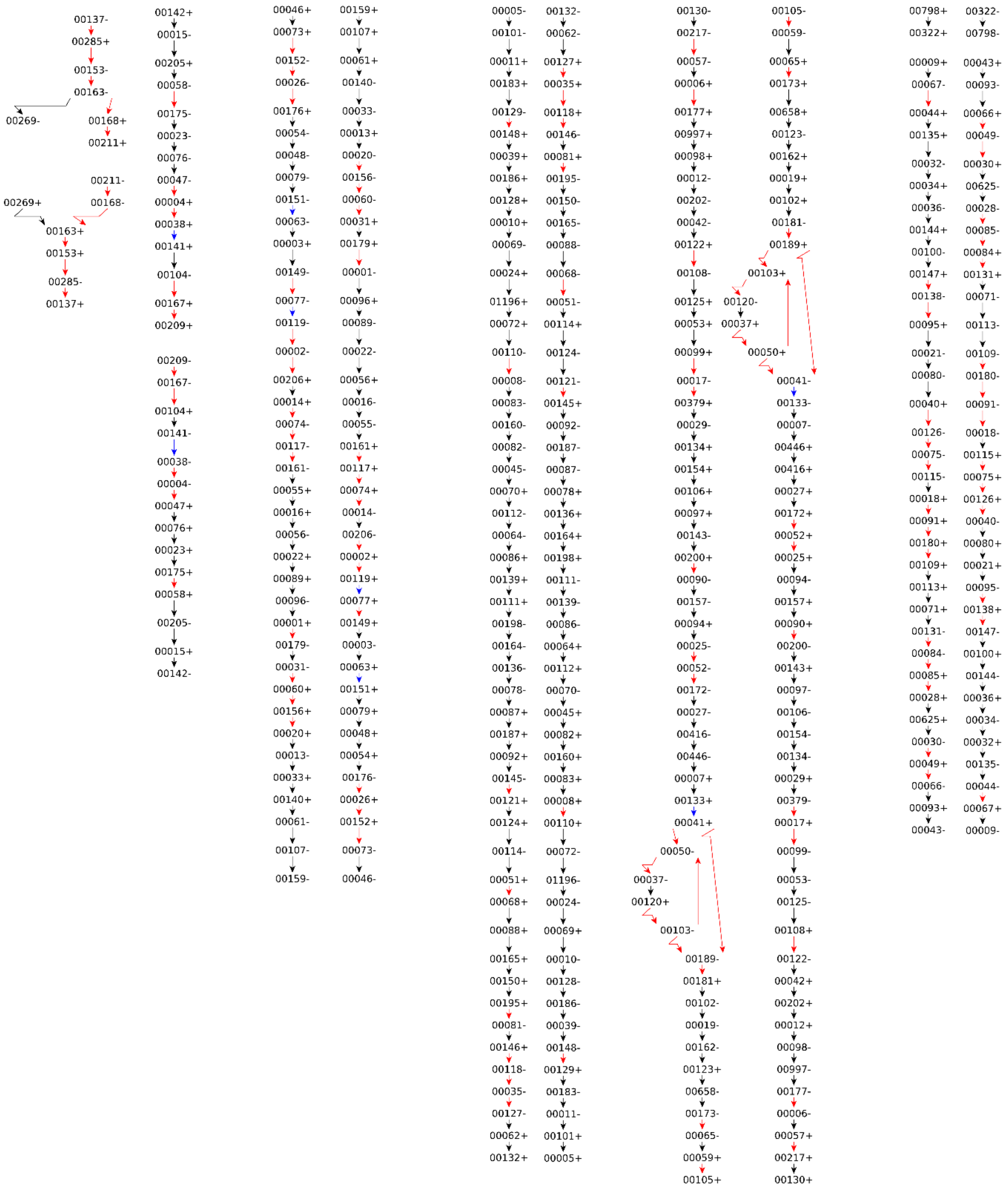

Black arrows indicate the linkages inferred from the SDA stain of An. stephensi; Red arrows indicate the linkages inferred from other species as reference; Blue arrows indicate the linkages based on genome rearrangements. Linkages from both directions are showed

Figure 4.6.2 Phylogenetic tree based on genome rearrangements

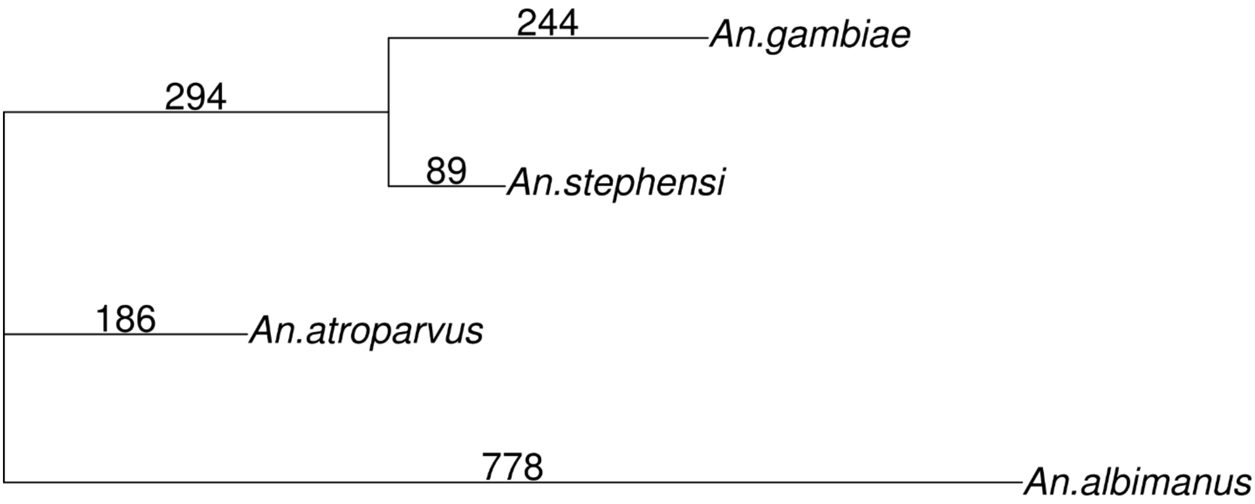

Figure 4.7.2. Phylogenetic tree based on genome rearrangements.

The number of rearrangements is labeled on the branches.

Figure 4.6.3 Chromosomal rearrangement rates

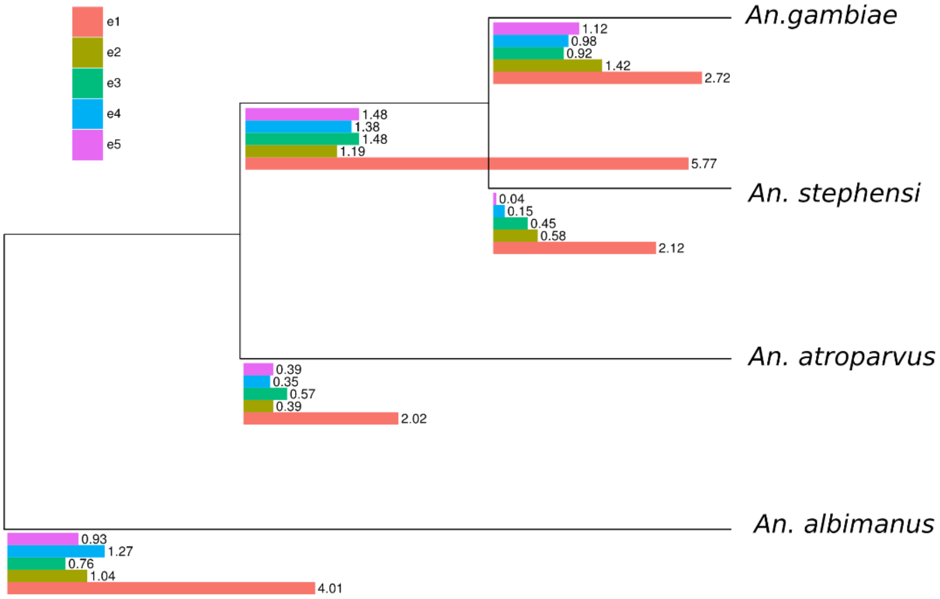

Figure 4.6.4: Improved map *An. stephensi*

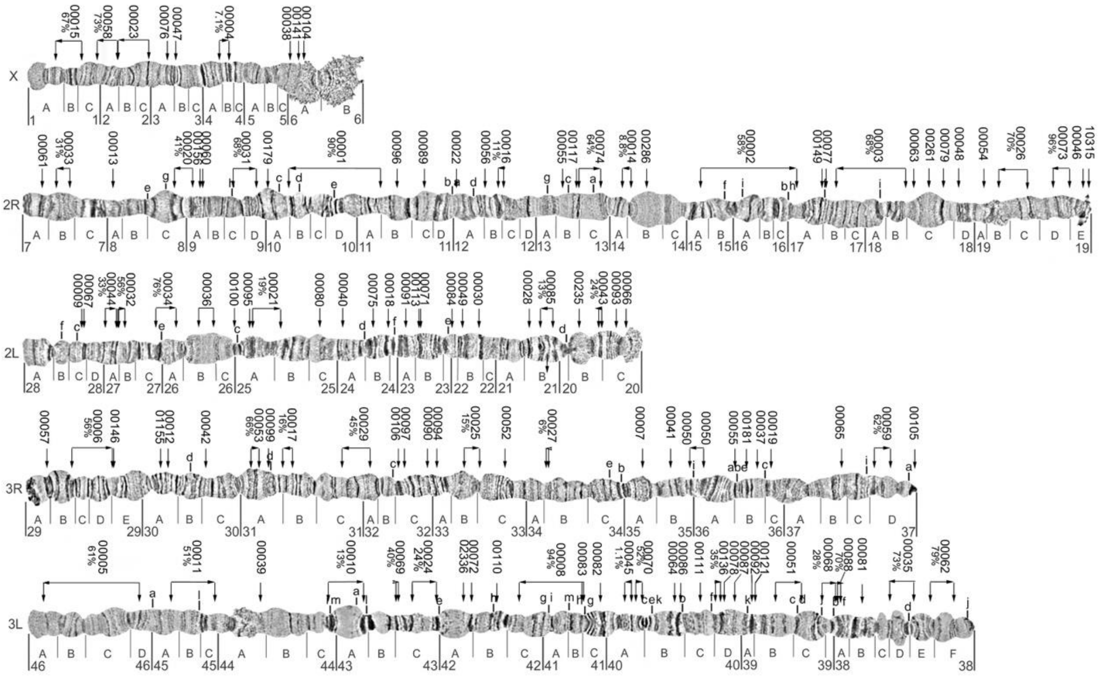

Figure 4.6.5: Comparison of Repeats in 4 Species

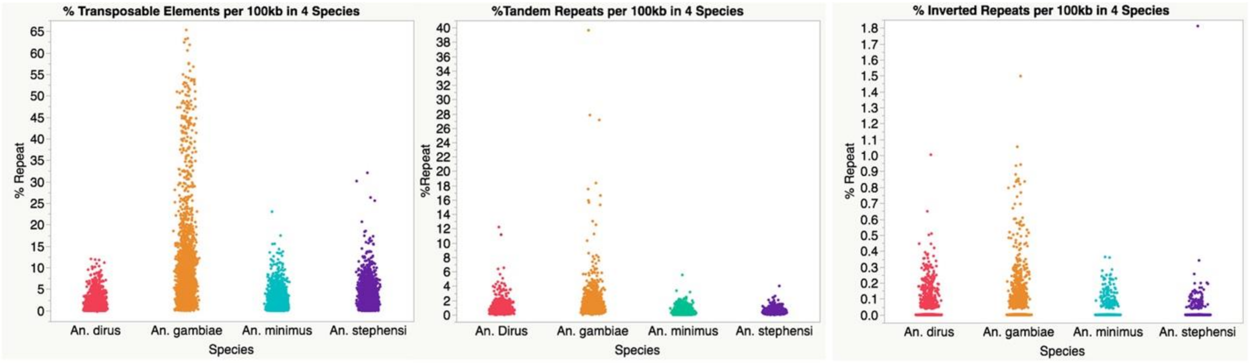

Figure 4.6.6: % Repeats in 4 Species by Element

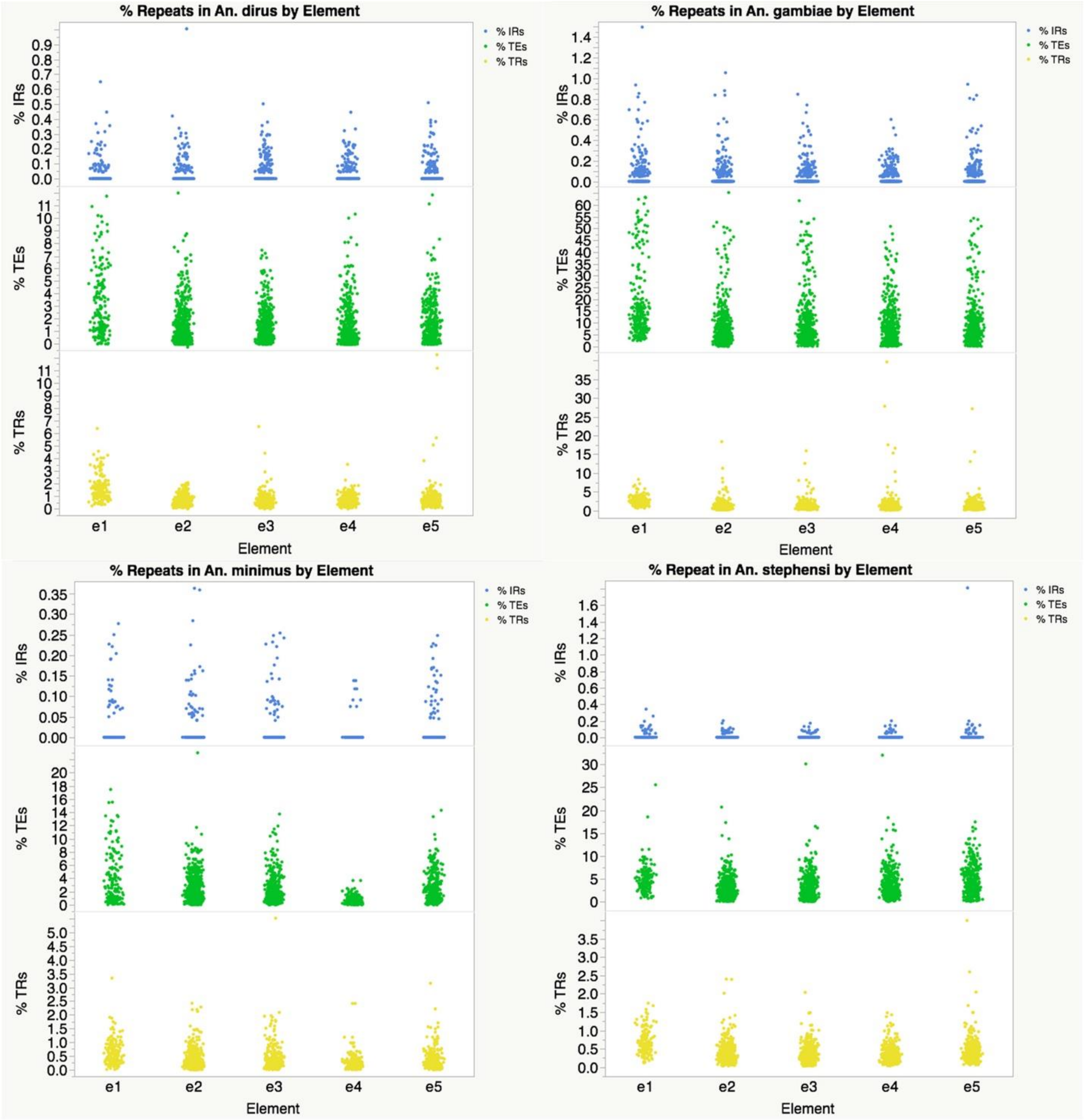

Figure 4.6.7: Mean % Repeats in 4 Species by Element

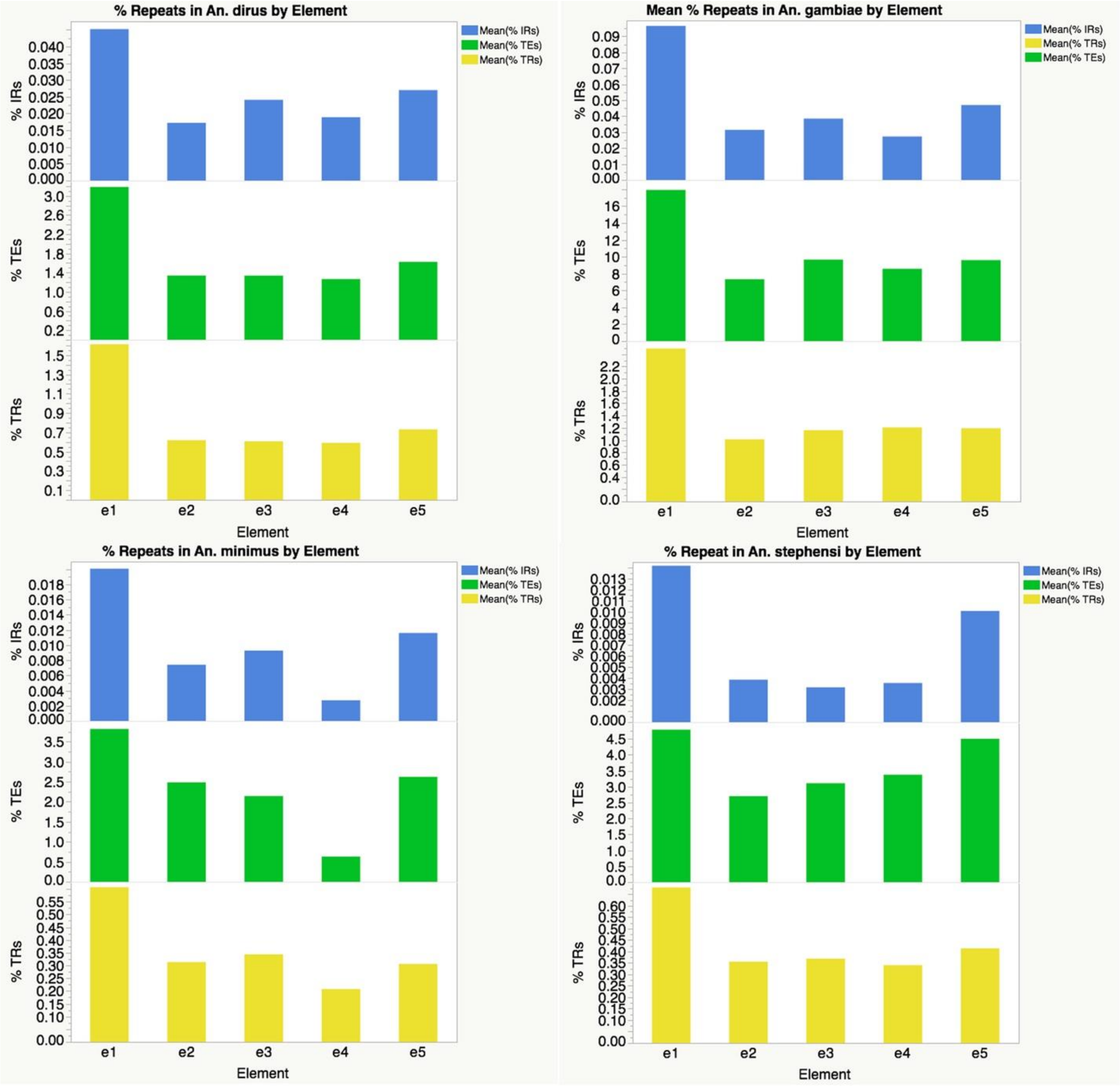

Figure 4.6.8: Repeats in Breaks vs. Whole Genome

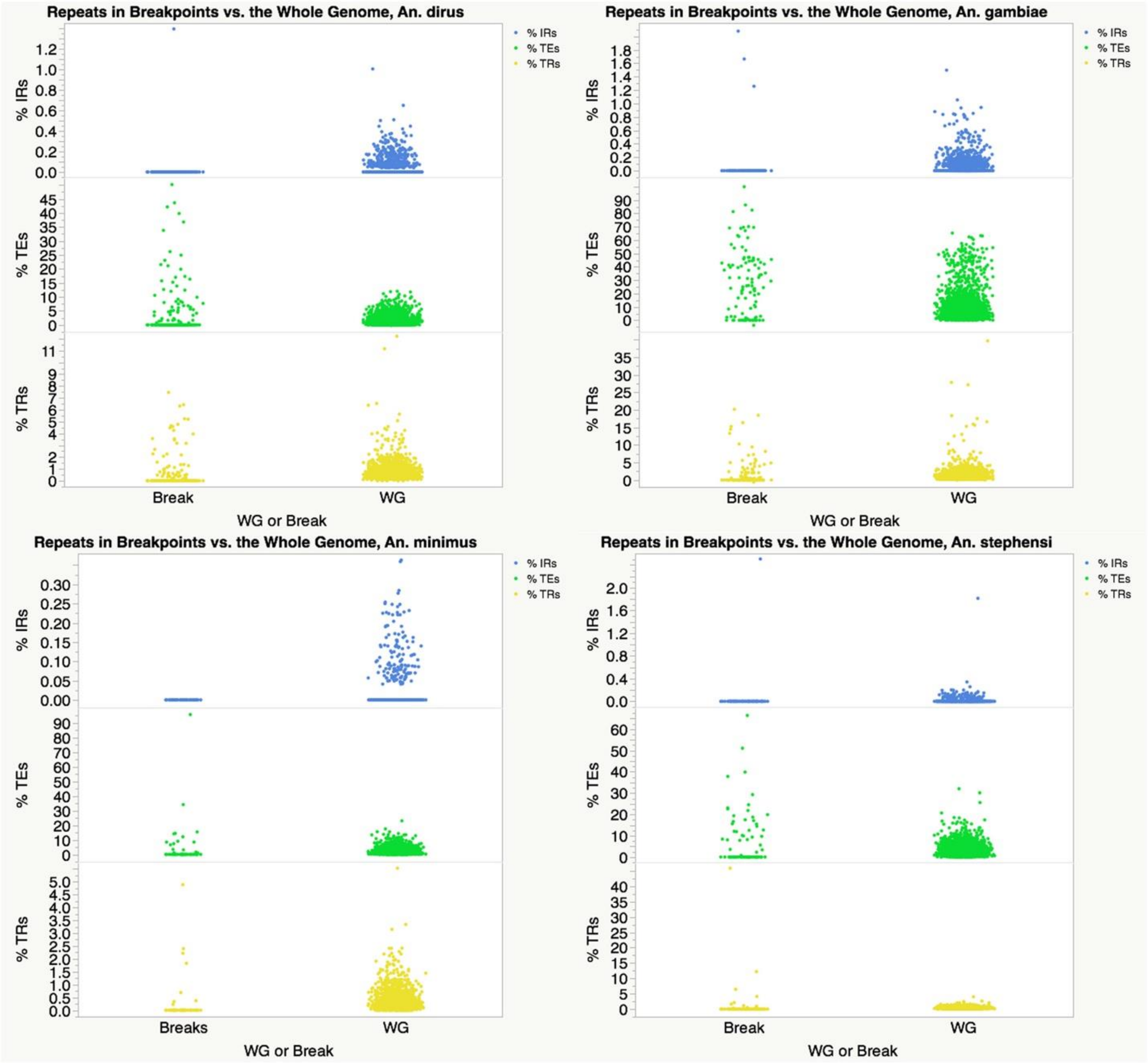

Figure 4.6.9 Mean %Repeat Breaks vs. Whole Genome

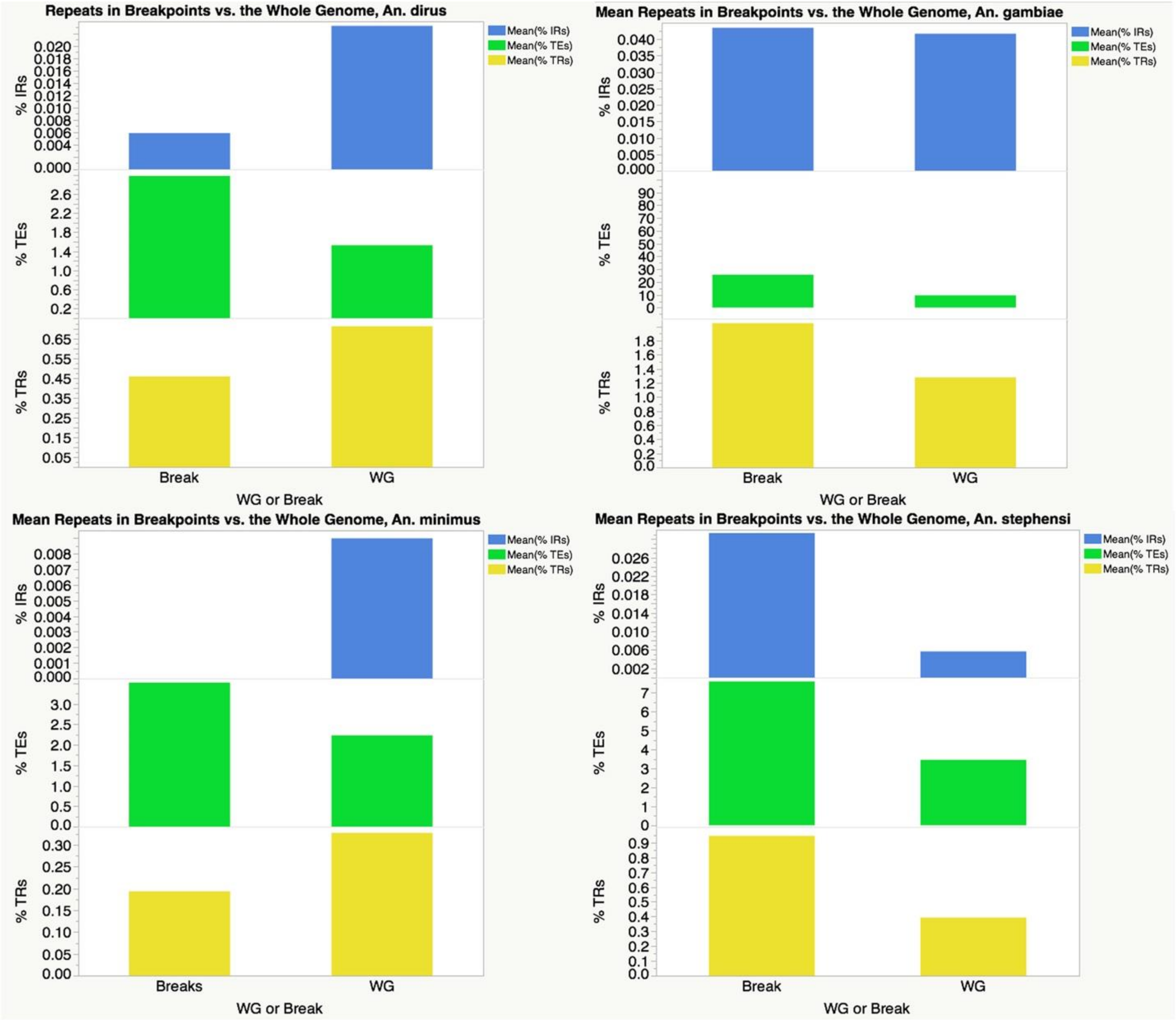

Figure 4.6.10 %TEs in WG or break by element

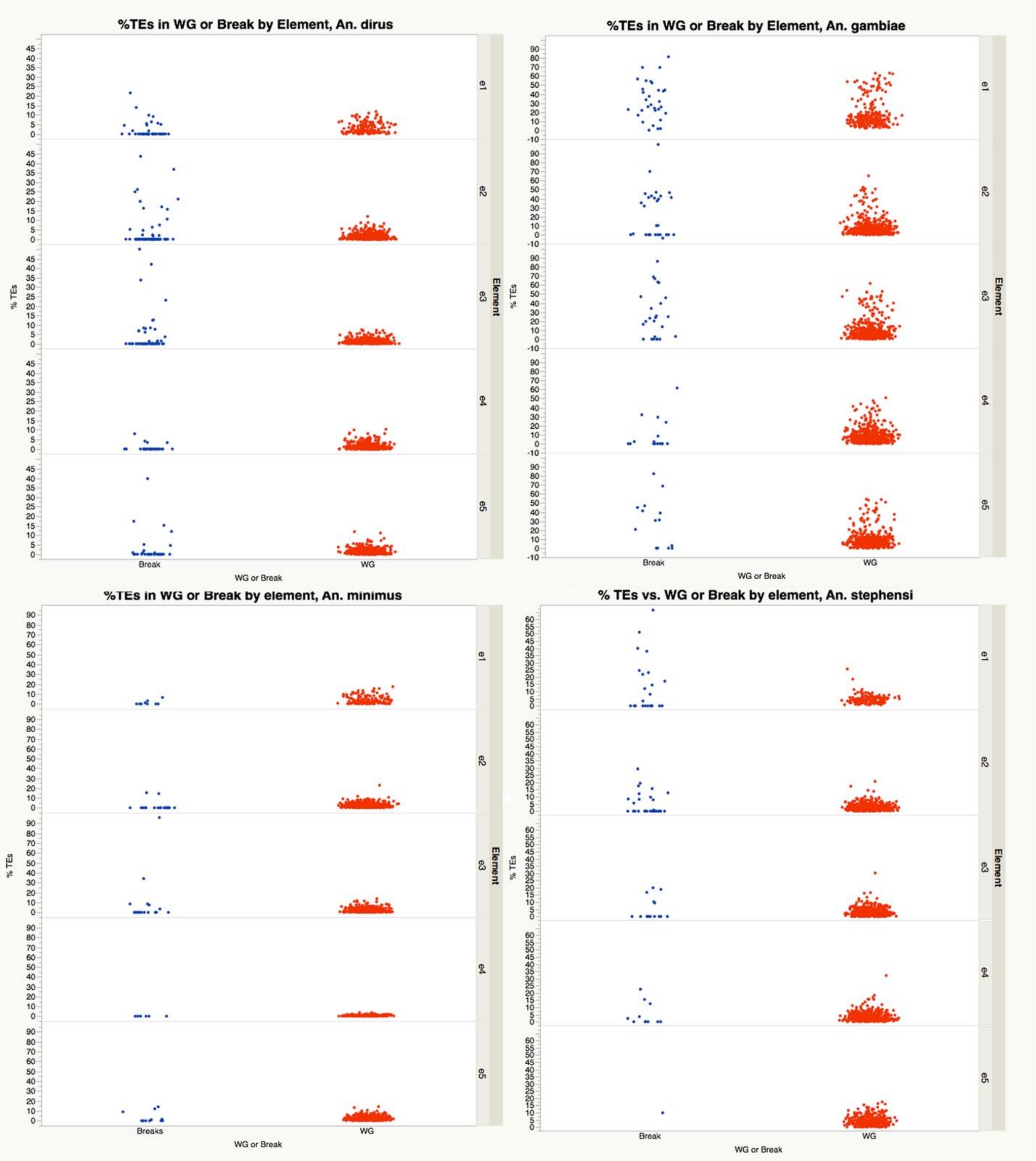

Figure 4.6.11 TRs in WG or break by element

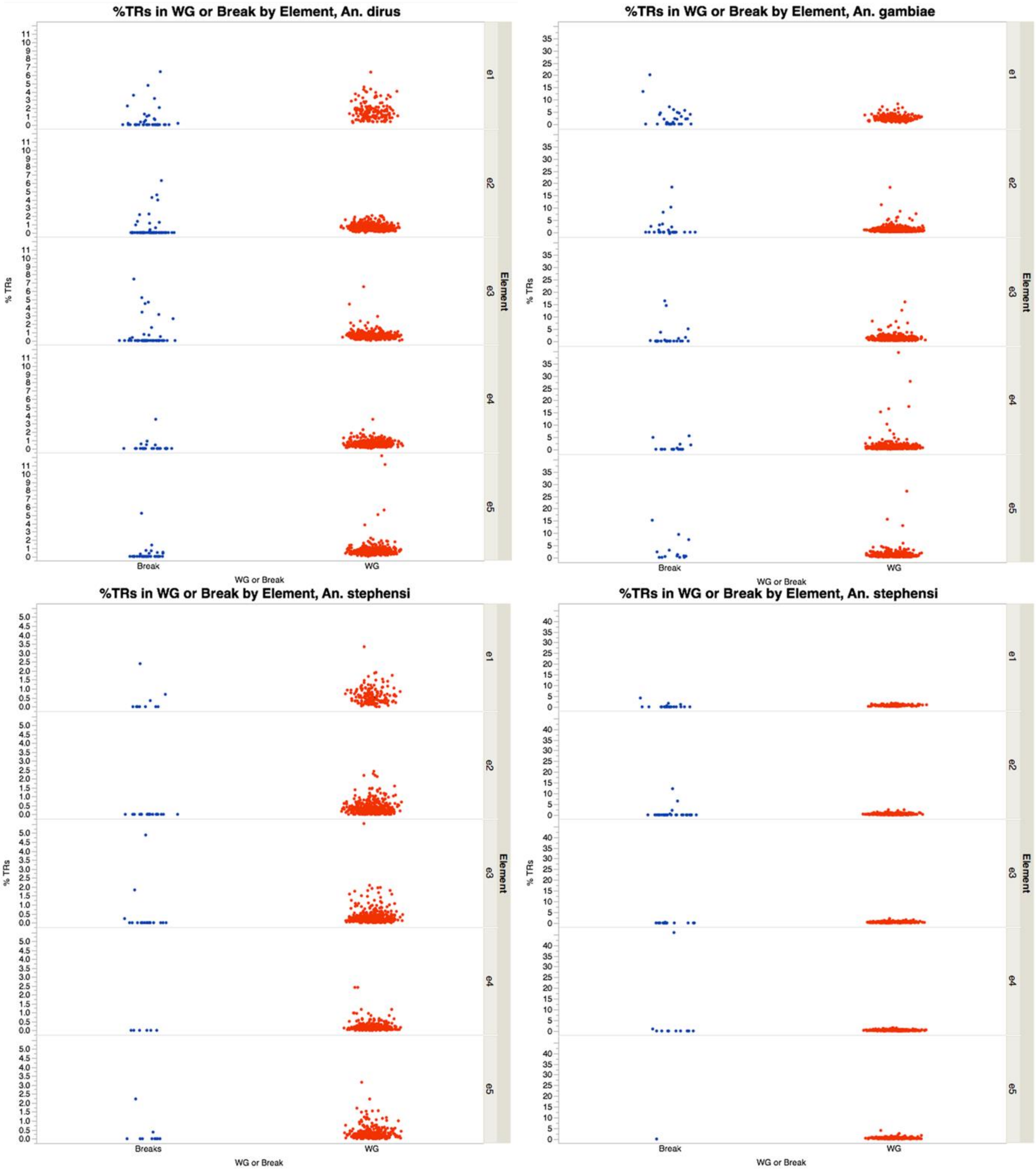

Figure 4.6.12 IRs in WG or break by element

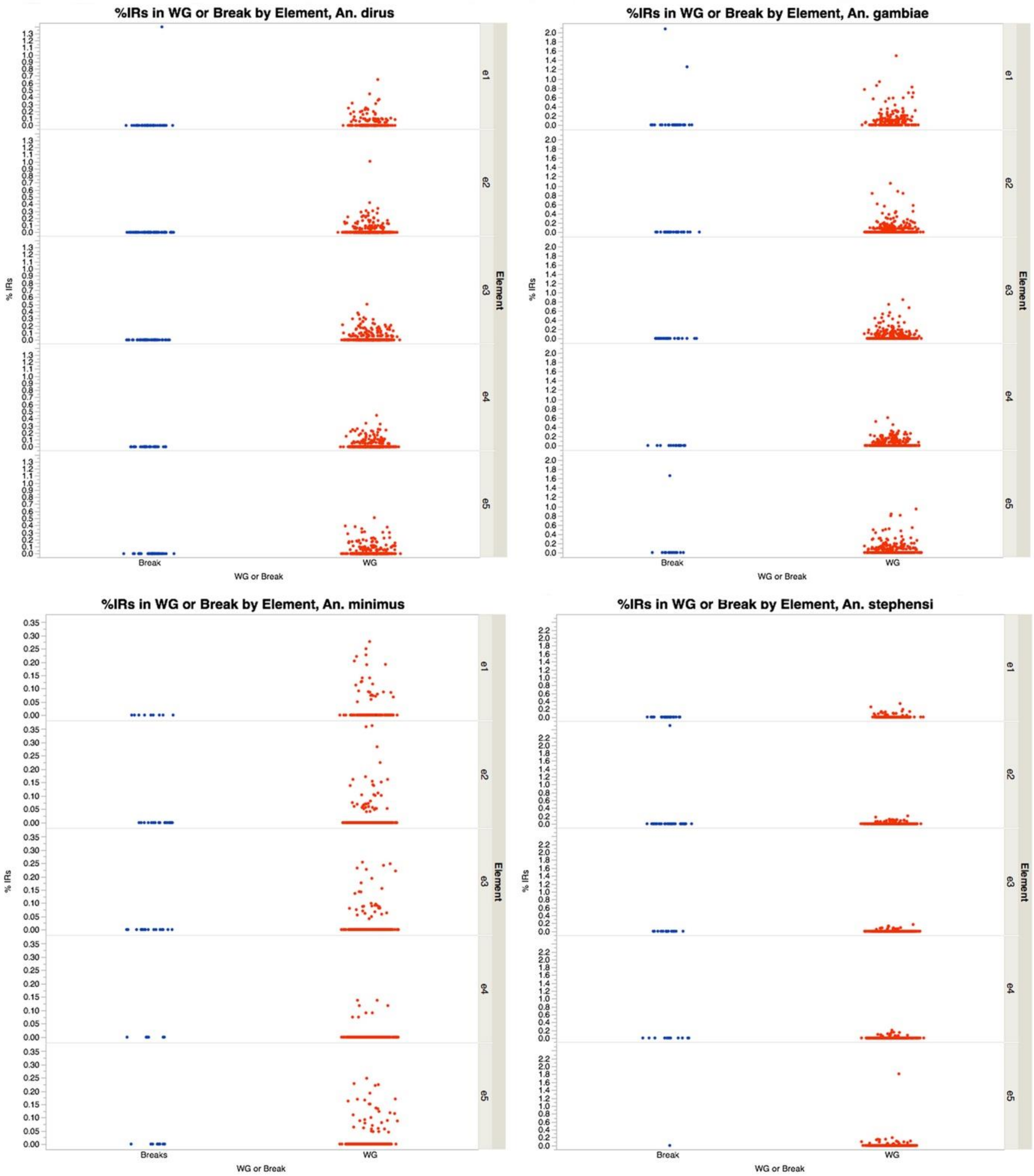

4.7 Methods

4.7.1 Identification of genome misassemblies

In the evolution of *Anophelines*, chromosomal inversions are assumed to be paracentric and translocations are at the whole chromosome arm level. As a result, the gene exchange between chromosomal elements is expected to be limited to gene transposition. As gene transposition is not frequent and generally limited to single genes, if large blocks of genes on the same scaffold have orthologs on different chromosomal elements, the scaffold is likely misassembled. A Hidden Markov model (HMM) was used to identify misassemblies in 18 *Anopheles* genomes, namely *An. albimanus*, *An. arabiensis, An. atroparvus, An. christyi*, *An. culicifacies, An, durus, An.epiroticus, An. farauti*, *An. funestus*, *An. gambiae, An. maculatus, An. melas*, *An. merus*, *An. minimus, An. quadriannutatus, An. sinensis, An. stephensi* Indian strain and SDA strain. Genomes and annotations of these species were downloaded from VectorBase and *Anophelinae* orthology information was obtained from OrthoDB. The probability of each ortholog located on a chromosomal element was estimated based on its chromosomal distribution in *An. gambiae*. Combined with arbitrary transposition rate, the emission probability matrix was constructed. The chance of misassembly occurred between two neighboring genes can be represented by a state transition rate to build transition probability matrix. The Viterbi algorithm was used to predict the most likely chromosomal element each gene is on. Scaffolds with genes assigned to more than one chromosomal element were considered misassembled.

4.7.2 Scaffolding genomes based on conserved syntenic segments and genome rearrangement

The order of scaffolds can be inferred from the conserved synteny. As shown in **Figure 1**, if the last gene on scaffold A and the first gene on scaffold B in Indian strain *An. stephensi* are neighboring genes in the SDA strain, the three prime end of scaffold A should be linked to the five prime end of scaffold B in the Indian strain assembly. This approach can also be used to link scaffolds inferred from a close species if the synteny is conserved. This approach will be invalid if a recent genome rearrangement resulted in a breakpoint between scaffolds. If the breakpoint occurred within a scaffold, as in **Figure 2**, further scaffolding is possible.

4.7.3 Genome rearrangement analysis

Physical mapping information was used to order scaffolds for *An. albimanus*, *An. atroparvus* and the *An. stephensi* Indian strain (Supplementary Information: **Order_of_Mapped_Scaffolds.xlsx**). The above three species and *An. gambiae* were used for the genome rearrangement analysis. Single-copy orthologs presented in four species were determined and used to identify synteny blocks. Synteny blocks were defined as genomic regions where the order and orientation of genes were conserved in all species. Synteny blocks were numbered and signed based on the gene order and orientation in *An. gambiae*. Phylogenies were constructed based on the order of synteny blocks for multi-chromosomal genomes using the Multiple Genome Rearrangements (MGR) tool. The same analysis was applied to individual chromosomal elements. The scaffolding predicted by the HMM approach was not used for the rearrangement analysis because:

a. The evidence based the synteny from different species can be inconsistent making the decision which arrangement to choose difficult.

b. Even if the evidence is consistent, it can be incorrect if there is a recent chromosomal inversion.

The only genome used from the HMM approach was *An. stephensi* as shown in **Figure 3**.

4.7.4 Physical mapping and confirmation of gluing predictions in *An. stephensi* Indian strain

Physical mapping by fluorescence in-situ hybridization (FISH) was used to confirm gluing predictions in *An. stephensi.* DNA probes sized 800-2000 bp were designed from gene exons at each end of glued supercontigs. To target only the largest unmapped supercontigs we chose only to map supercontigs numbered 00001-00100 that had not been previously mapped. DNA probes were amplified using PCR with Immomix(citation for company) and gene product was then labeled with Cy3, Cy5, or fluorescein dyes via “nick translation” protocols that have been described before [124]. FISH and subsequent image processing and mapping was performed as previously described.

4.7.5 Transposable elements

We quantified transposable elements in 4 *Anopheles* species possessing both a repeat library and at least some information regarding order and orientation of supercontigs along the chromosomal elements. *Anopheles gambiae, An. stephensi, An. minimus* and *An. dirus* satisfied these criteria and their genomes were analyzed using RepeatMasker via NCBI's RMBLAST, version 2.2.27+. *Anopheles gambiae, An. dirus* and *An. minimus* were repeat masked against the repeat library for the species available at Vectorbase.org. *Anopheles stephensi* Indian was repeat masked against the repeat library for this strain obtained from Z. Tu. Prior to repeat detection, each genome was broken into 100kb windows and sorted by chromosomal coordinates. The output was filtered in Microsoft Excel to remove simple repeats, low complexity repeats, unknown repeat families and redundant repeats with more than 80% domain overlap. Filtered results were then sorted by Window ID using the ".groupby" function in the pandas module for Python and then summed to find the total number of repeat base pairs per window. The statistics software, JMP, was used to test for statistically significant differences between different species, as well as differences between whole genome and breakpoint regions, and different chromosomal elements within species.

4.7.6 Inverted repeats

Inverted repeats were assessed in *An. dirus, An. gambiae, An. minimus, and An. stephensi* using the linux compatible version of Inverted Repeats Finder available at: https://tandem.bu.edu/irf/irf307.linux.download.html. Specifically, our study was interested in quantifying IRs which cause genetic instability. To target small IRs suspected of being recombinogenic in other species we used IRF parameters 2 3 5 80 10 40 200 7 -t4 207 -d -h. Relevant lines of the resulting .dat file were extracted using awk and formatted into a .csv file using find and replace. IRs with less that 80% match were removed from the dataset using awk. Nested IRs were detected using a Perl script that detected overlapping repeats (provided my NAK, also used for detection of overlapping TRs). Overlapping repeats with the greatest Smith-Waterman score were retained in the dataset while redundant repeats with lower scores were removed. The filtered and formatted .csv was then analyzed in the pandas module for python to obtain total bp IRs in each 100 KB window. Percent IRs were calculated and these data were imported into JMP Pro11 software to check for statistically significant differences between the whole genome mean %IRs in different species, element differences in mean, and mean %IRs between breakpoint regions and the whole genome.

4.7.7 Simple tandem repeats

Simple Tandem Repeats were quantified in *An. dirus, An. gambiae, An. minimus, and An. stephensi* using the linux compatible version of Tandem Repeats finder available at: https://tandem.bu.edu/trf/trf407b.linux.download.html. Parameters 2 7 7 80 10 50 500 –f –d were used when running the program. The resulting .dat file was filtered to remove repeats with <80% match and <2 copy number using awk. Overlapping and nested repeats were detected using a Perl script provided by NAK and redundant repeats with lower Smith-Waterman scores were removed from the dataset. Tandem Repeat bp were summed using the pandas module for python as described for the other repeat types. Percent tandem repeat for each 100kb window was then calculated and statistically significant differences were then assessed in JMP as described for other repeat types.

4.7.8 Comparison of breakpoints to the whole genome

Predicted breakpoints greater than 20kb in size were removed from our datasets. This left 237 breaks in *An. dirus*, 115 in *An. gambiae,* 67 in *An. minimus* and 80 in *An. stephensi*. Mean %TE, %IR, and %TR were compared to the corresponding mean in the whole genome for each species and statistically significant differences were determined by a one-way ANOVA.

4.7.9 Statistical tests for molecular features

Statistical tests were performed using JMP Statistical software. Our study used post hoc statistics to make comparisons of mean %TEs, mean %TRs, and mean %IRs between: species, chromosomal elements (within species), and breakpoints vs. the whole genome (within species). Species and chromosomal element differences in each repeat type were determined using an ANOVA followed by a Tukeys HSD test to examine which groups were different from each other. A Tukeys HSD was selected to control for experiment wise error as we were comparing 4 species groups and 5 chromosomal elements.

Mean coverage of molecular features in breakpoints within a species were compared to the whole genome means for that species using a one-way ANOVA

4.7.10 Rates of inversion in *anopheles*

We calculated rates of inversion in *An. albimanus, An. atroparvus, An. gambiae,* and *An. stephensi* by dividing the number of chromosomal rearrangements on each chromosomal arm by arm size in MB and MY divergence multiplied by 2. To restate, rate of rearrangement= #breaks/arm size (MB)/(2*MY divergence time). To determine whether the sex chromosome is evolving faster than the autosomes we ran a student's T-test on the rates of chromosomal breakage/MY for all elements pooled across all species.

4.7.11 Correlations of repeats with rates of chromosomal breakage

Rates of chromosomal breakage for each chromosomal arm were correlated with mean %TEs, IRs, and TRs in *An. gambiae* and *An. stephensi.* Correlations were performed in JMP using the Multivariate function. To test for confounding effects due to the much greater repeat density on the sex chromosome, correlation was calculated with and without e1 means. To test for arm specific differences each autosome was excluded from that analysis one at a time.

Acknowledgements: We would like to acknowledge members of the Sharakhov lab especially, Nick Kinney for assistance with perl scripts.

Chapter 5: Summary

5.1 General discussion and overview

Malaria vectors possess great ability to adapt. The evolution of behavioral and metabolic resistance to insecticides threatens to unravel recent success in reducing the global burden of malaria. As malaria vectors continue to adapt, and overcome the weapons we use against them, government agencies are in want of new tools to employ in the fight to eliminate vector borne disease. In this battle, a better understanding traits such as insecticide resistance and spreading to new environments is crucial to the future of malaria control. Hugely collaborative genome sequencing projects have produced genome sequences for more than 20 vector and non-vector mosquitoes and the raw materials are now available for the creation of many new genetic tools. Progress in genetic and physical mapping eases the process of assembling genomes to the chromosomal level and has provided an opportunity for comparative genomics studies with many members of genus *Anopheles.* Multi-species comparison of many members of this group can elucidate the evolutionary processes that have produced such efficient vectors of disease. Additionally, genome maps and knowledge of genome landscapes can greatly assist in understanding the genetic basis for epidemiologically important traits, and understanding modes of adaptation. This information in turn aids in the search for novel gene targets for genetic control of mosquitoes.

5.2 Review of chapter 2

Anopheles stephensi is an important vector of malaria in India and the middle east. We sequenced and assembled the Indian strain by employing a combination of Illumina, 454 and PacBio sequencing. This combined approach allowed us to take advantage of the long reads of PacBio to bridge gaps, and balance that with the greater accuracy of the shorter read Ilumina and 454 technologies. Our genome sequence is accompanied by a physical map representing 62% of the *An. stephensi* genome. Despite the fragmentation of this chromosomal assembly, gene order comparisons between *An. gambiae* and *An. stephensi* allowed quantification of chromosomal rearrangements that have occurred in the 30.4 million years since these two species diverged. Our results indicate a much faster rate of chromosomal rearrangement on the sex chromosome, despite a distinct lack of polymorphic inversions this arm. Additionally the faster rate of evolution corresponds with higher densities of TEs and satellite DNA. A comparison of the rates of evolution between *An. stephensi* and *An. gambiae* to those of *Drosophila* indicates that fast rates of rearrangement observed in *Anopheles* are a feature common to *Diptera.*

Our genome study includes an RNA-seq based analysis of transcriptomics that generated expression profiles for many life stage and gender specific genes. This information will be useful for later studies seeking to discern the genetic basis for important traits and behaviors. A few very important subsets of genes including those related to immunity, the sialome and the Y chromosome. Insights gained from these targeted analyses promise to enrich further studies of these vital aspects of mosquito biology.

5.3 Review of chapter 3

Anopheles albimanus is a dominant vector of malaria in central America whose genome was recently sequenced as part of the *Anopheles* 16 genomes project. This mosquito possesses a compact genome of ~170 MB, which has been assembled into a small number of very large supercontigs. These genomic attributes combined with the availability of high quality polytene chromosomes from the salivary glands make this vector a good candidate for chromosomal mapping. Additionally, this species is evolutionarily distant from other physically mapped species *An. gambiae* and *An. stephensi*. The addition of a physical map for *An. albimanus* would permit studies of genome rearrangement over both short and long distances within genus *Anopheles*.

A low coverage physical map was published for this species in 2000 by Cornell and Collins which allowed 75% of the genome to be placed to chromosomes. Although this photomap vastly improves the clarity of banding patterns over previous drawn maps, some chromosomal subdivisions were lacking and images were not completely flattened or straightened. These shortcomings could obscure relative distance between bands and render this map insufficient for physical mapping of the whole genome. Our new cytogenetic map for *An. albimanus* corrects these inadequacies and offers detailed description of chromosomal landmarks. Our improvements will permit use of this map by a wider audience within the scientific community.

Physical mapping of genomic supercontigs onto *An. albimanus* chromosomes via fluorescent *in situ* hybridization (FISH) allowed us to localize 98% of the sequenced genome to chromosomal locations. In the course of our physical mapping we identified 9 misassemblies within 5 supercontigs. These misassemblies broke some of the largest supercontigs into 2-4 pieces of variable size. Further investigation of sites of misassembly indicate that 100% of misassembly co-occur with physical gaps between contigs of the genomic sequence that were incorrectly bridged. These findings underscore the importance of physical mapping for validation of computational approaches and ensuring accuracy in genome assemblies.

Our physical map which comprises 98% of the *An. albimanus* genome is the highest coverage genome map for any mosquito species to date. This map is a high quality tool that improves upon previous physical maps and corrects mistakes within the assembly. The order of supercontigs on our map is in very high agreement with a previous cytogenetic map published in 2009. Our high coverage map is a valuable tool that can be applied to study of genome evolution in *Anopheles* and promises to help uncover patterns and modes of genomic rearrangement in malaria vectors.

5.4 Review of chapter 4

As part of global efforts at malaria eradication, 16 vector and non-vector *Anopheles* genomes were sequenced and made available to researchers. This is a huge milestone for the malaria research community and will undoubtedly play a critical role in research that will eventually eliminate this devastating disease. In the initial publication of the 16 genomes project, orthologs within the low coverage chromosomal assemblies for *An. albimanus, An. funestus, An. stephensi,* and *An. atroparvus* were compared to *An. gambiae* to study chromosomal evolution over 100 million years. This study yielded several important insights into modes of evolution in malaria vectors and provides a foundation for many future works

Since the 16 genomes concentrated efforts have improved the quality of chromosomal assemblies; *An. stephensi, An. atroparvus* and *An. albimanus* now possess relatively complete genome assemblies at ~80 or greater. Syntenic relationships have also been leveraged to predict the chromosomal order of supercontigs in *An. stephensi, An. dirus* and *An. minimus.* New computational approaches have also enabled multispecies alignments for identifying lineage specific inversion breakpoints rather than the pairwise alignments that were used in the original publication. We utilized these resources for a detailed analysis of genome rearrangement breakpoints wherein repetitive DNA including transposable elements(TEs), tandem repeats(TRs) and inverted repeats(IRs) were quantified and compared to the whole genome.

Our study found that syntenic relationships provide a reliable prediction of supercontig order along mosquito chromosomes. We were able to test the validity of this approach in *An. stephensi* Indian strain and found very high agreement between the physical map and predicted order of supercontigs. Although this approach requires further evaluation in other species, these results support syntenic scaffolding as a viable method for assembly of genomes to the chromosomal level. The combination of computational methods such as syntenic scaffolding with physical mapping promises to speed the process of chromosomal assembly in future studies.

Our examination of rates of evolution corroborated previous works which demonstrate that the X chromosome evolves much faster and hosts much higher densities of repeats relative to the autosomes. Correlations of repeats to the rate of breakage for each arm in *An. stephensi* and *An. gambiae* reveals strong, positive correlations but only if the sex chromosome is included in the analysis. Without the sex chromosome correlations become moderately negative or disappear all together. An arm by arm correlation analysis suggests that different repeat types may contribute to chromosomal breakage on different chromosomal arms. In *An. gambiae* e2 accounts for the negative correlation between autosomal breakage and %TRs. In *An. stephensi* removal of e1 and e5 results in a strong positive correlation between rates of inversion of e2, e3, and e4 and coverage of TRs. This indicates that TRs may play a major role in the genesis of inversions on all autosomes except e5.

Investigation of the molecular content of breakpoints revealed transposable elements are consistently overrepresented in breakpoint regions of all species across all arms. These findings contradict negative correlations between autosomal rates of breakage and coverage of TEs. These contradictory results could suggest that some other molecular feature is at work, perhaps in addition to TEs, on the autosomes. Based on previous work, one good candidate for genomic instability on autosomes are Segmental duplications (SDs) which were found in greater density on several autosomes than on the sex chromosome. Other possible explanations for the contradiction between correlations and the molecular content of breakpoints include a lack of distinction in our study between autonomous and non autonomous TEs within breakpoints. Further analysis is required to filter out TEs that are not capable of creating chromosomal breaks. It is also possible that the greater coverage of TEs in breakpoint regions reflects a confounding association unrelated to the generation of chromosomal inversions. Our study cannot rule out differential effects of selection on different chromosomal arms which could also account for differences in rates of breakage independently of repeat content.

Although this study has focused primarily on the parts of mosquito genomes that have changed, the blocks of genes which have remained intact over evolutionary time are also important. Evolutionarily conserved regions presumably contain genes of vital function to survival of the organism. As such, characterization of these genes can perhaps provide more detailed insights into the genetic basis of many aspects of mosquito biology. From the applied standpoint, characterization of these genes will perhaps reveal novel genes that can be repurposed into “genetic kill switches” in the genetic control of mosquitoes.

References

1. Sinka, M.E., et al., *The dominant Anopheles vectors of human malaria in the Asia-Pacific region: occurrence data, distribution maps and bionomic précis.* Parasites & Vectors, 2011. **4**(1): p. 1-46.
2. Sinka, M.E., et al., *The dominant Anopheles vectors of human malaria in Africa, Europe and the Middle East: occurrence data, distribution maps and bionomic précis.* Parasites & Vectors, 2010. **3**(1): p. 1-34.
3. Sinka, M.E., et al., *The dominant Anopheles vectors of human malaria in the Americas: occurrence data, distribution maps and bionomic précis.* Parasit Vectors, 2010. **3**.
4. Organization, W.H. *World Malaria Report 2015*. 2015 [cited 2015.
5. Coetzee, M. and L.L. Koekemoer, *Molecular systematics and insecticide resistance in the major African malaria vector Anopheles funestus.* Annu Rev Entomol, 2013. **58**: p. 393-412.

6. Djouaka, R., et al., *Exploring Mechanisms of Multiple Insecticide Resistance in a Population of the Malaria Vector <italic>Anopheles funestus</italic> in Benin.* PLoS ONE, 2011. **6**(11): p. e27760.
7. Riveron, J.M., et al., *Rise of multiple insecticide resistance in Anopheles funestus in Malawi: a major concern for malaria vector control.* Malaria Journal, 2015. **14**: p. 344.
8. Sande, S., et al., *The emergence of insecticide resistance in the major malaria vector Anopheles funestus (Diptera: Culicidae) from sentinel sites in Mutare and Mutasa Districts, Zimbabwe.* Malaria Journal, 2015. **14**: p. 466.
9. Neafsey, D.E., et al., *Mosquito genomics. Highly evolvable malaria vectors: the genomes of 16 Anopheles mosquitoes.* Science, 2015. **347**(6217): p. 1258522.
10. Alphey, L., *Genetic control of mosquitoes.* Annu Rev Entomol, 2014. **59**: p. 205-24.
11. Alphey, L. and N. Alphey, *Five things to know about genetically modified (GM) insects for vector control.* PLoS Pathog, 2014. **10**(3).
12. Reichard, R.E., *Area-wide biological control of disease vectors and agents affecting wildlife.* Rev Sci Tech, 2002. **21**(1): p. 179-85.
13. Alphey, L., *Sterile-Insect Methods for Control of Mosquito-Borne Diseases: An.* 2010. **10**(3): p. 295-311.
14. Readshaw, J.L., *Screwworm eradication a grand delusion?* Nature, 1986. **320**(6061): p. 407-10.
15. Aryan, A., et al., *TALEN-based gene disruption in the dengue vector Aedes aegypti.* PLoS One, 2013. **8**.
16. Hammond, A., et al., *A CRISPR-Cas9 gene drive system targeting female reproduction in the malaria mosquito vector Anopheles gambiae.* Nat Biotech, 2016. **34**(1): p. 78-83.
17. Kistler, Kathryn E., Leslie B. Vosshall, and Benjamin J. Matthews, *Genome Engineering with CRISPR-Cas9 in the Mosquito <em>Aedes aegypti</em>.* Cell Reports. **11**(1): p. 51-60.
18. DeGennaro, M., et al., *Orco mutant mosquitoes lose strong preference for humans and are not repelled by volatile DEET.* Nature, 2013. **498**.
19. Fu, G., et al., *Female-specific flightless phenotype for mosquito control.* Proc Natl Acad Sci U S A, 2010. **107**.
20. Gentile, J.E., S.S.C. Rund, and G.R. Madey, *Modelling sterile insect technique to control the population of Anopheles gambiae.* Malaria Journal, 2015. **14**: p. 92.
21. Zeh, D.W., J.A. Zeh, and M.M. Bonilla, *Wolbachia, sex ratio bias and apparent male killing in the harlequin beetle riding pseudoscorpion.* Heredity, 2005. **95**(1): p. 41-49.
22. Fry, A.J., M.R. Palmer, and D.M. Rand, *Variable fitness effects of Wolbachia infection in Drosophila melanogaster.* Heredity, 2004. **93**(4): p. 379-389.
23. Riparbelli, M.G., et al., *Wolbachia-Mediated Male Killing Is Associated with Defective Chromatin Remodeling.* PLoS ONE, 2012. **7**(1): p. e30045.
24. Martinez, J., et al., *Should Symbionts Be Nice or Selfish? Antiviral Effects of Wolbachia Are Costly but Reproductive Parasitism Is Not.* PLoS Pathog, 2015. **11**(7): p. e1005021.
25. Hedges, L.M., et al., *Wolbachia and virus protection in insects.* Science, 2008. **322**(5902): p. 702.
26. Hoffmann, A.A., et al., *Successful establishment of Wolbachia in Aedes populations to suppress dengue transmission.* Nature, 2011. **476**(7361): p. 454-7.
27. Hoffmann, A.A., et al., *Stability of the wMel Wolbachia Infection following invasion into Aedes aegypti populations.* PLoS Negl Trop Dis, 2014. **8**(9): p. e3115.

28. Bian, G., et al., *Wolbachia invades Anopheles stephensi populations and induces refractoriness to Plasmodium infection.* Science, 2013. **340**(6133): p. 748-51.

29. Bourtzis, K., et al., *Harnessing mosquito-Wolbachia symbiosis for vector and disease control.* Acta Trop, 2014. **132**(63): p. 16.

30. Dodson, B.L., et al., *<italic>Wolbachia</italic> Enhances West Nile Virus (WNV) Infection in the Mosquito <italic>Culex tarsalis</italic>.* PLoS Negl Trop Dis, 2014. **8**(7): p. e2965.

31. Hughes, G.L., et al., *Wolbachia strain wAlbB enhances infection by the rodent malaria parasite Plasmodium berghei in Anopheles gambiae mosquitoes.* Appl Environ Microbiol, 2012. **78**(5): p. 1491-5.

32. *Evolution of genes and genomes on the Drosophila phylogeny.* Nature, 2007. **450**(7167): p. 203-218.

33. Brown, S.E., et al., *Integration of the Aedes aegypti mosquito genetic linkage and physical maps.* Genetics, 2001. **157**(3): p. 1299-305.

34. Severson, D.W., *RFLP analysis of insect genomes*, in *The Molecular Biology of Insect Disease Vectors: A Methods Manual*, J.M. Crampton, C.B. Beard, and C. Louis, Editors. 1997, Springer Netherlands: Dordrecht. p. 309-320.

35. *Genomes, 2nd edition*. 2nd ed. 2002, Oxford, U.K.: BIOS Scientific Publishers. 572.

36. Pringle, E.G., et al., *Synteny and Chromosome Evolution in the Lepidoptera: Evidence From Mapping in Heliconius melpomene*. Genetics. 2007 Sep;177(1):417-26. doi:10.1534/genetics.107.073122.

37. Hickner, P.V., et al., *Composite linkage map and enhanced genome map for Culex pipiens complex mosquitoes.* J Hered, 2013. **104**(5): p. 649-55.

38. Juneja, P., et al., *Assembly of the Genome of the Disease Vector <italic>Aedes aegypti</italic> onto a Genetic Linkage Map Allows Mapping of Genes Affecting Disease Transmission.* PLoS Negl Trop Dis, 2014. **8**(1): p. e2652.

39. Witzig, C., et al., *Genetic mapping identifies a major locus spanning P450 clusters associated with pyrethroid resistance in kdr-free Anopheles arabiensis from Chad.* Heredity, 2013. **110**(4): p. 389-397.

40. Fansiri, T., et al., *Genetic Mapping of Specific Interactions between <italic>Aedes aegypti</italic> Mosquitoes and Dengue Viruses.* PLoS Genet, 2013. **9**(8): p. e1003621.

41. Schaeffer, S.W., et al., *Polytene chromosomal maps of 11 Drosophila species: the order of genomic scaffolds inferred from genetic and physical maps.* Genetics, 2008. **179**(3): p. 1601-1655.

42. Bhutkar, A., et al., *Chromosomal rearrangement inferred from comparisons of 12 Drosophila genomes.* Genetics, 2008. **179**(3): p. 1657-1680.

43. Holt, R.A., et al., *The genome sequence of the malaria mosquito Anopheles gambiae.* Science, 2002. **298**(5591): p. 129-49.

44. Sharakhova, M.V., et al., *Update of the Anopheles gambiae PEST genome assembly.* Genome Biol, 2007. **8**(1): p. R5.

45. Sharakhova, M.V., et al., *A standard cytogenetic photomap for the mosquito Anopheles stephensi (Diptera: Culicidae): application for physical mapping.* J Med Entomol, 2006. **43**(5): p. 861-6.

46. Artemov, G.N., et al., *A standard photomap of ovarian nurse cell chromosomes in the European malaria vector Anopheles atroparvus.* Med Vet Entomol, 2015. **17**(10): p. 12113.

47. Cornel, A.J. and F.H. Collins, *Maintenance of chromosome arm integrity between two Anopheles mosquito subgenera.* J Hered, 2000. **91**(5): p. 364-70.

48. Sharakhova, M.V., et al., *Cytogenetic map for Anopheles nili: application for population genetics and comparative physical mapping.* Infection, genetics

and evolution : journal of molecular epidemiology and evolutionary genetics in infectious diseases, 2011. **11**(4): p. 746-754.

49. Sharakhova, M.V., et al., *Arm-specific dynamics of chromosome evolution in malaria mosquitoes.* BMC Evol Biol, 2011. **11**: p. 91.

50. Xia, A., et al., *Genome landscape and evolutionary plasticity of chromosomes in malaria mosquitoes.* PLoS One, 2010. **5**(5): p. e10592.

51. Timoshevskiy, V.A., et al., *An Integrated Linkage, Chromosome, and Genome Map for the Yellow Fever Mosquito <italic>Aedes aegypti</italic>.* PLoS Negl Trop Dis, 2013. **7**(2): p. e2052.

52. Timoshevskiy, V., et al., *Genomic composition and evolution of Aedes aegypti chromosomes revealed by the analysis of physically mapped supercontigs.* BMC Biology, 2014. **12**(1): p. 27.

53. Penilla, R.P., et al., *Towards a Genetic Map for Anopheles albimanus: Identification of Microsatellite Markers and a Preliminary Linkage Map for Chromosome 2.* The American Journal of Tropical Medicine and Hygiene, 2009. **81**(6): p. 1007-1012.

54. Coluzzi, M., *Heterogeneities of the malaria vectorial system in tropical Africa and their significance in malaria epidemiology and control.* Bull World Health Organ, 1984. **62**(Suppl): p. 107-13.

55. Sharakhov, I.V., G.N. Artemov, and M.V. Sharakhova, *Chromosome evolution in malaria mosquitoes inferred from physically mapped genome assemblies.* Journal of Bioinformatics and Computational Biology, 2016. **14**(02): p. 1630003.

56. Brooke, B.D., et al., *Stable chromosomal inversion polymorphisms and insecticide resistance in the malaria vector mosquito Anopheles gambiae (Diptera: Culicidae).* J Med Entomol, 2002. **39**(4): p. 568-73.

57. Fouet, C., et al., *Adaptation to aridity in the malaria mosquito Anopheles gambiae: chromosomal inversion polymorphism and body size influence resistance to desiccation.* PLoS One, 2012. **7**(4): p. e34841.

58. Mnzava, A.E., M.J. Mutinga, and C. Staak, *Host blood meals and chromosomal inversion polymorphism in Anopheles arabiensis in the Baringo District of Kenya.* J Am Mosq Control Assoc, 1994. **10**(4): p. 507-10.

59. Ayala D, U.A.a.G.J., *Adaptation through chromosomal inversions in Anopheles.* Front. Genet. , (2014).

60. Coluzzi, M., et al., *A polytene chromosome analysis of the Anopheles gambiae species complex.* Science, 2002. **298**(5597): p. 1415-8.

61. Pombi, M., et al., *Chromosomal plasticity and evolutionary potential in the malaria vector Anopheles gambiae sensu stricto: insights from three decades of rare paracentric inversions.* BMC Evol Biol, 2008. **8**.

62. González, J., F. Casals, and A. Ruiz, *Testing chromosomal phylogenies and inversion breakpoint reuse in Drosophila.* Genetics, 2007. **175**.

63. Puerma, E., et al., *Characterization of the Breakpoints of a Polymorphic Inversion Complex Detects Strict and Broad Breakpoint Reuse at the Molecular Level.* Molecular Biology and Evolution, 2014. **31**(9): p. 2331-2341.

64. Pevzner, P. and G. Tesler, *Human and mouse genomic sequences reveal extensive breakpoint reuse in mammalian evolution.* Proceedings of the National Academy of Sciences, 2003. **100**(13): p. 7672-7677.

65. Ruiz-Herrera, A., J. Castresana, and T.J. Robinson, *Is mammalian chromosomal evolution driven by regions of genome fragility?* Genome Biol, 2006. **7**(12): p. R115.

66. Grotthuss, M.v.o.n., M. Ashburner, and J. Ranz, *Fragile regions and not functional constraints predominate in shaping gene organization in the genus Drosophila.* Genome Research, 2010. **20**.

67. Diaz-Castillo, C., X.Q. Xia, and J.M. Ranz, *Evaluation of the role of functional constraints on the integrity of an ultraconserved region in the genus Drosophila.* PLoS Genet, 2012. **8**(2): p. e1002475.

68. Kamali, M., et al., *A new chromosomal phylogeny supports the repeated origin of vectorial capacity in malaria mosquitoes of the Anopheles gambiae complex.* PLoS Pathog, 2012. **8**(10): p. e1002960.

69. Coulibaly, M.B., et al., *Segmental Duplication Implicated in the Genesis of Inversion 2<italic>Rj</italic> of <italic>Anopheles gambiae</italic>.* PLoS One, 2007. **2**(9): p. e849.

70. Cáceres, M., M. Puig, and A. Ruiz, *Molecular characterization of two natural hotspots in the Drosophila buzzatii genome induced by transposon insertions.* Genome research, 2001. **11**.

71. Delprat, A., et al., *The transposon Galileo generates natural chromosomal inversions in Drosophila by ectopic recombination.* PloS One, 2009. **4**.

72. Sharakhov, I.V., et al., *Breakpoint structure reveals the unique origin of an interspecific chromosomal inversion (2La) in the Anopheles gambiae complex.* Proceedings of the National Academy of Sciences of the United States of America, 2006. **103**(16): p. 6258-6262.

73. Lobo, N.F., et al., *Breakpoint structure of the Anopheles gambiae 2Rb chromosomal inversion.* Malar J, 2010. **9**: p. 293.

74. Feuk, L., et al., *Discovery of Human Inversion Polymorphisms by Comparative Analysis of Human and Chimpanzee DNA Sequence Assemblies.* PLoS Genet, 2005. **1**(4): p. e56.

75. Lu, S., et al., *Short Inverted Repeats Are Hotspots for Genetic Instability: Relevance to Cancer Genomes.* Cell Reports, 2015. **10**(10): p. 1674-1680.

76. Mathiopoulos, K.D., et al., *Cloning of inversion breakpoints in the Anopheles gambiae complex traces a transposable element at the inversion junction.* Proc Natl Acad Sci U S A, 1998. **95**(21): p. 12444-9.

77. Wesley, C.S. and W.F. Eanes, *Isolation and analysis of the breakpoint sequences of chromosome inversion In(3L)Payne in Drosophila melanogaster.* Proceedings of the National Academy of Sciences, 1994. **91**(8): p. 3132-3136.

78. Matzkin, L.M., et al., *The structure and population genetics of the breakpoints associated with the cosmopolitan chromosomal inversion In(3R)Payne in Drosophila melanogaster.* Genetics, 2005. **170**(3): p. 1143-52.

79. Ranz, J.M., et al., *Principles of genome evolution in the Drosophila melanogaster species group.* PLoS Biology, 2007. **5**.

80. Feachem, R.G.A., et al., *Shrinking the malaria map: progress and prospects.* Lancet, 2010. **376**.

81. Cheng, C., et al., *Ecological genomics of Anopheles gambiae along a latitudinal cline: a population-resequencing approach.* Genetics, 2012. **190**(4): p. 1417-32.

82. Rafinejad, J., et al., *Effect of washing on the bioefficacy of insecticide-treated nets (ITNs) and long-lasting insecticidal nets (LLINs) against main malaria vector Anopheles stephensi by three bioassay methods.* J Vector Borne Dis, 2008. **45**.

83. Sharma, V.P., *Current scenario of malaria in India.* Parassitologia, 1999. **41**.

84. Gakhar, S.K., R. Sharma, and A. Sharma, *Population genetic structure of malaria vector Anopheles stephensi Liston (Diptera: Culicidae).* Indian J Exp Biol, 2013. **51**.

85. Murray, C.J.L., et al., *Global malaria mortality between 1980 and 2010: A systematic analysis.* Lancet, 2012. **2012**.

86. Alonso, P.L., et al., *A research agenda to underpin malaria eradication.* PLoS Med, 2011. **8**.

87. Nolan, T., et al., *piggyBac-mediated germline transformation of the malaria mosquito Anopheles stephensi using the red fluorescent protein dsRED as a selectable marker.* J Biol Chem, 2002. **277**.

88. O'Brochta, D.A., et al., *piggyBac transposon remobilization and enhancer detection in Anopheles mosquitoes.* Proceedings of the National Academy of Sciences, 2011. **108**(39): p. 16339-16344.

89. Isaacs, A.T., et al., *Transgenic Anopheles stephensi coexpressing single-chain antibodies resist Plasmodium falciparum development.* Proc Natl Acad Sci U S A, 2012. **109**.

90. Smidler, A.L., et al., *Targeted mutagenesis in the malaria mosquito using TALE nucleases.* PLoS One, 2013. **8**.

91. Brown, A.E., et al., *Stable and heritable gene silencing in the malaria vector Anopheles stephensi.* Nucleic Acids Res, 2003. **31**.

92. Dong, Y., et al., *Engineered anopheles immunity to Plasmodium infection.* PLoS Pathog, 2011. **7**.

93. Garver, L.S., Y. Dong, and G. Dimopoulos, *Caspar controls resistance to plasmodium falciparum in diverse anopheline species.* PLoS Pathog, 2009. **5**.

94. Luckhart, S., et al., *Sustained activation of Akt elicits mitochondrial dysfunction to block Plasmodium falciparum infection in the mosquito host.* PLoS Pathog, 2013. **9**.

95. Mitri, C., et al., *Density-dependent impact of the human malaria parasite Plasmodium falciparum gametocyte sex ratio on mosquito infection rates.* Proc Roy Soc Lond B Biol Sci, 2009. **276**.

96. Pakpour, N., et al., *Ingested human insulin inhibits the mosquito NF-κB-dependent immune response to Plasmodium falciparum.* Infect Immun, 2012. **80**.

97. Rai, K.S. and W.C. Black Iv, *Mosquito Genomes: Structure, Organization, and Evolution.* Advances in Genetics, 1999. **41**: p. 1-33.

98. Marinotti, O., et al., *The genome of Anopheles darlingi, the main neotropical malaria vector.* Nucleic Acids Res, 2013. **41**.

99. Zhou, D., et al., *Genome sequence of Anopheles sinensis provides insight into genetics basis of mosquito competence for malaria parasites.* BMC Genomics, 2014. **15**.

100. Criscione, F., et al., *A unique Y gene in the Asian malaria mosquito Anopheles stephensi encodes a small lysine-rich protein and is transcribed at the onset of embryonic development.* Insect Mol Biol, 2013. **22**.

101. Göpfert, M.C. and D. Robert, *Active auditory mechanics in mosquitoes.* Proc Roy Soc Lond B Biol Sci, 2001. **268**.

102. Gibson, G., B. Warren, and I.J. Russell, *Humming in tune: sex and species recognition by mosquitoes on the wing.* J Assoc Res Otolaryngol, 2010. **11**.

103. Xi, Z., J.L. Ramirez, and G. Dimopoulos, *The Aedes aegypti toll pathway controls dengue virus infection.* PLoS Pathog, 2008. **4**.

104. Price, I., et al., *In vivo, in vitro, and in silico studies suggest a conserved immune module that regulates malaria parasite transmission from mammals to mosquitoes.* J Theor Biol, 2013. **334**.

105. Horton, A.A., et al., *The mitogen-activated protein kinome from Anopheles gambiae: identification, phylogeny and functional characterization of the ERK, JNK and p38 MAP kinases.* BMC Genomics, 2011. **12**.

106. Riehle, M.M., et al., *Anopheles gambiae APL1 is a family of variable LRR proteins required for Rel1-mediated protection from themalaria parasite, Plasmodium berghei.* PLoS ONE, 2008. **3**.

107. Baker, D.A., et al., *A comprehensive gene expression atlas of sex- and tissue-specificity in the malaria vector.* Anopheles gambiae BMC Genomics, 2011. **12**.

108. Choi, J., et al., *Structure of the FKBP12-rapamycin complex interacting with the binding domain of human FRAP.* Science (New York, NY), 1996. **273**.
109. Laplante, M. and D.M. Sabatini, *mTOR signaling in growth control and disease.* Cell, 2012. **149**.
110. Grewal, S.S., *Insulin/TOR signaling in growth and homeostasis: A view from the fly world.* Int J Biochem Cell Biol, 2009. **41**.
111. Arsic, D. and P.M. Guerin, *Nutrient content of diet affects the signaling activity of the insulin/target of rapamycin/p70 S6 kinase pathway in the African malaria mosquito Anopheles gambiae.* J Insect Physiol, 2008. **54**.
112. Anderson, K.V., L. Bokla, and C. Nüsslein-Volhard, *Establishment of dorsal-ventral polarity in the Drosophila embryo: the induction of polarity by the Toll gene product.* Cell, 1985. **42**.
113. Valenzuela, J.G., et al., *Exploring the salivary gland transcriptome and proteome of the Anopheles stephensi mosquito.* Insect Biochem Mol Biol, 2003. **33**.
114. Ribeiro, J.M.C., B.J. Mans, and B. Arcà, *An insight into the sialome of blood-feeding Nematocera.* Insect Biochem Mol Biol, 2010. **40**.
115. Mahmood, F. and R.K. Sakai, *Inversion polymorphisms in natural populations of Anopheles stephensi.* Can J Genet Cytol, 1984. **26**(5): p. 538-46.
116. Hoffmann, A.A., C.M. Sgrò, and A.R. Weeks, *Chromosomal inversion polymorphisms and adaptation.* Trends Ecol Evol, 2004. **19**.
117. Baricheva, E.A., et al., *DNA from Drosophila melanogaster β-heterochromatin binds specifically to nuclear lamins in vitro and the nuclear envelope in situ.* Gene, 1996. **171**.
118. Dechat, T., et al., *Nuclear lamins: major factors in the structural organization and function of the nucleus and chromatin.* Genes Dev, 2008. **22**.
119. Baker, R.H. and R.K. Sakai, *Triploids and male determination in the mosquito, Anopheles culicifacies.* J Hered, 1979. **70**.
120. Hall, A.B., et al., *Six novel Y chromosome genes in Anopheles mosquitoes discovered by independently sequencing males and females.* BMC Genomics, 2013. **14**.
121. Chin, C.S., et al., *Nonhybrid, finished microbial genome assemblies from long-read SMRT sequencing data.* Nat Methods, 2013. **10**.
122. Tesler, G., *GRIMM: genome rearrangements web server.* Bioinformatics, 2002. **18**(3): p. 492-3.
123. Lin, Y.C., et al., *SPRING: a tool for the analysis of genome rearrangement using reversals and block-interchanges.* Nucleic Acids Res, 2006. **34**(Web Server issue): p. W696-9.
124. Sharakhova, M., et al., *Genome mapping and characterization of the Anopheles gambiae heterochromatin.* BMC Genomics, 2010. **11**(1): p. 459.
125. Sharakhov, I.V., et al., *Inversions and gene order shuffling in Anopheles gambiae and A. funestus.* Science, 2002. **298**(5591): p. 182-5.
126. Schaeffer, S.W., et al., *Polytene chromosomal maps of 11 Drosophila species: the order of genomic scaffolds inferred from genetic and physical maps.* Genetics, 2008. **179**.
127. Ranz, J.M., et al., *Principles of genome evolution in the Drosophila melanogaster species group.* PLoS Biol, 2007. **5**.
128. Ranz, J.M., F. Casals, and A. Ruiz, *How malleable is the eukaryotic genome? Extreme rate of chromosomal rearrangement in the genus Drosophila.* Genome Res, 2001. **11**(2): p. 230-239.
129. Peng, Q., P.A. Pevzner, and G. Tesler, *The fragile breakage versus random breakage models of chromosome evolution.* PLoS Comput Biol, 2006. **2**.
130. Chaisson, M.J., B.J. Raphael, and P.A. Pevzner, *Microinversions in mammalian evolution.* Proc Natl Acad Sci U S A, 2006. **103**.

131. Bourque, G. and P.A. Pevzner, *Genome-scale evolution: reconstructing gene orders in the ancestral species.* Genome Res, 2002. **12**(1): p. 26-36.

132. Wurm, Y., et al., *The genome of the fire ant Solenopsis invicta.* Proc Natl Acad Sci U S A, 2011. **108**.

133. Kumar, S. and M.L. Blaxter, *Comparing de novo assemblers for 454 transcriptome data.* BMC Genomics, 2010. **11**.

134. Denisov, G., et al., *Consensus generation and variant detection by Celera Assembler.* Bioinformatics, 2008. **24**.

135. English, A.C., et al., *Mind the gap: upgrading genomes with Pacific Biosciences RS long-read sequencing technology.* PLoS One, 2012. **7**.

136. Pop, M., D.S. Kosack, and S.L. Salzberg, *Hierarchical scaffolding with Bambus.* Genome Res, 2004. **14**.

137. Kurtz, S., et al., *Versatile and open software for comparing large genomes.* Genome Biol, 2004. **5**.

138. Parra, G., K. Bradnam, and I. Korf, *CEGMA: a pipeline to accurately annotate core genes in eukaryotic genomes.* Bioinformatics, 2007. **23**.

139. Wu, T.D. and C.K. Watanabe, *GMAP: a genomic mapping and alignment program for mRNA and EST sequences.* Bioinformatics, 2005. **21**.

140. Sharakhova, M.V., et al., *Genome mapping and characterization of the Anopheles gambiae heterochromatin.* BMC Genomics, 2010. **11**.

141. Cantarel, B.L., et al., *MAKER: an easy-to-use annotation pipeline designed for emerging model organism genomes.* Genome Res, 2008. **18**.

142. Tempel, S., *Using and understanding RepeatMasker.* Methods Mol Biol, 2012. **859**.

143. Korf, I., *Gene finding in novel genomes.* BMC Bioinformatics, 2004. **5**.

144. Stanke, M., et al., *AUGUSTUS: a web server for gene finding in eukaryotes.* Nucleic Acids Res, 2004. **32**.

145. Waterhouse, R.M., et al., *OrthoDB: a hierarchical catalog of animal, fungal and bacterial orthologs.* Nucleic Acids Res, 2013. **41**.

146. Trapnell, C., L. Pachter, and S.L. Salzberg, *TopHat: discovering splice junctions with RNA-Seq.* Bioinformatics, 2009. **25**.

147. Anders, S., P.T. Pyl, and W. Huber, *HTSeq - A Python framework to work with high-throughput sequencing data.* Bioinformatics, 2014.

148. Si, Y., et al., *Model-based clustering for RNA-seq data.* Bioinformatics, 2014. **30**.

149. Love, M.I., W. Huber, and S. Anders, *Moderated estimation of fold change and dispersion for RNA-Seq data with DESeq2*. 2014.

150. Wickham, H., *ggplot2.* Wiley Interdiscipl Rev Comput Stat, 2011. **3**.

151. Conesa, A., et al., *Blast2GO: a universal tool for annotation, visualization and analysis in functional genomics research.* Bioinformatics, 2005. **21**.

152. Quevillon, E., et al., *InterProScan: protein domains identifier.* Nucleic Acids Res, 2005. **33**.

153. Falcon, S. and R. Gentleman, *Using GOstats to test gene lists for GO term association.* Bioinformatics, 2007. **23**.

154. Lowe, T.M. and S.R. Eddy, *tRNAscan-SE: a program for improved detection of transfer RNA genes in genomic sequence.* Nucleic Acids Res, 1997. **25**.

155. Nawrocki, E.P., D.L. Kolbe, and S.R. Eddy, *Infernal 1.0: inference of RNA alignments.* Bioinformatics, 2009. **25**.

156. Griffiths-Jones, S., et al., *Rfam: an RNA family database.* Nucleic Acids Res, 2003. **31**.

157. Nene, V., et al., *Genome sequence of Aedes aegypti, a major arbovirus vector.* Science, 2007. **316**.

158. Benson, G., *Tandem repeats finder: a program to analyze DNA sequences.* Nucleic Acids Res, 1999. **27**(2): p. 573-80.

159. van Hoof, A., et al., *Exosome-mediated recognition and degradation of mRNAs lacking a termination codon.* Science, 2002. **295**(5563): p. 2262-4.
160. Sinka, M.E., et al., *The dominant Anopheles vectors of human malaria in the Americas: occurrence data, distribution maps and bionomic précis.* Parasites & Vectors, 2010. **3**(1): p. 1-26.
161. Arredondo-Jimenez, J.I., et al., *Tests for the existence of genetic determination or conditioning in host selection by Anopheles albimanus (Diptera: Culicidae).* J Med Entomol, 1992. **29**(5): p. 894-7.
162. Narang, S.K., J.A. Seawright, and M.F. Suarez, *Genetic structure of natural populations of Anopheles albimanus in Colombia.* J Am Mosq Control Assoc, 1991. **7**(3): p. 437-45.
163. Narang, S.K. and J.A. Seawright, *Linkage map of the mosquito (Anopheles albimanus) (2n=6)*, in *Genetic maps, locus maps of complex genomes*, S.J. O'Brein, Editor. 1989, Cold Spring Harbor Laboratory Press: New York. p. 3269-3272.
164. Hobbs, J.H., *Cytogenetics of Anopheles albimanus (Diptera:Culicidae).* Ann Entomol Soc Am, 1962. **55**: p. 245-251.
165. Keppler, W.J., J.B. Kitzmiller, and M.G. Rabbani, *The salivary gland chromosomes of Anopheles albimanus.* J Am Mosq Control Assoc, 1973. **33**: p. 42-49.
166. Narang, S.K. and J.A. Seawright, *In situ hybridization mapping of histone genes in Anopheles albimanus.* J Am Mosq Control Assoc, 1993. **9**(2): p. 147-9.
167. Zheng, L., et al., *Low-resolution genome map of the malaria mosquito Anopheles gambiae.* Proc Natl Acad Sci U S A, 1991. **88**(24): p. 11187-91.
168. della Torre, A., et al., *Physical map of the malaria vector Anopheles gambiae.* Genetics, 1996. **143**(3): p. 1307-11.
169. Sharakhova, M.V., et al., *A physical map for an Asian malaria mosquito, Anopheles stephensi.* Am J Trop Med Hyg, 2010. **83**(5): p. 1023-7.
170. Neafsey, D.E., et al., *The evolution of the Anopheles 16 genomes project.* G3 (Bethesda), 2013. **3**(7): p. 1191-4.
171. Schatz, M.C., A.L. Delcher, and S.L. Salzberg, *Assembly of large genomes using second-generation sequencing.* Genome Res, 2010. **20**(9): p. 1165-73.
172. Henson, J., G. Tischler, and Z. Ning, *Next-generation sequencing and large genome assemblies.* Pharmacogenomics, 2012. **13**(8): p. 901-15.
173. Simpson, J.T. and M. Pop, *The Theory and Practice of Genome Sequence Assembly.* Annu Rev Genomics Hum Genet, 2015. **16**: p. 153-72.
174. Gabrieli, P., A. Smidler, and F. Catteruccia, *Engineering the control of mosquito-borne infectious diseases.* Genome Biology, 2014. **15**(11): p. 1-9.
175. Mlakar, J., et al., *Zika Virus Associated with Microcephaly.* New England Journal of Medicine, 2016. **374**(10): p. 951-958.
176. Liu, N., *Insecticide Resistance in Mosquitoes: Impact, Mechanisms, and Research Directions.* Annual Review of Entomology, 2015. **60**(1): p. 537-559.
177. Russell, T.L., et al., *Increased proportions of outdoor feeding among residual malaria vector populations following increased use of insecticide-treated nets in rural Tanzania.* Malar J, 2011. **10**.
178. Sougoufara, S., et al., *Biting by Anopheles funestus in broad daylight after use of long-lasting insecticidal nets: a new challenge to malaria elimination.* Malar J, 2014. **13**.
179. Zdobnov, E.M., et al., *Comparative Genome and Proteome Analysis of Anopheles gambiae and Drosophila melanogaster.* Science, 2002. **298**(5591): p. 149-159.
180. Kamali, M., et al., *Multigene Phylogenetics Reveals Temporal Diversification of Major African Malaria Vectors.* PLoS One, 2014. **9**(4): p. e93580.

181. Guillén, Y. and A. Ruiz, *Gene alterations at Drosophila inversion breakpoints provide prima facie evidence for natural selection as an explanation for rapid chromosomal evolution.* BMC Genomics, 2012. **13**(1): p. 1-18.

182. Aganezov, S., N. Sitdykova, and M.A. Alekseyev, *Scaffold assembly based on genome rearrangement analysis.* Comput Biol Chem, 2015. **57**: p. 46-53.

183. Jiang, X., et al., *Genome analysis of a major urban malaria vector mosquito, Anopheles stephensi.* Genome Biology.

184. Johnson, N.A., *The genetics of sex chromosomes: evolution and implications for hybrid incompatibility.* 2012. **1256**: p. E1-22.

185. Cattani, M.V. and D.C. Presgraves, *Incompatibility Between X Chromosome Factor and Pericentric Heterochromatic Region Causes Lethality in Hybrids Between Drosophila melanogaster and Its Sibling Species.* Genetics, 2012. **191**(2): p. 549-59.

186. Crawford, J.E., et al., *Reticulate Speciation and Barriers to Introgression in the Anopheles gambiae Species Complex.* Genome Biology and Evolution, 2015. **7**(11): p. 3116-3131.

187. Krzywinski, J., et al., *Isolation and Characterization of Y Chromosome Sequences From the African Malaria Mosquito Anopheles gambiae.* Genetics, 2004. **166**(3): p. 1291-1302.

188. Hall, A.B., et al., *Radical remodeling of the Y chromosome in a recent radiation of malaria mosquitoes.* Proceedings of the National Academy of Sciences, 2016.

189. Sakai, R.K., et al., *Crossing-over in the long arm of the X and Y chromosomes in Anopheles culicifacies.* Chromosoma. **74**(2): p. 209-218.

190. Fraccaro, M., et al., *Karyotype, DNA replication and origin of sex chromosomes in Anopheles atroparvus.* Chromosoma. **55**(1): p. 27-36.

191. Goidts, V., et al., *Segmental duplication associated with the human-specific inversion of chromosome 18: a further example of the impact of segmental duplications on karyotype and genome evolution in primates.* Hum Genet, 2004. **115**(2): p. 116-22.

192. Bailey, J.A. and E.E. Eichler, *Primate segmental duplications: crucibles of evolution, diversity and disease.* Nat Rev Genet, 2006. **7**(7): p. 552-564.

193. Calvete, O., et al., *Segmental duplication, microinversion, and gene loss associated with a complex inversion breakpoint region in Drosophila.* Mol Biol Evol, 2012. **29**(7): p. 1875-1889.

194. Di Rienzi, S.C., et al., *Fragile Genomic Sites Are Associated with Origins of Replication.* Genome Biology and Evolution, 2009. **1**: p. 350-363.

195. Kirkpatrick, M., *How and why chromosome inversions evolve.* PLoS Biology, 2010. **8**.

196. Naseeb, S., et al., *Widespread Impact of Chromosomal Inversions on Gene Expression Uncovers Robustness via Phenotypic Buffering.* Molecular Biology and Evolution, 2016.

197. de Jong, S., et al., *Common inversion polymorphism at 17q21.31 affects expression of multiple genes in tissue-specific manner.* BMC Genomics, 2012. **13**(1): p. 1-6.

198. Lee, Y., et al., *Chromosome Inversions, Genomic Differentiation and Speciation in the African Malaria Mosquito Anopheles gambiae.* PLoS One, 2013. **8**(3).

199. Woolfe, A., et al., *Highly conserved non-coding sequences are associated with vertebrate development.* PLoS Biol, 2005. **3**(1): p. e7.